Optimal Single-Tuned Passive Filter Design for Harmonics Mitigation using Mixed Integer Distributed Ant-Colony Optimization

By

Nor Hidayah Binti Abdul Kahar

Supervised by: Dr Ahmed F. Zobaa

Electronic and Computer Engineering Research

Brunel University London

A dissertation is submitted for the degree of

Doctor of Philosophy

Abstract

Power system harmonics has existed since the distorted current and voltage were observed in the power system. As newly advanced and developed technologies and the ongoing research efforts were made, awareness and interest were developed by pollution in the system created through harmonics. This research showed an advanced optimization solver called mixed-integer distributed ant colony optimization (MIDACO). The simulation is based on a single optimization of four objective functions, which minimizes the total of harmonic voltage distortions, maximizes the power factor, maximizes the transmission efficiency, and minimizes the resistor losses of the impedance of Thevenin. The presented solver is aimed at optimizing the size of a single-tuned passive filter based on harmonics elimination for all the objective functions involved. A completed and detailed study was conducted considering several significant constraints in designing the best filter. The global maximum and minimum can be achieved by maintaining the quality factor in a particular range, such as the harmonic resonance constraints and the capacitors that do not violate the limits of Institute of Electrical and Electronics Engineers (IEEE) standard 18-2012. The constraints also considered the design in which the harmonic voltage was below the standard limit, thus maintaining the desired range of power factor. The results are evaluated based on the system performance in four different cases in the study to be compared with the genetic algorithm (GA), particle swarm optimization (PSO), and previously published journals. In this research, a single-tuned filter design with and without damping resistor of the inductance was investigated. Then, the comparative study between the advantages and the disadvantages of damping over undamped filter was also presented in this research. Additionally, the numerical results were analyzed considering two objective functions simultaneously, which are total harmonic distortion (THD) and transmission losses. The results of the nondominated solution for the simulation of the multiobjective problem with different search effort on the part of the Pareto front have also been investigated. The advantages of multiobjective over single objective optimization are also presented and highlighted in this thesis.

Acknowledgment

A very high appreciation and recognition go to Dr. Ahmed F. Zobaa, who has been a tremendous inspiration, a great mentor, and the best supervisor throughout my PhD journey. I am truly grateful for his time, guidance, and encouragement from the start until I completed my study. Besides, I would also like to thank Dr. Shady Abdel Aleem, May Higher Institute Engineering, Egypt, and Mr. Ahmed Mohamed Zobaa, Faculty of Engineering, Cairo University, Egypt, for their technical support during the early stage of preparation of this work.

I would also like to recognize the scholarship given by the government of my beloved home country, Malaysia, known as Majlis Amanah Rakyat, for this opportunity to pursue my PhD at Brunel University London. I will always be indefinitely grateful for the financial support I have received throughout the 4 years of my study and living in the United Kingdom.

An extraordinary acknowledgment goes to my beloved husband, Mr. Mohd Hairulzihan Burhanuddin, for his love, understanding, and tolerance and for being the one who always believed and supported me to get to this point. Not to forget, my parent, families, and friends for their moral support and motivation throughout this journey.

Last but not least, I thank my children Hannah and Harison, who were born during my second and third year of my PhD; both of them were indeed the real inspiration for me to remain and achieve my PhD.

Table of Contents

List of Tables

List of Figures

List of Acronyms

AC	Alternating current
DC	Direct current
PPF	Passive power filter
APF	Active power filter
MIDACO	Mixed integer ant colony optimization
IEEE	Institute of electrical and electronics engineer
IEC	International Electrotechnical Commission
MATLAB	Matrix laboratory
THD	Total harmonic distortion
TDD	Total demand distortions
HVDC	High voltage direct current
SQP	Sequential quadratic programming solver
FFSQP	Fortran sequential quadratic programming optimization
SI	Swarm intelligence
GS	Gravitational search
GA	Genetic algorithm
ACO	Ant colony optimization
(MMAS)	$MAX - MIN$ Ant System
ACS	Ant Colony System
NSGA	Non-dominated sorting genetic algorithm
SS	Scatter search
PSO	Particle swarm optimisation
DE	Differential evaluation
PSO-NTVENN	Particle swarm optimisation with nonlinear time-varying evolution built on neural network
PSO-NTVEOA	Particle swarm optimisation with nonlinear time-varying evolution built on orthogonal arrays
BFO	Bacterial foraging optimization

ABFO	Adaptive bacterial foraging optimization
BA	Bat algorithm
CSA	Crow search algorithm
SA	Simulated annealing
SCR	Silicon-controlled rectifiers
ASD	Adjustable speed drives
CFL	Compact fluorescent lamps
LED	Light emitting diodes
SMPS	Switch-mode power supplies
VFD	Variable frequency drive
VSD	Variable speed drive
UPS	Uninterruptible power supplies
AFD	Adjustable frequency drives
RMS	Root mean square
OPM	Oracle penalty method
ACOmi	Hybrid strategy of MIDACO
SDT	Single dimension tuning heuristic
WABA	Weighted average best ant heuristic
PCC	Point of common coupling
cPDF	Continuous probability density function
dPDF	Discrete probability density function
LC	Inductor-Capacitor filter

List of Nomenclature

f_0	Fundamental frequency
h, h_{DF}	Harmonic order
h_r, h_{DFr}	Harmonic order activating resonance
f_n	Filter resonant frequency
n, k	An integer
$V_{k.rms}$	*K*-th harmonic number of RMS voltage
$I_{k.rms}$	*K*-th harmonic number of RMS current
V_1	1st harmonic number of RMS voltage
I_1	1st harmonic number of RMS current
I_h	Harmonic current (per unit)
p	Number of pulses
K	K-factor
Z	Total impedance (Ω)
X_L, X_{LU}, X_{LF}	Inductive reactance (ohms)
X_C, X_{CU}, X_{CF}	Capacitive reactance (ohms)
R, R_{DF}	Intrinsic resistance of inductance (ohms)
L	Inductor (Henry)
C	Capacitor (Farad)
Z_{THK}, Z_{LK}	*K*-th harmonic number of Thevenin and load impedance (Ω)
R_{THK}, X_{THK}	*K*-th harmonic number of Thevenin resistance and reactance (Ω)
X_{TH1}	1st harmonic number of Thevenin reactance (Ω)
V_{THK}	*K*-th harmonic number of Thevenin voltage (V)
V_{TH}	Thevenin voltage in RMS (V)
V_{LK}	*K*-th harmonic number of Load voltage (V)
V_{L1}	Fundamental load voltage in RMS(V)
V_L	Load voltage in RMS (V)
V_{CK}, V_{CFK}	*K*-th harmonic number of capacitor voltage (V)

V_C, V_{CF}	Capacitor voltage in RMS (V)
V_{CP}	Peak capacitor voltage (V)
I_{SK}, I_{SFK}	*K*-th harmonic number of source current (A)
I_{LK}	*K*-th harmonic number of load current (A)
I_L	Load harmonic current in RMS (A)
I_{CK}, I_{CFK}	*K*-th harmonic number of capacitor current (A)
I_C, I_{CF}	Capacitor current in RMS (A)
P_L	Load power (W)
Q_C, Q_{CF}	Reactive power of capacitor (kVAR)
THD_V	Voltage Total Harmonic Distortion (%)
THD_i	Current Total Harmonic Distortion (%)
θ_K	*K*-th angle of load voltage (rad)
ϕ_K	*K*-th angle of line current (rad)
P_S	Supply power (W)
dpf	Displacement power factor
QF	Quality factor
PB	Pass band
p_j	The chance of ants visiting node *j*
$\tau(i,j)$	Pheromone level on the path (*i,j)*
$\eta(i,j)$	Visibility factor on the path (*i,j)*
α, β	Weighting parameters
hO	The ants unvisited node
ρ	Evaporation rate
$\Delta\tau_k$	The amount of pheromone laid by ant *k*
Q	Value of constant
F_L	Distance of the path
i	Dimension of the search domain
$G^i(x)$	Gaussian PDFs
w_k^i	Weight for the individual Gaussian functions
$g_k^i(x)$	Individual Gaussian functions
K	Size of the solution archive (SA)
v	Size of the generation of individual ants

k	Number of each kernel of individual G^i
σ^i	Standard deviations for the individual Gaussian functions
μ_k^i	Means for the individual Gaussian functions
x_i^k	Individual ants
s_k	Solution with low index
x_{new}^k	New generated ant
n_{ants}	Minimum size of ants
Pop_{size}	Actual population size of ants
dyn_{max}	Actual population of ants reach the maximum size
dyn_{mean}	Mean number of iterations
s_1	Current best solution
SA	Solution archive
x_{sdt}^i	A new created ant
x_{rand}^i	Vector of component n with a random number
x_{waba}^i	Weighted average best ant
dc_{max}, $dc_{average}$	Successive generations of ant
W_{final}	Weight to compare with successive generations of ant
ACOmain	First stage of ACO search process (Stage 1)
$stage_{final}$	End generation in the final stage heuristics
ACOfinal	Final stage of ACO search process (Stage 2)
MAXEVAL	Maximum number of function evaluation.
MAXTIME	Maximal limit budget of CPU-time
X	Decision variables.
F(X)	Objective function.
G(X)	Constraint values
fex	Feasible solution achieves
Ω	Omega/Oracle
$p(x)$	Penalty function
h_i and g_j	Equality and inequality constraints
V_i^{k+i}	Modified velocity

Pbest	Fitness best solution
Gbest.	Best value in the population
C_1	Cognitive attraction
C_2	Social attraction
$rand_1$ and $rand_2$	Two random sequences
X_i^k	Current position of individual *i* at iteration *k*.
$\omega = 2\pi f$	Angular frequency (rad/s)
PF	Power factor
η	Efficiency for transmission
P_{LOSS}	The losses in the resistor of the Thevenin's impedance
$P(x)dx$	continuous Probability Density Function
$Q(d)$	discrete Probability Density Function
$\mathbb{R}$	Set of real numbers
$\mathbb{R}_0^+$	Set of positive real numbers (include zero)
$\mathbb{Z}$	Set of integer numbers
ξ	General evolutionary operator
n_{int}	Integer variables
U_i	Utopia
N_i	Nadir
$B_j(x)$	Balance
$d_i^j(x)$	Weighted distance
$D_j(x)$	Average distance
w_i^j	weights
$T_j(x)$	Target function
$\check{\mathrm{T}}_j(x)$	Initial target function

Chapter 1

Introduction

1.1 General Overview About the Research

In the power system, there are some types of loads from power electronically controlled device widely used in most of the facilities such as rectifiers, uninterruptible power supply (UPS), variable speed drive and switch-mode power supplies which certainly change the pure sinusoidal power of alternating current (AC) [1], [2]. The nonlinear load charges distort waveforms with high frequencies known as power system harmonics. These higher frequencies are the main concerns of all the issues related to the power quality problem in which the engineers are required to design a reliable supply system for the utilities [3], [4].

Power system harmonics can cause many problems in the power system, such as the increase in the power losses that overall affects the efficiency and power quality reduction. Additionally, it will cause communication disturbance and the unpredicted failure of electrical appliances, which inconsiderably affects the rate of the production mainly in large industrial plants. With the growth of nonlinear loads and sensitive electronic equipment that can mostly be obtained at all power levels, thus, the harmonic problems will increase and continue to be a challenge for engineers in the future [5], [6]. Also, engineers have recently faced new challenges in maintaining the power quality due to other developments in power systems, such as the expansion of the

interconnected power grid and the massive renewable energy generation technologies [7]–[10].

Several methods have been used to reduce harmonics, such as 18-pulse converter, active power filter (APF), direct current (DC) choke, hybrid power filter, isolation transformers, linear reactor, passive power filter (PPF), and shifting transformer. Passive power filter is one of the many techniques used to eliminate harmonics because it is simple, robust, economical and almost free for the maintenance operation. The reactive compensation by the PPF has become an advantage for the utility and users in particular, where the filter not only increases the power factor but also reduces the power losses. Nevertheless, it can cause harmonic resonance when the filter is integrated into the circuit, which can damage the circuit as a whole.

The topology and the parameters of the passive components need to be selected wisely to have the best PPF performance. It is not an easy task for engineers in the design of PPF because conditions, measurements and practical standard need to be studied and considered carefully. Because of the difficulties for the engineers have in obtaining the optimal PPF when designing using experimental procedures, nature has inspired many researchers to provide practical ways to solve the problem that include PPF designs. In recent years, there have been numerous PPF design methods in the power system, such as adaptive bacterial foraging optimization (BFO), adaptive carrier frequency optimization, artificial bee colony, genetic problem, and particle swarm optimisation have been numerous in the power system. With the inspiration from the scavenging behavior of artificial ants, MIDACO was proposed in its algorithm to extend the mixed-integer search domains. This research presents the first application of MIDACO in passive filter design. The significant contribution of MIDACO is the ability to achieve rapid convergence to the global maximum or minimum, which was proven by comparison with the previous approaches.

The effective method of PPF has been proved especially useful in improving power factor, along with reducing the power losses, as well as for eliminating harmonics. Because of the requirements in power factor specifications and standard limitation to the voltage THD, the power system design should be handled with caution as the problem is not straightforward as the careful design of PPF can reduce any harmful effects of harmonics. There were numerous strategies that have been proposed and

addressed in the previous literature for the optimal design of passive harmonic filters considering several objectives; nonetheless, the goal is the same, which is to mitigate harmonics. The objective functions include minimization of voltage THD, minimization of current THD, power factor maximization, transmission efficiency maximization, transmission losses minimization, filter loss minimization, and filter investment cost minimization.

From the literature, finding an optimal PPF considering maximization of power factor as objective function has been widely used and become the top priority [11]–[13], whereas designing PPF by maximizing the load power factor and minimizing transmission losses as well as maximizing transmission efficiency has been commonly used as a main objective with the aim of achieving a practical level of THD [14], [15]. Nevertheless, maximizing only power factor may not succeed to reduce total voltage and current harmonic distortion in the power system, although it may work to reduce them [16]. Therefore, there is another goal to minimize voltage THDV [17], [18] to obtain an optimal passive filter design while considering the nonlinearity of the load in which having the load PF at an acceptable, pre-specified level is used as a constraint. Additionally, the previous study also considered several elements in the design of passive filters, such as capacitor size, cost, harmonic standard, locations, power factor, resonance, the system structure, and the source of harmonics. However, less information is needed when designing this type of filter, wherein it considers only two or three aspects from the previous. Therefore, this thesis considers four important objectives that have been widely used for harmonics elimination, which are (i) minimization of voltage THD, (ii) power factor maximization, (iii) transmission efficiency maximization, and (iv) losses in Thevenin's resistor. The design PPF also will consider the quality factor, the range of power factor to ensure efficiency, voltage THD, harmonic resonances and an adequate standard of capacitors using the application of MIDACO. Besides, this research will design a filter according the latest standard by the IEEE which is IEEE Std. 18-2012 and IEEE Std. 519-2014.

1.2 The Purposes and Targets to Be Achieved in This Research

The primary objective of the study is to design an optimal single-tuned passive filter under nonsinusoidal conditions using new executed optimization tool called MIDACO. The optimization is based on four objective functions to design the best filter. In this research, two designs are considered as follows:

- Undamped single-tuned filter—The previous studies have proposed several optimization techniques for the design of undamped single-tuned filters. However, the efficiency of the previous design lacked all the vital information when planning this type of filter. Therefore, the first objective of this research is to find the parameter of inductance and capacitance considering the design of the filter to avoid the harmonic resonance, at least minimum of 90% limit of power factor. The harmonic voltage limitation is required to comply with IEEE Std. 519-2014, and the power capacitor value is required to comply with IEEE Std. 18-2012.

- Damped single-tuned filter—The second objective of this research is to consider the damping resistance value when finding the optimal parameter of the single-tuned filter, considering similar constraints such as when designing the undamped single-tuned filter. However, this design considers the performance of the filter as one of the important critical constraints to be taken into consideration.

The third objective of this research is to verify convergence capability and robustness when using MIDACO. This is completed in comparison with other published approaches and articles in which MIDACO is expected to reach global solutions that satisfy all the constraints that are faster than other techniques.

The fourth objective of this research is to simulate the multiobjective problem of damped single-tuned filter considering two objective functions simultaneously, which are the total voltage harmonic distortion and the resistor losses of the impedance of Thevenin. To solve this problem, the simulations use the same constraints when solving single-objective optimization for the damped single-tuned filter. The numerical results

of nondominated solutions for all four cases are evaluated, which allows the selection parameters of the proposed algorithm to reach the best solution. The objectives of this research are summarized as follows:

1. To discover the optimal value of inductance and capacitance based on the four objective functions while satisfying all the implied constraints
2. To determine the optimal value of capacitance, inductance, and resistance, based on the four objective functions while satisfying all the implied constraints. The intrinsic resistance of inductance in which there is damping resistance is one of the variables that need to be optimized in this study
3. To analyze the system performance of the optimal filter size obtained in which the consequences of the results are used to evaluate other functions
4. To evaluate the efficiency and demonstrate the significant contribution of MIDACO to other techniques and other published articles
5. To analyze and study the comparison between damped and undamped single-tuned filter
6. To determine the optimal value of resistance, inductance, and capacitance based on the two objective functions instantaneously while satisfying all the implied constraints
7. To evaluate and analyze the Pareto front of the multiobjective problem and the effects of the selection parameters to the nondominated solutions
8. To analyze and study the comparison between optimization of the multiobjective and single-objective problem for all cases.

1.3 Contributions of the Research

This research contributes to the knowledge that the new advanced optimization solver known as MIDACO is used in its first design of PPF. The contributions developed in this thesis are highlighted and detailed as follows:

1. This research proposed a new technique for finding the optimal single-tuned filter subject to all constraints involved. In the simulation, the proposed method is tested using matrix laboratory (MATLAB) software. Overall, the results of the proposed method appeared to achieve different optimal solutions to four different objective functions with the satisfaction of constraints.

2. Two other evolutionary techniques are used to test the same power system implemented in IEEE Std. 519-1992 examples. The comparison with the other published methods showed that MIDACO has improved the solutions and satisfied all the constraints involved.
3. Also, the proposed method proved the ability of the algorithm to process thousands of ideal solutions within a few seconds.
4. The results of this research revealed that the resistor in the single-tuned filter had to be considered, and it was essential to take the power losses in the filter into consideration because it can affect the performance of the system.
5. This research was also involved solving multiobjective damped single-tuned design problems with two objective functions concurrently. The improvements in multiobjectives over single-objective optimization are also highlighted.

1.4 Thesis Outline

In this thesis, there are seven chapters are structured and explained as follows:

- Chapter 1 summarizes the research background in which its scope and the extent to which the specific research problem have been successfully studied. In this chapter, the ideas and the purposes of this research are clearly defined in which the contributions of the research are addressed.
- Chapter 2 explains the preliminary design of a PPF in detail. The literature reviews on the previous simulation studies are cited that consider the different topologies of a passive filter, the advantages and disadvantages, and the earlier optimization techniques that the earlier researcher considers to find the optimal solution including the objective functions and constraints considered.
- Chapter 3 describes the background study of the presence of harmonics and the previous methods that were used to remove the harmonics. Details of the explanation using single-tuned passive filter are also presented and discussed in this chapter.
- The implementation of MIDACO, in general, is explained in detail in Chapter 4. Besides, this chapter also includes all the mathematical background, the parameter selection, the flowchart, and the advantages and disadvantages of this method.

- Chapter 5 applies the proposed method of designing the optimal undamped single-tuned filter. The numerical results specifying the general design of the filter are then compared to the other published techniques and articles. The performance results of the filter were analyzed and are discussed in this chapter.
- Chapter 6 presents the design of an optimal damped single-tuned filter that considers the damping resistance to inductance. The results are also compared to other published techniques. In this chapter, a comparative study between the damped and the undamped filters is also presented. Additionally, the design of this filter considering two objectives simultaneously was also analyzed, whereas the advantages of multiobjective over single objective are presented in this chapter.
- Chapter 7 summarizes the overall findings of this research and explains the contributions made. Besides, this chapter also discussed the work that can be conducted to continue the investigation in the future.

1.5 List of Publications Conducted from This Study

In this research, there are few lists of papers that have successfully published and still under review.

- N. H. A. Kahar and A. F. Zobaa, "Application of mixed integer distributed ant colony optimization to the design of undamped single-tuned passive filters based harmonics mitigation," *Swarm and Evolutionary Computation,* vol. 44, pp. 187-199, February 2019.
- N. H. A. Kahar and A. F. Zobaa, "Optimal single tuned damped filter for mitigating harmonics using MIDACO," in *17th International Conference Environment and Electrical Engineering,* 2017.
- N. H. A. Kahar, A. F. Zobaa, A. M Zobaa and S. H. E. Abdel Aleem, "Comparative analysis of optimal damped and undamped single tuned passive filters using mixed integer distributed ant colony optimization," submitted to *22nd International Middle East Power System Conference,* 2020.

Chapter 2

Literature Review

2.1 Introduction

The extensive use of power electronic applications technology in the power system continues to develop. The nonlinear loads that are efficient and controllable can be discovered at all power levels with different applications, such as commercial, industrial, and residential. However, electrical pollution due to power system harmonics, such as current distortions or voltage and/or resonances, has become profoundly dangerous in which the problem can lead to overvoltage or overcurrent malfunctions in the facilities. Hence, it is indispensable for engineers to design a filter that can solve the problem of harmonics problem by reducing the harmonics to certain restrictions, for example, the limits as proposed by IEEE standard to improve the quality factor while keeping the investment costs to the lowest level possible.

Passive power filter is the most cost-effective approach to eliminate harmonics in the power system. In the design of this type of filter, few considerations should be taken into account and given as follows: (a) power factor, (b) resonance, (c) source of harmonics, (d) positions, (e) price, (f) voltage/current harmonic standard, (g) capacitor, and (h) the system structure. The design of PPF has become a significant task and challenge for engineers because of measurements, conditions, and practical standard that need to be studied carefully, as in the previously mentioned (a–h) factors in which

the previous design addressed only parts of it [19]. This chapter explains the previous experimental and simulation methods when designing PPF. This study also includes the effects of the filter and equipment connected to the source network. These previous methodologies effectively deal with constraints and integer variables, as well as the selection of single-objective and multiobjective optimization. Besides, the research gap of this study will also be discussed in this chapter. The section covers any missing information from the previous literature and is covered in this research.

2.2 Literature Review on PPF Design

In the 1940s, the first PPF was successfully installed in the power system in which the advantages of the filter make the solutions attractive until today [20]. Although active filters are proven to be the most effective method for improving power quality problem, however, most engineers are still selecting PPF when planning a power system. It is done to eliminate harmonics because it is economical, efficient, reliable, and requires only simple configurations of passive components [21].

Passive power filter can be categorized using either series or shunt filter connection. At the tuning frequency, the PPF series blocks the harmonics from entering by representing as series high-impedance series. On the contrary, the PPF shunt acts as a small impedance path. The advantages of shunt PPF, which are being capable of supporting voltage and compensating reactive power, have increased the interests among the researchers in this type of filter [22].

Besides, PPF also can be categorized into several topologies with different characteristics of frequency response. The most common design of PPF can be categorized into the following types: (i) tuned filter [14], [18], [29]–[37], [19], [21], [23]–[28], (ii) high-pass filter [38]–[41], and (iii) combination of both [42]–[44]. The single-tuned PPF design was commonly used in many applications, including distribution systems and industrial applications. However, double-tuned filter was widely used in high-voltage DC (HVDC) system, whereas triple-tuned filter in high-voltage applications [42].

Contrariwise, a high-pass filter or a damped filter is used to reduce harmonics at the wide range of frequencies. Generally, the filter is installed in the distribution system,

HVDC system, industrial system, and transmission system [13], [45]. The main issues for engineers are with the concern of the selection topology, which is not only effective but also economical. Therefore, in [46], the investigation was carried out to evaluate the effectiveness and the overall performance of various PPF topologies in which the results show that the single-tuned filter is sufficiently effective to reduce the voltage harmonics. Also, the authors in [47] also proved that a single-tuned filter was also considered as cost-effective in comparison with the damped filter.

It is a lot of effort and challenge for engineers to produce good PPF design because of several objectives and constraints that need to be considered carefully. In previous literature, two methodologies were suggested for the optimal planning of the PPF design, including optimization of single-objective [13], [14], [50], [18], [19], [21], [24], [31], [39], [48], [49] and multiobjective approaches [26], [30], [35], [38], [51]–[53].

The objective of the PPF design for single-objective optimization approach is either to maximize the power factor [13], [14], minimize the current THD [18], [49] or voltage THD [18], [19], [24], [49], or minimize the transmission losses [14] including the power losses [19], [24], [48]. Additionally, the objective also minimizes the cost that includes total filter installation cost [31], total investment cost [24], [48], total filter cost [19], [21], [39] and the overall costs [18]. While some previous studies in [13], [14], [50], [18], [19], [21], [24], [31], [39], [48], [49] solve the multiobjective problem by explaining each of the objectives individually, the studies in [26], [30], [35], [38], [51]–[53] implemented multiobjective optimization approach to optimize multiple objectives optimization when designing PPF. In [30], the bi-objective is applied to minimize the individual harmonic voltages and the cost of the filter. However, the multibjectives in [26], [35] are to minimize the NPV compensation and to reduce THD of the voltages as well as total demand distortions (TDD) of the current at the PCC. The optimization for the study in [51], includes three objectives: first reactive power compensation, investment costs, and losses. In [38], the author presented a PPF design with the objective functions of minimizing the budget for the installation while maximizing the power factor. Besides, the author in [52] also proposed PPF design based on bi-objective that minimizes voltage and current THD.

Practically, testing and error methods are widely used in the design of PPF. A basic guideline for designing LC filter has been proposed in [54], where the experimental

investigations were prepared in Lappeenranta University of Technology. However, this method is challenging for engineers to obtain optimal solutions to solve the problems with many objectives and nonlinear constraints involved. Therefore, the field of optimization has promptly developed over the last few decades to solve the problems. Different algorithms have been used to optimize the selection or topology of the passive filter using either exhaustive search [46], deterministic optimization approaches or heuristic/metaheuristic algorithms [29].

In solving optimization problems of PPF design, it is usually preferred to select the components of the filter with the best performance. The classic optimization algorithms using the exact techniques [46] is not suitable for solving the problem especially with a high-dimensional problem of search space. As the search space increases, the problem size will also increase, and the exhaustive search is shown to be impractical and not feasible because of being time-consuming in the search space. The authors in [55] also stated that the combination of preferred values to obtain the optimal design of the filter is also not realistic once the components are selected from the tighter tolerance series over a wide decade range. Thus, some intelligent search algorithms have to be found in filter design that requires high accuracy in a short computation time.

Numerous methods have been proposed using optimization methods in order to improve solution at a reasonable computational time and to find the near-optimal solution to a problem that cannot be solved by classic methods. The recent developments in optimization techniques are therefore divided mainly into two approaches: deterministic approach and heuristic/metaheuristics approach.

From literature, the deterministic method is used to solve the single optimization, where the sequence of a point converges to a global optimal or nearly global solution. The sequential quadratic programming (SQP) solver [31] and the golden section search method [15] are examples of deterministic methods.

Sequential quadratic programming solver is a technique that solves constrained nonlinear optimization problem, where the minimization of single-tuned filter total installation price has been proposed in [31]. By combining two algorithms based on SQP, Zhou has implemented Fortran Feasible Sequential Quadratic Programming (FFSQP) optimization, which guarantees many benefits, such as fast convergence,

improvement in the accuracy, and robust to the optimal solution. FFSQP has been successfully applied in the design of C-type high-pass filters [17], [18] that minimized THD of the supply line current [18], minimized of voltage THD [17], [18], and minimized of the total cost [18]. The main drawbacks of this method are that it needs to be analyzed before iterating the solution that is cumbersome with massive problems, especially for C-type filter with conflicting objectives and constraints.

The algorithm created based on nature has inspired many researchers in which the techniques are undergoing increasing development recently [56]–[58]. The heuristic algorithm, which is found to be more efficient and flexible, has been introduced in comparison with the deterministic approach. Besides, many researchers use these algorithms gradually to solve complex computational problems, such as filter modeling, objective functions and pattern recognition [59]–[62]. A heuristic technique is problem-dependent, in which it attempts to gain full advantage of the problem, which makes it too avaricious. As a result, the algorithm is usually trapped to the local optimum and subsequently failing to achieve an optimal global solution. Some procedures have improved the resolution for some specific problems than others and consequently, there will be a problem when new heuristic algorithms are penetrated.

The metaheuristic algorithm, on the other hand, is a high-level problem-independent technique for solving wide-ranging issues. It is not avaricious and would not take advantage of any particularity problem. Randomization is implemented in the formulation of the algorithm that allows them to start the search for solution space thoroughly on a global scale, thus making this algorithm a better solution and suitable for global optimization. The metaheuristic algorithms inspired by nature can be categorized into swarm intelligence (SI), bioinspired without SI basis, and the physical or chemical system has been actively used to solve PPF problems [63]. In recent years, the most popular to design PPF in the power system is based on an SI-based algorithm, such as ant colony optimization (ACO), bat algorithm (BA), crow search algorithm (CSA), GA, and PSO. All the algorithms are inspired by the cooperative performance of social insects, such as ants, bees, termites, and wasps. It was also inspired by the behavior of flocks of birds and fish. However, there is an algorithm that is bioinspired but does not directly use swarming behavior, such as differential evolution (DE), which can only be found in the application of active filters. [27]. The metaheuristic algorithm

is also categorized according to a physical and chemical system in which the algorithm imitates specific physical/chemical laws, such as gravity and river systems. The example of this algorithm can be found in simulated annealing (SA) and gravitational search in designing PPF.

Holland invented GA, which was further described by Goldberg, which used artificial intelligence to solve the method of optimization [64]. In GA, the potential solution refers to the individual or chromosomes in a population where the algorithm modifies a population repeatedly to produce a new individual that is close to the optimal results. From the current population, GA selects random individuals at each step as parents use it to produce children for the next generation [65]. This search process will continue until a satisfied termination condition is met. Genetic algorithm has been widely used in many design applications involving locating and sizing of passive filter [19], [32], [36], [66], [67]. In [66], the objective is to minimize the harmonic voltage with regard to the optimal solution for the location of the bus, the quality factor, and the size of the passive shunt filter using GA and micro-GA applications. By using an actual three-phase distribution system, [32] proposed GA to solve solution of replacing existent capacitor banks in [68] to harmonic filters where GA is used to find optimal filter size while minimizing the voltage distortions subject to all implied constraints. Reference [67] describes the application of GA with new coding in which the optimal parameters for the dimension and position of the filters are determined, which is cost-effective and below the standard harmonic distortion level following IEEE 519. Although GA is performed successfully in many different applications, the results of low efficiency and long running time overall degrade the effectiveness of this method. Kahar and Zobaa have recently designed an optimal undamped single-tuned filter using a new method, where the overall results have proven that GA is the least effective with a high computational burden and slow convergence time compared to other methods [14].

With the inspiration concept by Goldberg, Srivinas and Deb suggested a nondominated sorting GA (NSGA) from an extension of GA to optimize multiobjectives problem [69]. The updated version from classic NSGA known as NSGA-II succeeded in optimizing the design of PPF based on three independent objectives [26], [35]. Three predefined configurations of PPF have been proposed, where the user can select the filter-type algorithm before the optimization is completed. This algorithm was used to find Pareto

front, where NSGA shows better convergence and spread of solutions. However, the algorithm is restricted to the uniformity of few problems and requires few modifications to improve efficiency [70].

The first ACO was introduced in 1992 by Marco Dorigo, where the algorithm mimics the biological behavior with artificial ants. The ability of the ants is the way in which they find food where a certain amount of pheromone trails will be leaving on the ground. This pheromone trail acts as a communication, which is preferred by the ants to travel along the path rich with pheromones [71]. However, the simulation based on real ant colonies has increased the interest where the first ant ACO algorithm known as ant system has been proposed in 1996 by Marco, Alberto and Vittorio [72]. Based on the originality of the ant system, the algorithms known as Max–Min Ant System (MMAS) and ant colony system (ACS) have been successfully implemented in [73] and [74], respectively, to improvise variants of the ant system. This system introduces ant algorithm where the major advantages of these artificial ants are some memories where they are not totally blind, which operates on a time-discrete signal. Many applications of ACO with different problems can be found in [75]–[77]. There are some researchers who have combined ACO with another algorithm, such as scatter search [78], beam search [79], and nearest neighbor [80], to improve ACO.

The PSO was introduced in 1995, wherein the initial idea came from Dr. Kennerdy and Dr. Eberhart [81]. The traditional PSO was inspired by having a population or swarming behavior flocks of fish or birds. In PSO, each of the "bird," called as "particle," in the search space is represented by every single potential solution. The particles fly through the search space until the better positions are discovered. Then, it will guide the entire swarm best-known position. The process continues repetitively until an acceptable solution is eventually discovered. Although PSO shares many resemblances with GA, the information-sharing mechanism in PSO is entirely dissimilar.

Additionally, PSO is simpler and more convenient compared to GA without genetic operators such as crossover and mutation. For the past few years, PSO has increased the interest among the researchers involving optimal PPF planning [33], [82]–[85] because of its advantages, which are easy implementation, efficient, and robust when compared to the other heuristic techniques. For the first time, PSO has been applied in [82] to find optimal PPF filter, where the results overall show outstanding performance. In [33], the

reference proved that PSO is capable of obtaining results, which is better than the penalty function method. To solve multiobjective problems, PSO has been combined with another algorithm for using the advantages of both algorithms when planning large-scale passive harmonic filters. However, PSO might be slow to converge. Therefore, Ying Pin has proposed a deterministic method—SQP to be combined with the PSO (SQP-PSO) approach to improve the convergence time, while PSO will help to escape from local optimal tripping to achieve near-optimal solutions [86]. Additionally, Ying Pin has also proposed PSO to be combined with nonlinear time-varying evolution built on neural network [85] and orthogonal arrays [84].

Besides, Passino presented the first BFO in 2002, in which the technique was implemented from the behavior of bacteria [87]. In [48], the author proposed BFO in designing passive filter to define the dimension, harmonic tuning orders, and location of the filters. The aim is to reduce electricity losses and investment costs. The aim is to minimize power loss and investment costs. For a small-scale system, the comparison with GA, PSO, and ant-bee colony shows that BFO has fast convergence in a short computational time and better accuracy compared to other intelligence optimization methods. In [24], further investigation has been carried out in the large-scale system using the simplifies BFO algorithm known as adaptive BFO (ABFO). The study focused on optimization based on three objective functions: the investment costs, the minimization of the power loss, and THD.

In this respect, new nature-inspired optimization approaches, such as BA and CSA, are still being established. In 2010, Yang proposed BA that was based on the behavior of microbats [88]. In many applications, BA proved to be practical [89], [90]. The first design of PPF using BA with added inertia weight into the algorithm was proposed in [51], where the algorithm showed a promising future for solving any optimization problems. In 2016, Alireza introduced CSA to solve the optimization problem of constrained engineering, where the method was nature inspired by the behavior of crows [91]. The crows can recall the appearances, effectively use the tools, and interconnect, storing as well as hiding their foods. Also, the crows can escape their food and take back the food once required. The advantage of CSA with its fast convergence capability and high-level sensitivity has increased the interests of the researchers in solving the engineering problem [39], [91]–[93]. In [39], the first application of CSA has been

successfully implemented in the design shunt PPF based on the reduction of filtering costs with the assurance that electrical hazards are not present in the system.

In 1983, SA was recommended to solve complex nonlinear problems [94]. Simulated annealing is also known as one of the metaheuristic algorithms that inspire the creation of solid crystals in the process of heating and controlled cooling of the material. Authors proposed SA in [53] for optimal planning of PPF based on single optimization minimization of the current of the distribution bus root mean square (rms). On the contrary, the author in [50] solves the problems using SA after constructing four optimal subfunctions: (i) voltage THD, (ii) current THD, (iii) cost of the filter, and (iv) reactive power. SA has the ability to deal with multiobjectives and many constraints problems due to its advantages, which can be avoided by trapping the local optimal solutions. However, this method has no stopping characterization, where they cannot tell if the optimal solution has still been found [95].

2.3 Research Gap

In this thesis, several issues were not covered in the previous literature and were carried out in this research. In addition, this thesis highlights any conflicts in the existing literature and the attempt to study these conflicts in order to improve their performance. The issues and conflicts, as well as contributions developed in this thesis, are presented in the following sections:

2.3.1 Design of PPF

The high-pass filter has good suppression and efficiently dampens the resonance without changing the tuning frequency to a lower harmonic order. In [38]–[41], the installation cost such as the additional features in C-type filters and competitiveness with other traditional shunt PPF filters, especially single-tuned filter, makes it less selective because it is simpler and more convenient to use and maintains the overall simplicity of the PPF concept. Hence, most engineers preferred the single-tuned filter [14], [18], [29]–[37], [19], [21], [23]–[28] which has simple configurations and is cost-effective [47].

- In [14], [28], [33], [96], [97], the researchers ignored the resistive values when they found the optimal parameter of the single-tuned filter. However, this research revealed that the resistor in the single-tuned filter must be considered, and it is essential to evaluate the power losses in the filter into contemplation because it can affect the system performance.
- The author in [22] suggested that the harmonic order should be tuned between 3% and 10% of the harmonic frequency in order to overcome the problems caused by the effects of resonances. While some of the previous literature ignored the effects of resonance in its design [25], [37], [50], an author also determines the positions of the resonance in advance when designing PPF [36]. On the other hand, in this research, the positions of the resonance are set as the constraints and obtained by the optimization process when the optimal parameter of a single-tuned filter is found.

2.4 Summary

Many general recommendations from the relevant existing literature have been included using various methods describing the design of PPF, which includes the design topologies and the considerations of the objectives and constraints involved in order to improve the design of PPF. In summary, several topologies with different characteristics were previously used in many applications, where a single-tuned filter proved to be the most economical approach. A brief review was provided for the optimal planning of PPF, which includes single-objective and multiobjective optimization using various algorithms, such as exhaustive search, deterministic optimization approaches, and heuristic/metaheuristic algorithms. Besides, this chapter presents the research gap in which information from the previous literature covered in this research is missing in this section.

Chapter 3

Background of Power System Harmonics

3.1 Introduction

Power system harmonics is not a new problem in power system, where the phenomena occurred since the 18th and 19th centuries, in which Joseph Fourier and several mathematicians established the basic calculations of harmonics. Alexander in his review mentioned that in the second half of the 19th century, several mathematicians: Cantor, Heine, Riemann, Gibbs, Stokes, Seidel, and Dini, have attracted to Fourier's theory, which led to the discovery of the applications of Fourier series. From the equation of heat conduction in [99], the mathematicians extended the methods to many branches of physics and engineering, such as electricity, elasticity, and fluid mechanics [100]. However, at the end of the 1900s, only certain engineers–mathematicians were able to use the most necessary tool inherited from Fourier, where the tool was proven to be necessary for the expansion of electric power system [98].

In 1916, Steinmetz published a book on harmonics of the power system, in which his main concerns were the third harmonics in transformers and machinery. Besides, Steinmetz originally proposed the blocking third harmonic current using delta connections [101]. Then, the utilities recognized the effects of power system harmonics, where the distorted waveforms were observed in the transmission lines between the 1920s until the early 1930s [100]. However, the effects of harmonics on the

synchronous machine, power capacitor failures, circuit breakers, fuses, electronic equipment, and telephone interference have become the main concerns because of the increasing use of the nonlinear loads in the power electronics application. The research has found that 60% ± 10% of the power factor reduction and 2% increase in the line losses are due to the extensive usage of the nonlinear loads [102]. Besides, the hysteresis in generators, eddy current in the transformers, and core losses in the induction motors have overall led the power quality problems to be vital matters than ever [103]–[105].

Nowadays, electronic devices use silicon-controlled rectifiers (SCRs), diodes, inverters, and other electronic switches to control the power and convert fundamental frequency from AC to DC. Examples of power electronic loads include adjustable speed drives (ASDs), compact fluorescent lamps, air conditioners, and light-emitting diode lamps. The problems and challenges caused by harmonics in the modern system were restricted by Jain and Sing [106].

The problems of power quality problems are commonly caused by sags, harmonics, flickers, imbalances, and transient or steady-state voltage where the problems caused discomfort and economic losses to the consumers and industry [107]. The recent study has investigated the impacts of harmonic current and revealed that power losses in real low-voltage distribution networks increase by more than 20%. For various harmonic levels, the additional power losses are in the range between 4% and 8.5% for the distribution network [108].

In this chapter, the general background of power system harmonics is presented, which includes the definition, source, and identification of harmonics. In this chapter, technologies to eliminate harmonics were explained in order to solve the power quality problem, where the main focus is on the technique when using a single-tuned passive filter.

3.2 Power System Harmonics and Mitigation Techniques

3.2.1 Definition of Power System Harmonics

Harmonics refers to the periodical of a sinusoidal signal increasing its frequency with multiple integers with fundamental frequency [109]. Harmonic distortion can also be described as "wave distortions," where the term can be more easily understood by understanding the simple power system circuit network shown in Figure 3.1 below.

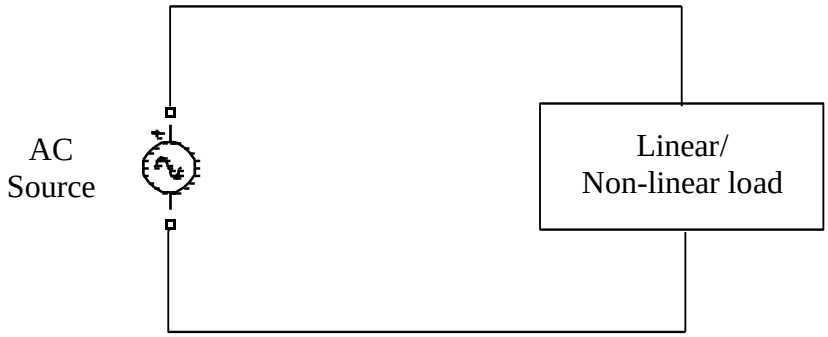

Figure 3.1: AC circuit network

The figure above shows a combination of the AC circuit and an electrical load connecting the source to the linear or nonlinear loads. However, different types of loads produce different outputs of current drawings, which affect the power quality of the power system. Figure 3.2(a) below shows a current or voltage drawn when the source is connected to the linear loads with an ideal sine wave output. However, the linear load, such as a resistor, is generally producing sinusoidal waveforms and creates zero harmonics. From the observation after comparing the waveforms in Figure 3.2, the nonlinear loads inject harmonics that produced distorted sinusoidal supply waveforms where the current drawn by the loads no longer appears to be an ideal sinusoidal wave and could affect other linear devices as well.

Today, the rapid development of the power electronics technology has affected the importance of DC as a power supply, which commonly converts the rectifier bridge from AC to DC power supply [110]. Hence, the uses of nonlinear loads in the power system are significant, especially in switching action and current disruptions.

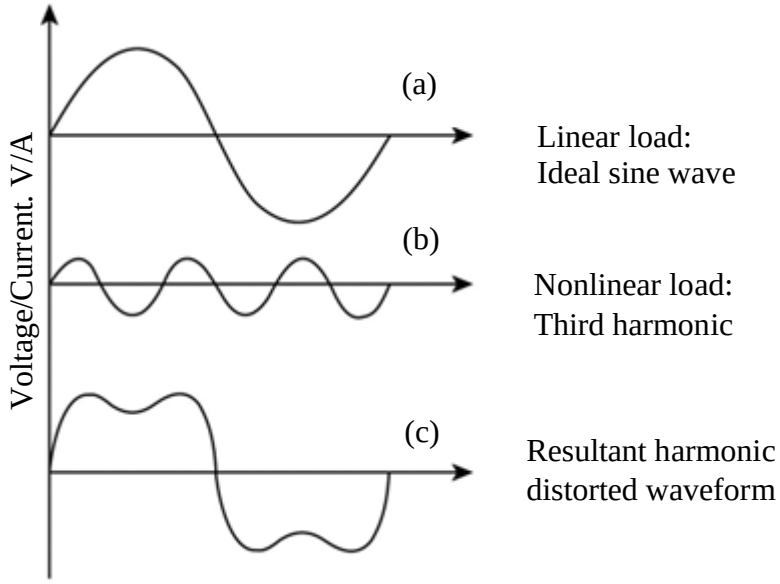

Figure 3.2: Sine waveforms, (a) ideal sine wave, (b) 3rd harmonic wave and (c) distorted waveform

There are a few types of "waveform distortion," where the appropriate term can distinguish between harmonic, interharmonic, and subharmonic components:

- *Harmonic distortion* is a sinusoidal waveform with a frequency f_h that multiplies 50/60 Hz by an integer number. For example, in the 60-Hz electrical power system, the second harmonics is 120 Hz, and the third harmonics is 180 Hz.

- *Interharmonic distortion* is a component in which the harmonics frequencies exist. Based on the International Electrotechnical Commission 61000-2-1, interharmonic distortion can be observed in cases where the nonintegral frequencies between harmonics occur between the two [111]. For example, in the 60-Hz electrical power system, the component with a frequency of 90 Hz is an interharmonic that exists between the first and second harmonics.

- *Subharmonic distortion* is where the value of the frequency is less than 50/60 Hz. For example, in the 60-Hz electrical power system, all the components with a frequency less than 60 Hz are called subharmonic components.

All of the explanations for harmonic, interharmonic, and subharmonic components are summarized as shown in Table 3.1.

Table 3.1: The mathematical descriptions for all type of harmonics

Type of harmonics	Classification	Comment
Harmonics	$f_n = n.f_0$	n is an integer, $n > 0$
Inter-Harmonics	$f_n \neq n.f_0$	n is an integer, $n > 0$
Sub-Harmonics	$0 < f_n < f_0$ or $f_h = n.f_0$	where $0 < n < 1$

In the power system, THD is the most common measure of distortion for harmonics. The voltage and current THDs are calculated as Equations (3.1) and (3.2), as shown below:

$$THD_v = \frac{\sqrt{\sum_{n=2}^{n_{max}} \left(V_{n,rms}^2\right)}}{V_1} = \frac{\sqrt{V_{2,rms}^2 + V_{3,rms}^2 + \cdots + V_{n,rms}^2}}{V_1} \tag{3.1}$$

$$THD_i = \frac{\sqrt{\sum_{n=2}^{n_{max}} \left(I_{n,rms}^2\right)}}{I_1} = \frac{\sqrt{I_{2,rms}^2 + I_{3,rms}^2 + \cdots + I_{n,rms}^2}}{I_1} \tag{3.2}$$

where $V_{n,rms}^2$ and $I_{n,rms}^2$ is the root mean the square (rms) voltage and current at *n*-th harmonics, respectively. The value of *n*th harmonics for both current and voltage is varies from 2 to maximum. Besides, the value of V_1 and I_1 is referred to the rms voltage and current at the fundamental frequency, respectively.

3.2.2 The Sources and Identification of Power System Harmonics

From the beginning of the first generators, harmonics problems existed. However, the effects of the harmonic component are too small and considered insignificant until the existence of nonlinear loads. Prof. Victor Gosbell pointed out that harmonic distortion did not exist until the 1960s until customer loads started using electronic power supplies [112]. By explaining the waveform from household and factory applications, Gosbell has proven that harmonic distortion occurs because of the connections between customers with the electric power system [112].

The harmonics are usually produced by low-distortion-level generation, transmission, and distribution equipment, whereas harmonics are produced by industrial and domestic loads at a high distortion level. Generally, nonlinear devices are known as power system

harmonic sources and can be categorized into two types of power electronic devices and saturable magnetic devices [3].

A) Harmonic Created by Saturable Magnetic Devices

Transformers, power generators, and motors are referred to as saturable magnetic devices that have been widely used in the power system. The harmonics produced by these types of devices are mainly due to the iron saturation. The saturable magnetic devices have been designed to operate slightly above the knee of the curve for commercial purposes in the iron core saturation curve. However, these have led to highly distorted magnetizing currents in third harmonic, causing unbalanced operation [113].

- *Transformer* - Transformer is one of the familiar sources of harmonics generally caused by the nonlinearity of iron saturation in the magnetic circuit of the windings [114]. Ohm's law states that voltages could be generated at the terminal for any currents that flow within the resistance or impedance. Therefore, Ohm's law also applies in transformers because transformers also have impedance, where harmonic current flows and leads to harmonics voltage. The large current that flows through the windings in the secondary terminals increases the harmonic voltages generated, thus creating voltage distortions. Therefore, the outcome of the harmonic to the transformer can be determined from the design of the transformer and harmonic current.

- *Power Generator* - Power generator is one of the primary sources of harmonic by comparing the utility power supplies. The problem is similar to the transformer, but the source of harmonics is very high because of the impedance of power generators, which is usually three to four times higher than the utility transformer. The significant impact of voltage and current distortions in power generator is due to the losses of iron and copper. However, unlike the transformer, the core iron is not the only source of harmonic in the generator, in which the generator produces a fifth harmonics nonsinusoidal flux distribution around the air gaps. The harmonics in the magnetic circuit can be minimized by changing the configurations of the stator windings in the generator. Besides, the selected pitch factor can also reduce and eliminate specific harmonics.

- *Motor* - In electric motor applications, there is an increasing use of variable frequency drive (VFD) connected to the motor. The sources of current and voltage from VFD that are used to power the motor have high harmonic frequency components. In the winding, there are also I^2R losses, which vary as the square of rms current and the actual losses are slightly higher because of the skin effect. The interaction between positive and negative sequence harmonics results in torsional oscillations of the motor shaft causing vibrations of the shaft. Meanwhile, zero-sequence harmonics only causes additional losses but does not ripen any usable torque in the motor. Therefore, it is essential to perform harmonic analyses and to regulate the levels of harmonic distortions in the large VFD motor installations and to evaluate their effect in the motor.

B) Harmonic Created by Power Electronic Devices

Several devices use power electronics devices, such as SCRs, diodes, and thyristors, where ASD and uninterruptable power supplies are commonly used. Another application of the power electronics device that has been used widely is static synchronous compensator and state VAR compensator, which is usually applied in the transmission system. The percentage load of all power electronic devices in the industrial power system has increased.

- *Static Synchronous Compensator/Condenser (STATCOM or STATCON)* – STATCOM is part of the flexible AC transmission system (FACTS), which is used to improve the voltage stability and increase the capability of the power transfer for the AC transmission of electrical energy on power grids [115], [116]. STATCOM regulates the voltage at its terminal by controlling the amount of reactive power to be absorbed from or injected into the power system. The inductive and capacitive components in its primary circuit may cause resonance under certain conditions, such as distorted line voltage [117]. Many STATCOM controllers have been industrialized and commercialized based on voltage source converter technologies with a combination of self-commutating solid-state turn-off devices such as gate turn-off thyristors, insulated gate bipolar transistors, or insulated gate commutated transistors under pulse width modulation switching principle [118]. In practice, the fundamental switching-

based 48-pulse converter topology is widely used in high-power-rating STATCOMs because of its excellent operational and harmonics performance. In contrast, low pulse-order compensators such as 12-, 18-, or 24-pulse configurations under the square-wave mode of operation are not adopted because of the high impact of voltage harmonics, creating unacceptable harmonic distortion.

- *Static VAR Compensator (SVC)* – SVC is also a member of FACTS, which is used to regulate grid voltage and control reactive power flow in the transmission network. The device acts in a similar way as STATCOM where SVC generates reactive power when the system voltage is low, whereas it absorbs reactive power when the system voltage is high [119], [120]. However, both STATCOM and SVC have a different way to operate. SVC operates as a dynamically controllable reactance connected in parallel compared to STATCOM, which works as a controllable voltage source. Negative phase sequence voltages within a three-phase power system are generally caused by unbalanced loads. Power utilities are generally required to limit the amount of negative phase sequence voltage on the grid because of the increased heating it causes in three-phase machines. SVC has been widely used to address unbalanced voltage problems in distribution, subtransmission, and transmission networks. Nevertheless, the SVC can introduce harmonic currents into the power system because of the power electronic switching of static reactive devices [121]..

- *Adjustable Speed Drive (ASD)* - ASD is also known as adjustable frequency drives, where the harmonic distortion is caused by the nature of front-end rectifier design. Today, the six-pulse rectifier is the typical standard power circuit configuration with diode bridge rectifiers for most pulse-width–modulated variable-speed devices. However, some of the manufacturers used 12-pulse rectifiers in large-horsepower configurations because this type of rectifier eliminates the fifth and seventh harmonics and extends the primary characteristics up to the 11th and 13th harmonics. Besides, the 12-pulse rectifier provides a smoother current waveform compared to the six-pulse rectifier.

- *Uninterruptible Power Supplies (UPS)* - UPS is also referred to as an uninterruptible power source or battery backup in which UPS supplies the

system from any disturbance in the primary power source. Besides, UPS considers fitting "in-line" between the main power supply and the loads in which UPS supplies energy stored in batteries to provide instant protection against interruptions input power. Therefore, UPS should also protect the main power supply by protecting the charges against harmonic charges generated by the loads. It is commonly known that UPS generates harmonic pollution by its design because of the rectifier connected to the main supply to convert the battery and inverter from AC to DC. In order to reduce harmonics, the passive filter can be installed next to the UPS. However, this can increase the cost of capital, wiring, and installation.

3.2.3 The Recommended Harmonic Standard

In the power system, the aims are to set goals for voltage and current waveform to keep the distortion below the standard limit as low as possible. Refer to Table 3.2 below, which shows the limit that applies following IEEE Std. 519-2014 [122].

Table 3.2: The recommended limit based on IEEE Std. 519-2014

Bus voltage at PCC, kV	Individual harmonics (%)	Total harmonic distortion, THD_v (%)
$V \leq 1$	3.0	8.0
$1 < V \leq 69$	3.0	5.0
$69 < V \leq 161$	1.5	2.5
$161 < V$	1.0	1.5^a

Based on the table above, the limit only applies to the PCC, and the characteristics of the system should be modified if the distortion level is exceeding the maximum limitations.

3.2.4 The Technologies for Harmonics Elimination

In the power system, harmonics can cause excessive heat in the equipment connected to the source of the harmonics if they affect the power factor-deficient and less-efficient system. Most harmonics techniques performances typically depend on the conditions of the system. Nonetheless, others require extensive system investigation to prevent from capacitor failure and resonance problems, where resonance can interrupt the operation

of the power system. Therefore, it is crucial and essential to controlling of harmonics voltages and currents. The selection of the best harmonic mitigation techniques can be a very complicated process, as the number of techniques available to eliminate harmonics that include passive and active methods is increasing. The most common approaches include phase multiplication [123], [124], linear reactors [125]–[127], passive harmonic filters [23], [37], [40], [128], phase-shifting transformers [129]–[131], isolation transformers [132], [133], k-factor transformer [134], [135], multi-pulse converter [136], and active harmonic filter [137]–[140].

A) Line Reactor

The line reactor is a series device that is also known as "choke" or "inductor," where it is the most cost-effective and straightforward technique classified by voltage, impedance, and current. The impedance in the line reactor acts as a current-limiting device in which the magnetic form from the coil of the inductor limits the current flow through it, thus reducing harmonics and protecting the drive from power surge or transients [141]. The installation of a series reactor for current limitation and control of power load flow has continuously increased, especially in a high-voltage-power system [142], [143]. The current-limiting series reactor can improve the transient recovery voltage for high-voltage transmission lines [144]. Besides, the reactors can also be found in series with nonlinear loads, such as arc furnace and VFD for harmonic attenuation and protection to the drive or motor itself [125], [126], [145]. Conversely, this technique is less preferred, because it is suitable only for small drives and can handle only full load current..

B) Phase Multiplication

Phase multiplication, which is also called phase cancellation, refers to the conversion of lower pulse device to higher pulse devices. By assuming three-phase, ideal converters with equal firing angles and perfect commutation angles, the harmonic order is given by the formula:

$$h = pk \pm 1$$

with p and k as the converter number of pulses and an integer, respectively.

Therefore, the quantities of the pulse increase the harmonic cancellation and eliminate several orders. This is because they feed the load because of the usual elimination of

harmonics within the converter connection circuits and the losses in the lines. The presence of positive and negative harmonics of the orders in the converter cancels one another.

C) Passive Harmonic Filter

The passive filter is a grouping of resistors, capacitors, and inductors in the network without external power supply and any active components. The classifications of passive filters are based on topologies, such as tuned filters and damped filters. Besides, it can also be categorized as series, shunt, and hybrid from its connection [146].

The tuned shunt filter acts as a low pass, whereas damped filter acts as a high pass. However, the connected tuned or damped filter acts as a low block or a high block. It is usually more convenient to use the shunt filter compared to the passive filter series. The shunt filter can improve the voltage profile and provide the reactive power. Besides, the shunt filter carries only part of the load current compared to the full load current series filter [147].

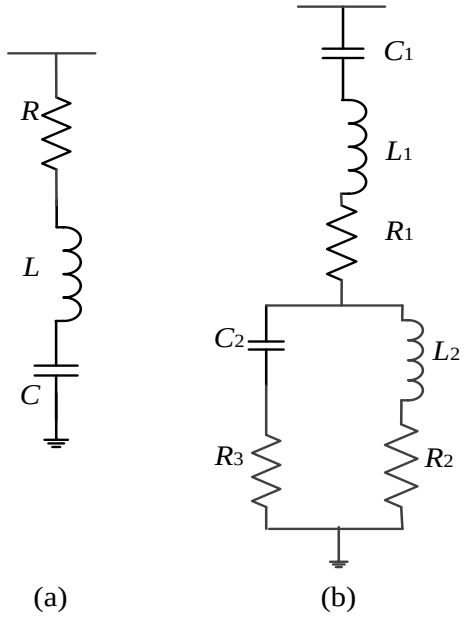

Figure 3.3: Typical shunt tuned filter, (a) single tuned and (b) double tuned.

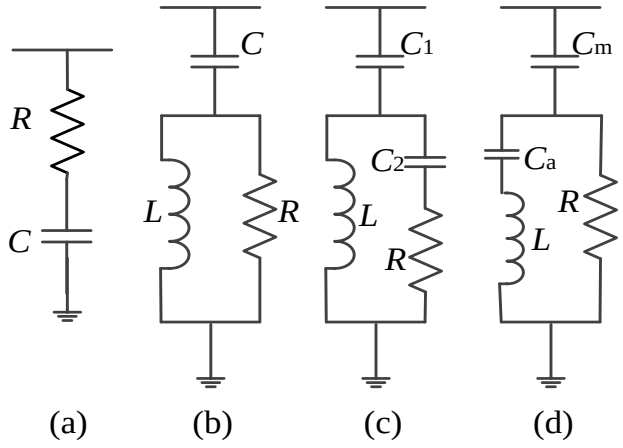

Figure 3.4: Typical shunt high pass filter, (a) 1st order, (b) 2nd order, (c) 3rd order and (d) c-type.

The typical type of passive tuned filter includes single-tuned [14], [28], [34] and double-tuned filter as shown in Figure 3.3 above. For the typical shunt, high-pass filter for the first order can be referred in Figure 3.4(a), second-order in Figure 3.4(b) [148], [149], third order [39] in Figure 3.4(c), and C-type filter [17], [41] in Figure 3.4(d)).

D) Phase-shifting Transformer

Phase-shifting transformer is also known as harmonic cancellation transformer, where this technique used built-in electromagnetic technology in the transformer to remove harmonic order from the 3rd until the 21st. Several countries have installed or are interested in installing the phase-shifting transformer [150]–[152]. Although the technology is considered old, the method that is basic and cost-effective for harmonics elimination has gained many interests [153]–[157].

In the first and secondary windings, the transformer can be connected to any arrangement of delta and wye for harmonics cancellation. For example, the connection of delta-wye transformer traps all the triple harmonics in the delta. [131]. The additional special winding transformer is the polygon and zigzag, and extended delta windings can be used to cancel other harmonics on balanced loads.

E) Isolation Transformer

This method is based on two isolated Faraday screen or shield principles [158]. The transformer is used to separate two circuits that are connected to the device and the source of input. Refer to Figure 3.5, where the shield used between primary and

secondary is made of pure copper and must be connected to earth [159]. For power quality purposes, the ratio of the transformer is unity, where the typical configurations of the isolation transformer are delta primary and wye secondary generally. Also, the isolation transformer also allows the transmission of the AC signal while blocking the transmission of the DC signal.

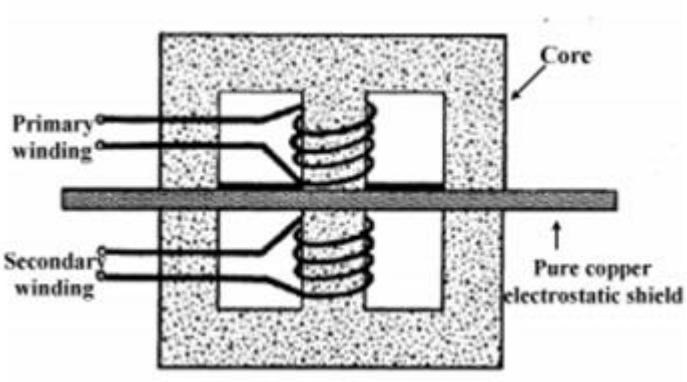

Figure 3.5: Isolation transformer [159].

Because of the capacitive coupling, the shield created a small impedance between each winding. This impedance acts as a path of reducing noise, transients, and zero sequence currents and avoiding any common disturbances caused by the acquisition and damage of sensitive electronic equipment. [159], [160].

F) K-factor Transformer

The harmonics produced due to nonlinear loads can result in high-temperature effects when the harmonics are entering the transformer where the core saturates and causes failure [161]. Therefore, the value of K-factor transformers is designed to ensure that the transformer can stand with the harmonics load currents and operate within a safe temperature range [162].

The K-factor can be defined based on the equation below [163].

$$K = \sum_{h=1}^{\infty} \left(I_{h(\mathrm{pu})}\right)^2 h^2 \tag{3.3}$$

where the harmonic current, I_h is expressed in per unit.

Besides, the transformer also incorporates the eddy current losses, where the method of derating of the transformer can be found in [164]. The rating of load K-factor depends on the harmonic levels as shown below [165].

Harmonic Level	**Load K-rating**
THD < 5%	K-1
THD < 35%	K-4
THD < 50%	K-7
THD < 75%	K-13
THD < 100%	K-20

G) Active Power Filter

Active power filter such as an amplifier and reactive elements, usually op-amps, improves power factor and stabilize the operation. An amplifier expands the performance and predictability of active filter, where it can also prevent the impedance of the load from disturbing the characteristic of the filter. In order to neutralize the distorted harmonic current, the opposite current phase is injected [166]. The active filter operates based on two parallel principles and series in which the filter acts as the current source and voltage source. Refer to Figures 3.6 and 3.7 for system configuration for shunt and series APF.

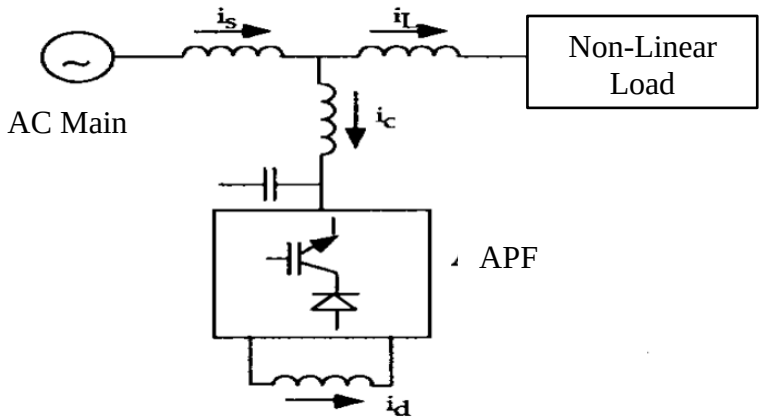

Figure 3.6: The system configuration of shunt APF [167].

Active power filter is characterized into few classifications, which are two-, three-, and four-wire APFs. Different configurations of two-wire APFs or single phase are available to fulfill the requirements of single-phase nonlinear loads, such as oven, air conditioners, and many more [168]–[174].

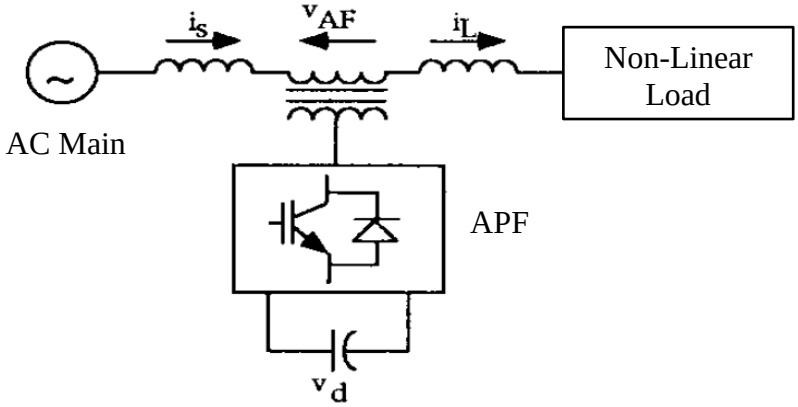

Figure 3.7: The system configuration of series APF [167].

For three-wire APFs, few articles and publications have been published with a typical configuration of the active shunt and series APFs along with a combination of passive filters with the active shunt and series APF. [175]–[181]. In addition, the system with four-wire APFs has been used with the system that has an excessive current neutral problem, mainly due to unbalanced nonlinear loads. Besides, the system with four-wire APFs was used with the system that has an excessive neutral current problem, mainly due to unbalanced nonlinear loads [182]–[185].

3.3 Single-tuned Passive Filter

The filter also known as series or notch filter is designed based on three non-intricate quantities. The filter includes a series of RLC configuration, which is tuned to resonate single harmonic frequency. Refer to Figure 3.8 below the filter schematic diagram, $R - X$ plot and its typical frequency response [14].

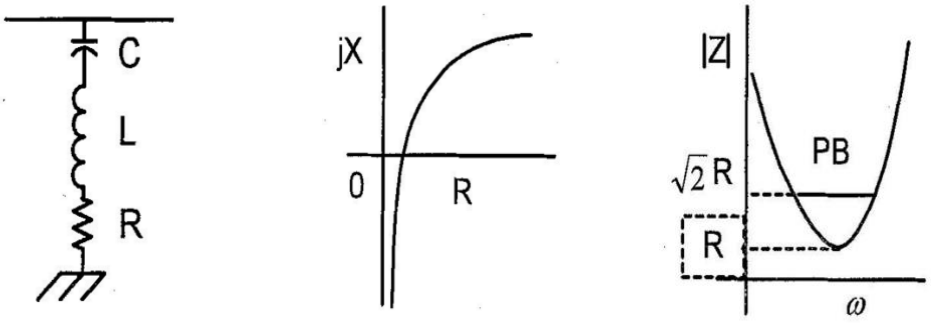

(a) (b) (c)

Figure 3.8: Single tuned (a) arrangement, (b) $R - X$ plot and (c) a typical characteristics of harmonic impedance

3.3.1 Design Equations

The total impedance can be formulated as

$$Z = R + j(X_L - X_C) \tag{3.3}$$

$$Z = R + j\left(\omega L - \frac{1}{\omega C}\right) \tag{3.4}$$

where the frequency in radians, $\omega = 2\pi f$. Note that R is ignored for undamped case.

An ideal filter is when the values of the capacitor and reactor have equal reactance at the tuned harmonic frequency, f_n [186].

$$f_n = h * f_0 = \frac{1}{2\pi\sqrt{LC}} \tag{3.5}$$

where the f_n = filter resonant frequency,f_0= fundamental frequency (50/60Hz), C = filter capacitance, and L = filter inductance. Then, h is tuning order and given as

$$h = \frac{f_n}{f_0} = \sqrt{\frac{X_c}{X_L}} \tag{3.6}$$

where X_C and X_L are the values of the capacitive and inductive reactances, respectively.

The resistance, R, in the Equation (3.3) is generally called "damping," which is referred as an intrinsic resistance to inductance. It usually causes small loss power in the filter, which cannot be merely ignored and must be taken into consideration when designing this type of filter. In contrast, the ohmic losses in the capacitor are usually insignificant [146], [187].

3.3.2 Design performance

The quality factor, *QF*, given in the Equation (3.7) defines the performance of the filter, which is related to energy loss in the filter.

$$QF = \frac{1}{R}\sqrt{\frac{L}{C}} \tag{3.7}$$

The definition of filter passband, *PB*, can be explained based on Figure 3.4(c) where the frequencies are bounded at which the value of reactance of the filter is equal to the resistance.

$$|Z| = \sqrt{2}R \tag{3.8}$$

From Figure 3.4(c), the graph shows an example impedance angle $= 45^{o}$ equal to the magnitude $\sqrt{2}R$. Then, the relationship between the quality factor and passband can be expressed as follows

$$PB = \frac{f_n}{QF} \tag{3.9}$$

The following facts regarding the *QF* are of importance:

- *QF* is infinite when a tuned circuit is said to be ideal (ignore R). However, there is always a particular *R* in the circuit that reduces the quality.
- The value of *QF* is irregularly measured regarding filtering action.
- *QF* can determine the sharpness of the resonance. At a specified tuned frequency, *QF* reveals the capability of the filter to provide a steady reduction of harmonic currents.
- At a higher value of *QF*, the resonant peak becomes sharper and less damping. This results in high-frequency selectivity and better harmonic attenuation. The passband is also reduced with higher *QF*. The impact of resistance and *QF* on the impedance and frequency response is shown in Figure 3.9 below.
- There are standard restrictions of QF where the typical value is between 20 and 100. However, the responses are virtually indistinguishable, except for the magnitude of the peak [42].
- The damping effect on the circuit bandwidth shown in Figure 3.9 can only be obtained from the value of the resistor in the parallel resonant circuit.

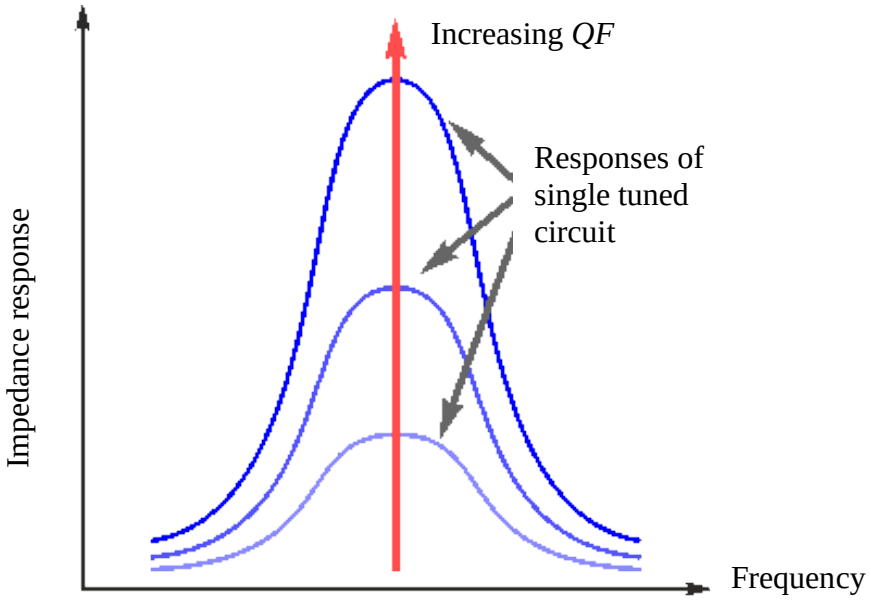

Figure 3.9: Single tuned circuit response with a different value of *QF*.

3.3.3 Design concerns

In the design of a single-tuned filter, the main drawback is the presence of resonances. The spike of current and voltage caused by series and parallel resonance, respectively, will result in damage to the circuit. Usually, the problem related to both resonances usually is caused by filter detuning, where the common operations are due to the capacitor fuse blowing, capacitance and inductance manufacturing tolerance, system variants, and temperature.

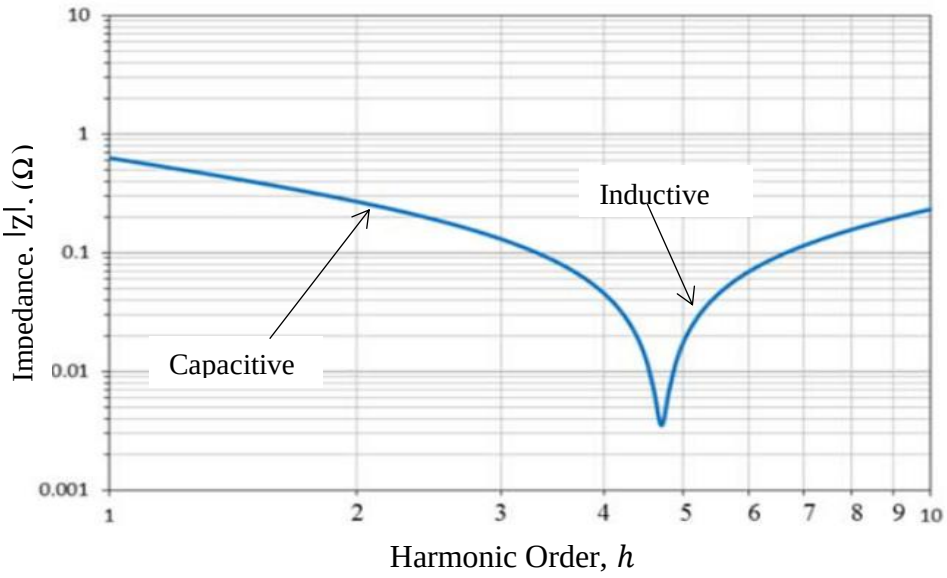

Figure 3.10: Impedance of the 5-the tuned filter [25].

Therefore, it is beneficial for the value in Equation (3.5) for the filter to be tuned 3% to 10% from the desired harmonic frequency in order to avoid both resonances [42]. Refer to Figure 3.10 above where the tuned frequency is slightly lower from the fifth harmonic order, where h = 4.7..

3.4 Summary

This chapter introduces the general background of power system harmonics. Then, the background study of the harmonics is also presented in this chapter, which includes the identifications of the problems found in the power system. This chapter also includes several typical nonlinear devices and several techniques for harmonics eliminations, while detailed explanation in this chapter focuses only on single-tuned filter.

Chapter 4

Mixed Integer Distributed Ant Colony Optimization

4.1 Introduction

This technique is one of the evolutionary computation techniques created from the extent of ACO metaheuristics [188]. Ant colony optimization was motivated to reflect the natural behavior and function of ants [71], [72], [189]. However, there are many additions have been added from original ACO for escalation of the competencies of the ACO algorithm in MIDACO.

In MIDACO, the innovative concept of general penalty method known as the Oracle penalty method is used to enhance the constraint handling, convergence, and general robustness of the algorithm. This technique subject to a single parameter known as Omega (Ω) directly linked to the objective function, which meant to be set near or slightly above the optimal solution [190].

In this chapter, a description of the proposed technique that was used during the thesis and the rationale behind the choice are presented. Section 4.2 explains some background of ACO and the additions of the algorithm added in MIDACO. Section 4.3 defines the mathematical background of this proposed method, whereas Section 4.4 is specifically about multiobjective optimization in MIDACO. In Section 4.5, the parameters selection

is clarified, while lastly, the advantages and disadvantages of MIDACO are highlighted in Section 4.6 of this chapter.

A relatively new problem-solving technique using SI was motivated by the behavior of insects and animals. Specifically, ants have inspired some methods and techniques in which the most effective optimization for the general purpose technique is when simulated using ACO.

4.2 Ant Colony Optimization (ACO)

A relatively new problem-solving technique using SI was motivated by the behavior of insects and animals. Specifically, ants have inspired some methods and techniques in which the most effective optimization for the general purpose technique is when simulated using ACO.

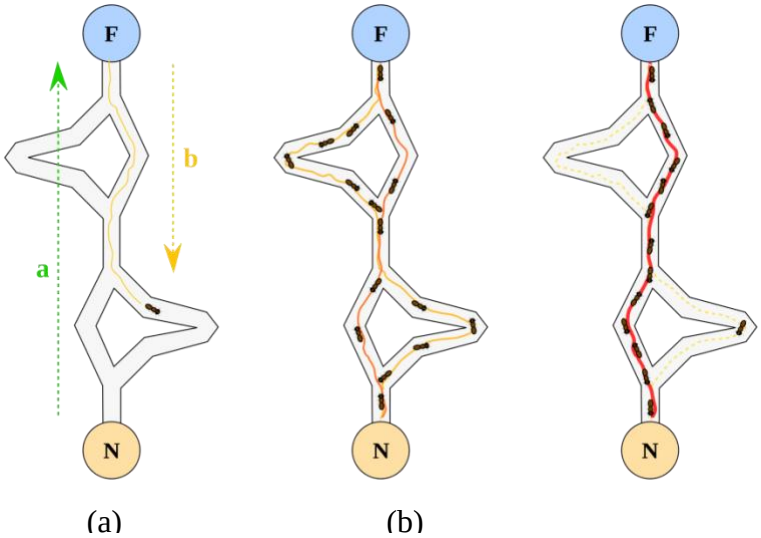

Figure 4.1: The biological behavior of ant, (a) the ants searching food from the nest; (b) ants track the path; (c) ants discover and choose the shortest trail [191].

In ACO, the biological ants start to explore randomly at the area around their nest to search for food. After locating the food source, the ants leave chemical pheromone on the ground while going back to their nest, in order to mark the trail path. This pheromone trail acts as a means of communication that attracts other ants to follow the path to search for the food. Subsequently, the trail paths start to disappear. Therefore, the ants will be attracted to other updated tracks with higher-concentration and fresh, pheromone. Finally, the ant colony will discover a concise way between the nest and

the food source with on-going time [71], [72], [189]. Refer to Figure 4.1, which shows the behavior of ants while finding the shortest path through the pheromone trail when searching for food [191]. This characteristic of ants is to solve combinatorial optimization problems by the artificial ant colonies [192].

In the ACO algorithms, the optimization problem needs to be converted into the problem of finding the shortest path on a weighted graph. Each ant is going from one path to the other paths to figure the solution in which the ant is restricted to visit the track that has been visited earlier as illustrated in Figure 4.2.

The ant colony is motivated to find the best solution in the shortest path. For every variable path, called a pheromone, the chance of an ant to select the route can be determined using the following basic ant system equation [72]:

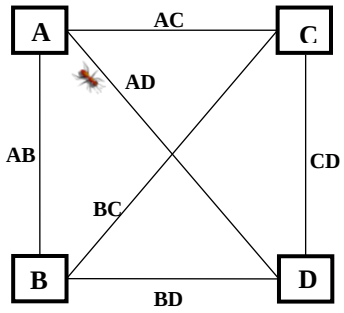

Figure 4.2: The graphical illustrations for the ant movement

The ant colony is motivated to find the best solution in the shortest path. For every variable path called as a pheromone, the chance of ant to select the route can be determined using the following basic ant system equation [72]:

$$p_j = \frac{\tau(i,j)^{\alpha}\eta(i,j)^{\beta}}{\sum_{hO\epsilon j}\tau(i,hO)^{\alpha}\eta(i,hO)^{\beta}} \quad (4.1)$$

where p_j represents the chance of ants visiting node *j*, $\tau(i,j)$, and □(*i*, *j*) is the pheromone level and visibility factor from node *i* to node *j*, respectively. The unvisited node is given by parameter hO, whereas α and β represent weighing parameters, the positive values that determine the relationship between pheromone information and heuristic information.

For the next path, the ants select the route according to a stochastic mechanism, whereby at each step of resolution construction influences the pheromone. Once all ants have

built a complete path and removed all loops, each of the ants will retrace its route to the source node and deposit the pheromones to each of the corresponding paths. Then, each of the iterations is allowed to evaporate before being reinforced from the newly constructed paths of pheromone in order to force the ants to explore more and avoid new convergence [193], [194].

$$\tau(i,j) = (1-\rho).\tau(i,j) + \sum_{k=1}^{m} \Delta\tau_k(i,j) \tag{4.2}$$

$$\Delta\tau_k(i,j) = \begin{Bmatrix} \frac{Q}{F_L} & \text{if ant } k \text{ uses curve } (i,j) \text{ in its tour} \\ 0 & \text{otherwise} \end{Bmatrix} \tag{4.3}$$

where ρ represents the evaporation rate while on the edge (*i, j)* laid by ant *k*, the amount of pheromone is given as $\Delta\tau_k$ for the number of ants *m*, *Q* is value the of constant, and F_L is the distance of the path.

Then, the steps algorithm for ACO metaheuristic is described as follows:

Step 1 Initialize input parameters
Set pheromone path
Step 2 Iteration
Reiteration for individual ant, *k*
Build ant solutions
Run a local search (optional)
Pheromones intensification and evaporation
Until termination conditions

Generally, the pheromone will be updated based on the good solution found earlier. There is a different way of updating pheromone in different ACO algorithm, for example, in ACS [74] and MMAS [73].

4.3 The Mathematical Background of MIDACO

4.3.1 The ACO Framework

In this thesis, the ACO framework considered is mainly based on the extended ACO for continuous domain proposed by Socha and Dorigo [195] and was extended to mixed-integer search domain. The biological visualization of ants choosing their way through

a graph-like search domain does not hold any longer for these problems, as these belong to a completely different class. However, Socha proved that there is no significant conceptual change for the extension of the original ACO metaheuristic to a continuous domain.

In this methodology, there are some standard well-known fundamental definitions to clearly define ACO metaheuristic for mixed-integer nonlinear programming, where the ACO algorithm requires stochastic samples, which correspond to the probability density function. The difference of this method is ACO, which works by the incremental construction of solutions regarding a probabilistic choice unlike original ACO, which requires a pheromone table. For the mixed-integer search domains, there are two types of probability density function (PDF) considered known as a continuous and discrete domain. The general equations are given in Equations (4.4) and (4.5) below. .

A continuous Probability Density Function (cPDF) is when function P: $\mathbb{R} \rightarrow \mathbb{R}_0^+$ with

$$\int_{-\infty}^{\infty} P(x)dx = 1 \tag{4.4}$$

A discrete Probability Density Function (dPDF) is when function Q: $\mathbb{Z} \rightarrow \mathbb{R}_0^+$ with

$$\sum_{d=-\infty}^{\infty} Q(d) = 1 \tag{4.5}$$

In the optimization problem, the ants that act as individual agents in ACO metaheuristics will explore the search areas. The fitness of the individuals is relating directly to the objective function where the individual belongs to a different generation. For a constrained problem, the fitness of the individuals is related directly to the penalty function where the problem will be transformed into an unconstrained problem.

The fittest individuals are chosen after each generation and kept in solution archive, which is stochastically used for the next generation. For this way, the algorithm aims to improvise the fitness of the individuals. Based on the information provided by the solution archive, a general evolutionary operator, ξ is responsible for the creation of a generation of individuals. A function ξ is given as:

$$\xi = (\mathbb{R}^{n_{con}} \times \mathbb{Z}^{n_{int}})^K \rightarrow (\mathbb{R}^{n_{con}} \times \mathbb{Z}^{n_{int}})^v \tag{4.6}$$

where the evolutionary operator creates *v* individuals based on the *K* individuals of solution archive *SA*..

$$SA = \{(x,y)^1, (x,y)^2, \dots, (x,y)^K\} \tag{4.7}$$

The size *K* and *v* are independent parameters and normally assumed that the size of *K* is less than the size of *v* of the generated individuals..

An extension to the ACO metaheuristics was implemented in MIDACO for integer variables, where the algorithm was based on stochastic Gauss approximation technique [196]. Fast sampling time and easy implementation are some strong advantages of this function [197]. On the contrary, a single Gaussian function is only able to focus on one mean and therefore not able to describe situations where two or more disjoint areas of the search domain are promising. To overcome this disadvantage by still keeping track of the benefits of a Gaussian function, a PDFs $G^i(x)$ consisting of a weighted sum of several one-dimensional Gaussian functions $g_l^i(x)$ is considered. To generate ants or individuals, the algorithmic search process given by Gaussian PDFs, $G^i(x)$ is defined as Equation (4.8) below..

$$G^i(x) = \sum_{k=1}^{K} w_k^i . g_k^i(x) = \sum_{k=1}^{K} w_k^i \frac{1}{\sigma^i \sqrt{2\pi}} e^{\frac{-\left(x-\mu_k^i\right)^2}{2\sigma^{i2}}} \tag{4.8}$$

Where:

$w_k^i =$ weights within G^i for every dimension *i* where $i = 1, \dots, n$

σ^i and $\mu_k^i =$ Standard deviations and means for corresponding G^i for every dimension *i*

$K =$ Size of the solution archive (*SA*)

$k =$ *k*-th kernel number of individual G^i

From Equation (4.8), the result of Gauss PDF G^i and individual Gaussian g_k^i applied in one of the dimensions *i* can be presented as illustrated in Figure 4.3(a), where g_k^i presented in orange line is used to generate G^i thick blue for continuous domain.

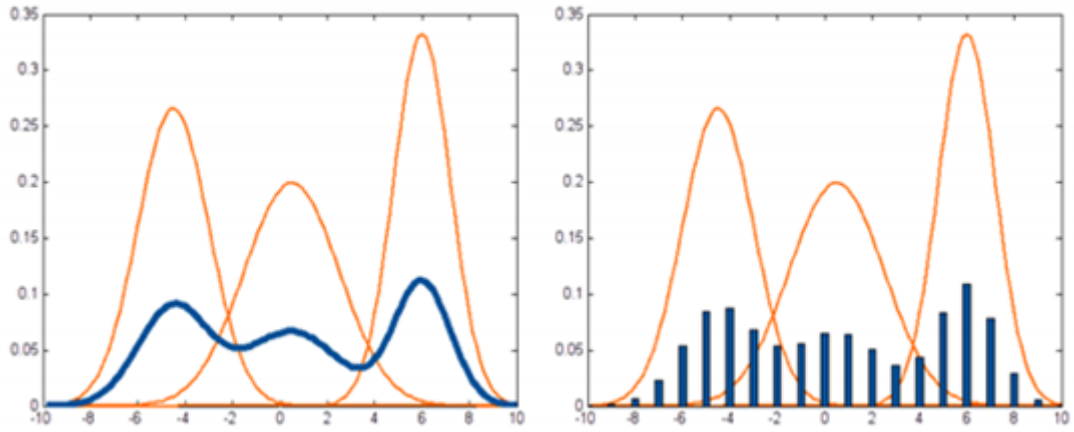

(a) (b)

Figure 4.3: Three individual kernels Gauss PDF, (a) continuous domain, (b) integer domain [188].

For the case of integer domain, a discretized version of multikernel Gauss probability density accumulating around an integer d in the interval $[d-\frac{1}{2}, d+\frac{1}{2}]$ is applied. Probability density functions known as cPDF and dPDF given in Equations (4.4) and (4.5) can be described as Equation (4.9) below:

$$P^i(x) = G^i(x) \qquad (i = 1, \dots, n_{con})$$
$$Q^j(d) = \int_{d-\frac{1}{2}}^{d+\frac{1}{2}} G^{n_{con}+j}(x)dx \quad (j = 1, \dots, n_{int}) \tag{4.9}$$

where $Q^j(d)$ is a discretized version of G^i around integer d between $(d + 0.5)$ and $(d - 0.5)$, which is illustrated as in Figure 4.3(b).

In this thesis, the research considered continuous search domain where $P^i(x)$ given in Equation (4.9) is determined by the triplet parameters $(w_k^i, \sigma_k^i, \mu_k^i)$, which also referred to pheromones. In ACO metaheuristics, the pheromones play a significant role because the process of pheromones is directly connected to the procedure of the updated solution in solution archive (*SA*). One of the triplet parameters, which is the weight w_k^i for the individual Gaussian function designating the importance of ants can be defined as:

$$w_k^i = \frac{(K-k)+1}{\sum_{k=1}^{K} k} \tag{4.10}$$

given that the total of all weights are equal to one, $\sum_{k=1}^{K} w_k^i = 1$.

The solution of the first kernel is more preferred compared to the last kernel. Therefore, starting with s_1 is the current solution found that is the most significant, and ending with s_k is the lowest interest that is saved in *SA.* For every new ant, solution is produced and evaluated; the attraction (penalty function value) is compared with the best solution found in *SA.*

The standard deviations σ_k^i, which is defined from a variety of solutions saved in *SA*, can be calculated from Equation (4.11) as described below:

$$\sigma_k^i = \frac{distance_{max}(i) - distance_{min}(i)}{\#generation} \tag{4.11}$$

where $distance_{max}(i) = \max\{x_i^p - x_i^q\}$ and $distance_{min}(i) = \min\{x_i^p - x_i^q\}$ are maximal and minimal distance between individual dimension *i* of the ants $x^{k=1,\dots,K}$ stored in *SA*, given that the value of *p,q*=1,…,*k* and $p \neq q$ for $i = 1, \dots n_{con}$.

The μ_k^i expresses the means of individual Gaussian g_k^i, which can be easily calculated using Equation (4.12) below.

$$\mu_k^i = x_i^k \tag{4.12}$$

μ_k^i is given directly by one component (the ants $x^{k=1,\dots,K}$) saved in the solution archive in respect to their dimension $i = 1, \dots n_{con}$.

From the three individual parameters given in Equation (4.10) until (4.12), the steps of a new ant can be described as below [195]:

Step 1	μ_k^i is chosen where the selection of means corresponds to w_k^i. This means that μ_1^i has a higher probability to be chosen compared to μ_k^i.
Step 2	Then, σ_k^i generates a random number for sampling μ_k^i.
Step 3	Repeat Steps 1 and 2. for *i* = 1,…,*n* x_{new}^k(new ant) is produced
Step 4	Steps 1 to 3 are repeated for any ants (number of ants per generation)
Step 5	Evaluate solutions (objective function value and constraint evaluations) Go to Step 1 again if the outcomes are not satisfied.

In this method, the algorithm proposed the modifications to the σ_k^i, which is different from Socha, wherein this method allows the algorithm to handle the mixed-integer search domain as shown in Equation (4.13) below.

$$\sigma_k^i = max\left\{\frac{distance_{max}(i) - distance_{min}(i)}{\#G}, \frac{1}{\#G}, \frac{\left(1 - \frac{1}{\sqrt{n_{int}}}\right)}{2}\right\} \qquad (4.13)$$

where $G = generation.$ The maximal and minimal distances are calculated using $distance_{max}(i) = \max\{y_p^{i-n_{con}} - y_q^{i-n_{con}}\}$ and $distance_{min}(i) = \min\{y_p^{i-n_{con}} - y_q^{i-n_{con}}\}$ between individual components s_k^i stored in *SA*, given that the value of p,q=1,…,k and $p \neq q$, where $i = n_{con} + 1, \dots n_{con} + n_{int}$.

By introducing fixed lower bound $\frac{\left(1-\frac{1}{\sqrt{n_{int}}}\right)}{2}$ for the deviation of integer variables, n_{int} enables the ACO metaheuristic to handle integer and continuous variable in the same framework, while the middle term $\frac{1}{\#G}$ in Equation (4.13) ensures convergence of the deviation that is not too fast.

From the above explanations of the equation to describe multikernel PDF$G^i(x)$, the evolutionary operator given in Equation (4.6) can be applied to the solution archive *SA* to create the next-generation G^{i+1} of *v* individuals $\{(\tilde{x})^1, (\tilde{x})^2, \dots, (\tilde{x})^K\}$ based on the *K* from solution archive $SA = \{(x)^1, (x)^2, \dots, (x)^K\}$, which is described in Equation (4.7).

4.3.2 The Oracle Penalty Method

In many real-world applications, the optimization problem that involved constraints has arisen and becomes essential in finding the best optimal solution. Generally, the constrained optimization problem is defined in Equation (4.14) below:

$$\begin{aligned} &\text{Minimize } f(x) = 0 \\ &\text{Subject to: } g_i(x) = 0, \quad i = 1, \dots, m_{eq} \in \mathbb{N} \\ &\qquad\qquad g_i(x) \geq 0, \quad i = m_{eq} + 1, \dots, m \in \mathbb{N} \end{aligned} \qquad (4.14)$$

where the vector of decision variables is given as $x = (x_1, \dots, x_n)$ of dimensional search space $n \in \mathbb{N}$. The objective function $f(x)$ has to be minimized subject to m_{eq} equality constraints $\left(g_1, \dots, g_{m_{eq}}\right)$ and $m - m_{eq}$ inequality constraints $\left(g_{m_{eq}} + 1, \dots, g_m\right)$. On the other hand, two inequality constraints can also be expressed for any equality constraint.

Penalty function method is simple and easy to use. However, the use of this method often becomes a challenging problem because of its difficulties in gaining adequate performance. Therefore, MIDACO introduced a new concept of general penalty method, called oracle penalty method, in order to enhance the control of the constraints. For a given problem, this method adjusts only a single parameter, called Oracle (**Ω**), which is allied to the objective functions in which this parameter will select the equal or slightly better optimal (feasible) solutions. The problem with applying this approach to the real-world problem is due to the unknown value of the target function. Thus, the performance of this method is essential to be acceptable even for bad selections of **Ω** [190].

Basic Oracle Penalty Function

The idea of the new formulation is to transform the objective function $f(x)$ into additional equality constraint $g_0(x) = f(x) - \Omega = 0$. An objective function is unnecessary in the transformed problem definition and can be declared as a constant zero function $\bar{f}(x)$ as described in the form below:

$$\begin{aligned} &\text{Minimize } \bar{f}(x) = 0 \\ &\text{Subject to: } g_0(x) = f(x) - \Omega = 0, \quad \Omega \in \mathbb{R} \\ &\qquad\qquad g_i(x) = 0, \quad i = 1, \dots, m_{eq} \in \mathbb{m} \\ &\qquad\qquad g_i(x) \geq 0, \quad i = m_{eq} + 1, \dots, m \in \mathbb{m} \end{aligned} \tag{4.15}$$

where $f(x)$ and Ω are the objective function and oracle parameter, respectively. If x^* represents the optimal global solution of the problem in (4.14), therefore, $\Omega = f(x^*)$ directly specifies that feasible solution of problem (4.15) is the global optimal of the problem (4.14). Therefore, by transforming to the equality constraint, the algorithm with minimizing new constraint $g_0(x)$ and minimizing the residual of the original constraints

$(g_1, \dots, g_m)$ will be directly comparable. The comparability can be exploited using basic oracle penalty function where the function balances the penalty weight on either the transformed objective function or the constraints. The basic oracle penalty function is described in Equation (4.16) below:

$$p(x) = \alpha . |f(x) - \Omega| + (1 - \alpha) . res(x) \tag{4.16}$$

Where α factor is specified as:

$$\alpha = \begin{cases} 1 - \dfrac{1}{2\sqrt{\dfrac{|f(x) - \Omega|}{res(x)}}} & \text{, if } res(x) \leq |f(x) - \Omega| \\ \dfrac{1}{2}\sqrt{\dfrac{|f(x) - \Omega|}{res(x)}} & \text{, if } res(x) > |f(x) - \Omega| \end{cases} \tag{4.17}$$

where $f(x)$ and Ω are the objective function and oracle parameter, respectively. The basic oracle penalty function (4.16) indirectly includes $|f(x) - \Omega|$, which is directly applicable to the optimization problem in (4.14) without the necessity of the problem transformation in Equation (4.15).

From Equation (4.17), the α factor will balance the penalty function $p(x)$ concerning the relationship between $|f(x) - \Omega|$ and $res(x)$, where the factor was constructed as a dynamic weight between 0 and 1. Let $res(x) \leq |f(x) - \Omega|$, the quotient $\frac{|f(x) - \Omega|}{res(x)}$ will be greater than 1, which results in a value of α between 0.5 and 1. Hence, the weight of the penalty function will concentrate on the transformed objective function. In case of $res(x) > |f(x) - \Omega|$, the quotient $\frac{|f(x) - \Omega|}{res(x)}$ will result in a value of α between 0 and 0.5. Therefore, the penalty function will focus its weight on the residual.

$$\begin{aligned} l^1 &: res(x) = \textstyle\sum_{i=1}^{m_{eq}} |g_i(x)| - \sum_{i=m_{eq}+1}^{m} \min\{0, g_i(x)\} \\ l^2 &: res(x) = \sqrt{\textstyle\sum_{i=1}^{m_{eq}} |g_i(x)|^2 - \sum_{i=m_{eq}+1}^{m} \min\{0, g_i(x)\}^2} \\ l^\infty &: res(x) = max\left\{ |g_i(x)|_{i=1,\dots,m_{eq},} \left| min\{0, g_i(x)\}_{i=m_{eq+1}+1,\dots m} \right| \right\} \end{aligned} \tag{4.18}$$

A residual function measures the constraint violations by applying a norm function over all *m* constraint violations of the problem (4.14). This approach is commonly used and

some explicit residual functions based on the l^1, l^2 and l^∞ listed in Equation (4.18), where the l^1 norm is assumed in this thesis..

Extension for the Basic Oracle Penalty Function

For the extension to the basic oracle penalty function, the modifications are still based on two conditions for oracle parameters: $\Omega \geq f(x^*)$ and at least one feasible solution $\tilde{x}$ exist, $\Omega = f(\tilde{x}) \geq f(x^*)$. For the first modification, the extension to the basic oracle penalty function is achieved by splitting the penalty function in Equation (4.16) into two cases as shown in Equation (4.19) below:

$$p(x) = \begin{cases} \alpha.|f(x) - \Omega| + (1-\alpha).res(x) & \text{, if } f(x) > \Omega \text{ or } res(x) > 0 \\ -|f(x) - \Omega| & \text{, if } f(x) \leq \Omega \text{ and } res(x) = 0 \end{cases} \quad (4.19)$$

where the first case affects any iteration with an objective function value higher than the oracle or any infeasible iterate, whereas the second case concerns only feasible iterates with an objective function value lower than the oracle.

For second modification, the concern is with the infeasible iterations corresponding to objective function values lower than Ω. Therefore, α factor is modified with the addition of a new case, which will overcome the problem. Refer to Equation (4.20) below in which the new case has been added in case of $f(x) \leq \Omega$; the α factor will be zero. In this case, by referring to Equation (4.19), the penalty function should penalize the iteration with $res(x)$.

$$\alpha = \begin{cases} 1 - \dfrac{1}{2\sqrt{\dfrac{|f(x)-\Omega|}{res(x)}}} & \text{, if } f(x) > \Omega \text{ and } res(x) \leq |f(x) - \Omega| \\ \dfrac{1}{2}\sqrt{\dfrac{|f(x)-\Omega|}{res(x)}} & \text{, if } f(x) > \Omega \text{ and } res(x) > |f(x) - \Omega| \\ 0 & \text{, if } f(x) \leq \Omega \end{cases} \quad (4.20)$$

For the third modification, the concern is for iterations (x) with $f(x) > \Omega$ and $res(x) \leq \frac{|f(x)-\Omega|}{3}$. Therefore, the new case for α factor can be obtained based on the calculation of the penalty function below:

Let

$$f(x) > \Omega \text{ and and } res(x) \leq |f(x) - \Omega|$$

Then

$$\alpha = 1 - \frac{1}{2\sqrt{\frac{|f(x) - \Omega|}{res(x)}}}$$

and

$$p(x) = \alpha . |f(x) - \Omega| + (1 - \alpha) . res(x)$$

$$\Longrightarrow \quad p(x) = 1 - \frac{1}{2\sqrt{\frac{|f(x) - \Omega|}{res(x)}}} . |f(x) - \Omega| + \left(1 - \left(1 - \frac{1}{2\sqrt{\frac{|f(x) - \Omega|}{res(x)}}} \right) \right) . res(x)$$

$$= |f(x) - \Omega| - 1 - \frac{|f(x) - \Omega|}{2\sqrt{\frac{|f(x) - \Omega|}{res(x)}}} . + \frac{1}{2\sqrt{\frac{|f(x) - \Omega|}{res(x)}}} . res(x)$$

$$= |f(x) - \Omega| - 1 - \frac{|f(x) - \Omega| \sqrt{res(x)}}{2\sqrt{\frac{|f(x) - \Omega|}{res(x)}}} . + \frac{res(x)\sqrt{res(x)}}{2\sqrt{\frac{|f(x) - \Omega|}{res(x)}}}$$

The residual function $res(x)$ is substituted with $\mathcal{R}$ and $p(\mathcal{R})$ can be expressed as follows:

$$\tilde{p}(\mathcal{R}) = 1 - \frac{1}{2\sqrt{\frac{|f(x) - \Omega|}{\mathcal{R}}}} . |f(x) - \Omega| + \left(1 - \left(1 - \frac{1}{2\sqrt{\frac{|f(x) - \Omega|}{\mathcal{R}}}} \right) \right) . \mathcal{R}$$

Then, the first derivative of $\tilde{p}(\mathcal{R})$ is given as:

$$\frac{d}{d\mathcal{R}}\tilde{p}(\mathcal{R}) = -\frac{|f(x)-\Omega|}{4\sqrt{|f(x)-\Omega|}\sqrt{\mathcal{R}}} + \frac{3\sqrt{\mathcal{R}}}{4\sqrt{|f(x)-\Omega|}}$$

Let if

$$\frac{d}{d\mathcal{R}}\tilde{p}(\mathcal{R}) = 0$$

Therefore

$$\frac{|f(x)-\Omega|}{4\sqrt{|f(x)-\Omega|}\sqrt{\mathcal{R}}} = \frac{3\sqrt{\mathcal{R}}}{4\sqrt{|f(x)-\Omega|}}$$

$$\frac{|f(x)-\Omega|}{\sqrt{\mathcal{R}}} = 3\sqrt{\mathcal{R}}$$

$$\mathcal{R} = \frac{|f(x)-\Omega|}{3}$$

Based on the above, the second derivate of $\tilde{p}(\mathcal{R})$ can be calculated as:

$$\frac{d^2}{d^2\mathcal{R}}\tilde{p}(\mathcal{R}) = \frac{\sqrt{|f(x)-\Omega|}}{8\mathcal{R}\sqrt{\mathcal{R}}} + \frac{3}{8\sqrt{\mathcal{R}}\sqrt{|f(x)-\Omega|}} > 0$$

Based on the assumptions, the penalty function takes it minimum for iterates (x) with $f(x)$ and $res(x) = \frac{|f(x)-\Omega|}{3}$. Then the penalty function for such an iterate can be calculated.

Let

$$f(x) > \Omega \text{ and } res(x) = \frac{|f(x)-\Omega|}{3}$$

Then

$$\alpha = 1 - \frac{1}{2\sqrt{3}}$$

$$\Longrightarrow \quad p(x) = 1 - \frac{1}{2\sqrt{3}}.|f(x)-\Omega| + \frac{1}{2\sqrt{3}}.\frac{|f(x)-\Omega|}{3}$$

$$= |f(x) - \Omega| - \frac{|f(x) - \Omega|}{2\sqrt{3}} + \frac{|f(x) - \Omega|}{6\sqrt{3}}$$

$$= |f(x) - \Omega|.\left(1 - \frac{1}{2\sqrt{3}} \pm \frac{1}{6\sqrt{3}}\right)$$

$$= |f(x) - \Omega|.\frac{6\sqrt{3} - 2}{6\sqrt{3}}$$

When penalty above is set equal to penalty function in equation (4.19), therefore the α factor is given as below.

$$\alpha.|f(x) - \Omega| + (1 - \alpha).res(x) = |f(x) - \Omega|.\frac{6\sqrt{3} - 2}{6\sqrt{3}}$$

Then

$$\alpha.\left(|f(x) - \Omega| - res(x)\right) + res(x) = |f(x) - \Omega|.\frac{6\sqrt{3} - 2}{6\sqrt{3}}$$

$$\Longrightarrow \quad \alpha.\left(|f(x) - \Omega| - res(x)\right) = |f(x) - \Omega|.\frac{6\sqrt{3} - 2}{6\sqrt{3}} - res(x)$$

$$\Longrightarrow \quad \alpha = \frac{|f(x) - \Omega|.\frac{6\sqrt{3} - 2}{6\sqrt{3}} - res(x)}{\left(|f(x) - \Omega| - res(x)\right)}$$

From the mathematical explanation of the third modification above, the value of the α factor above is now included in Equation (4.21) for iterations (x) with $f(x) > \Omega$ and $res(x) \leq |f(x) - \Omega|$. Then, all iterations (x) with $f(x) > \Omega$ and $res(x) \leq \frac{|f(x) - \Omega|}{3}$ will then be penalized with $|f(x) - \Omega|.\frac{6\sqrt{3} - 2}{6\sqrt{3}}$.

Extended Oracle Penalty Function in MIDACO

In MIDACO, the extension of oracle penalty function to handle constraints is based on the three modifications from the basic oracle penalty function explained above. Therefore, the extended oracle penalty function can be written as:

$$p(x) = \begin{cases} \alpha.|f(x) - \Omega| + (1-\alpha).res(x) & \text{, if } f(x) > \Omega \text{ or } res(x) > 0 \\ -|f(x) - \Omega| & \text{, if } f(x) \leq \Omega \text{ and } res(x) = 0 \end{cases} \quad (4.21)$$

Where α is given as:

$$\alpha = \begin{cases} \dfrac{|f(x) - \Omega|.\dfrac{6\sqrt{3}-2}{6\sqrt{3}} - res(x)}{\left(|f(x) - \Omega| - res(x)\right)} & \text{, if } f(x) > \Omega \text{ and } res(x) \leq \frac{|f(x)-\Omega|}{3} \\ 1 - \dfrac{1}{2\sqrt{\dfrac{|f(x) - \Omega|}{res(x)}}} & \text{, if } f(x) > \Omega \text{ and } \frac{|f(x)-\Omega|}{3} \leq res(x) \leq |f(x) - \Omega| \\ \dfrac{1}{2}\sqrt{\dfrac{|f(x) - \Omega|}{res(x)}} & \text{, if } f(x) > \Omega \text{ and } res(x) > |f(x) - \Omega| \\ 0 & \text{, if } f(x) \leq \Omega \end{cases}$$

(4.22)

In this chapter, a simple and effective updated rule for the oracle parameter **Ω** is also presented where the parameter is applied if no information about optimal feasible objective function value is known and several optimization runs are performed. The oracle parameter Ω^i is always equal to the lowest known feasible objective function value or sufficiently large for no feasible objective function value up until the feasible solution is found. Therefore, the proposed updated rule will initialize the oracle parameter Ω^1 for the very first run with a sufficiently large parameter, which is therefore given as $\Omega > f(x)$. Based on Equation (4.22), this means the method is focused entirely on the residual until a feasible solution is found.

Any further optimization updated rule oracle parameter $\Omega^{i=2,3,4,\cdots}$ should be calculated as follows:

$$\Omega^i = \begin{cases} f^{i-1}, & \text{, if } f^{i-1} < \Omega^{i-1},\ res^{i-1} = 0 \\ \Omega^{i-1}, & \text{, else} \end{cases} \quad (4.23)$$

where Ω^i is given as oracle parameter used for the *i*th optimization run. The objective function and residual function values obtained by the *i*th optimization are given by f^i and res^i.

The oracle parameter $\Omega^{i=2,3,4,\cdots}$ is updated with the latest feasible solution, which has a lower objective function value than the present oracle parameter or leaving the oracle

parameter unaffected, in case the solution is infeasible or has a larger objective function value than the present oracle parameter.

4.3.3 The Extended ACO Implementation (ACOmi)

In this section, more detailed explanations on implementation of ACOmi are discussed. This method followed the ACO framework strictly explained in Section 4.3.1. While the fitness of ants (or attraction) is considered for solving objective value for the unconstrained problem, the oracle penalty function as fitness criteria is considered for the problem that involved a problem with constrained.

Four new heuristic methods are included in the MIDACO execution in order to develop the global competency of the ACO algorithm, which are described as following:

A. Dynamic Population Heuristic

During the optimization process, the size for the number of ants per generation is not persistent, which allows additional ants to be used during the algorithm process, particularly for the critical parts. Based on a heuristic nature, the algorithm for the calculation of the dynamic population of ants and parameter selection is given in Algorithm I below::

Algorithm I

if $\#\boldsymbol{iteration} \leq \boldsymbol{dyn_{mean}}$

$Pop_{size} = \left[n_{ants} + (dyn_{max} - n_{ants}) \frac{\#iteration - 1}{dyn_{mean} - 1}\right]$

else

if $\#iteration > dyn_{mean}$ **and** $\#iteration \leq 2.dyn_{mean}$ **then**

$Pop_{\boldsymbol{size}} = \left[dyn_{\boldsymbol{max}} + (n_{\boldsymbol{ants}} - dyn_{\boldsymbol{max}}) \frac{\#iteration}{2dyn_{mean}}\right]$

else

$Pop_{\boldsymbol{size}} = n_{\boldsymbol{ants}}$

end if

end if

Based on the algorithm, the parameters of n_{ants}, dyn_{max}, and dyn_{mean} need to be selected to calculate the actual population size of ants Pop_{size} for a given generation ($\#iteration$). For each of every generation, n_{ants} is the minimum size of ants' population that is allowed, whereas the actual population will increase until it reaches the maximum size, dyn_{max} in the dyn_{mean}-th iteration. The first stage of the algorithm is actually the most critical in the search process, and therefore more ants that are active during the algorithm process can be useful where the Pop_{size} is enlarged equally to this point. Then, the size of ants will immediately be decreased about half of the population size after reaching dyn_{mean}-th generation, and it will keep reducing until reaching the minimum size of n_{ants}. Refer to Figure 4.4 for a detailed explanation of the algorithm.

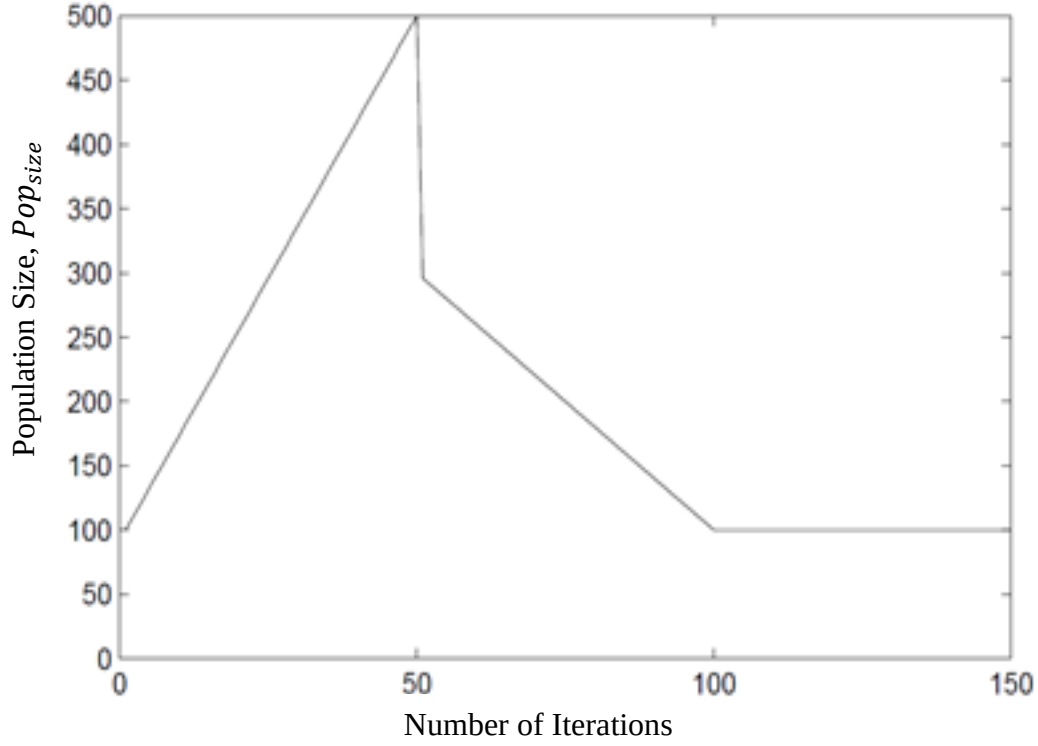

Figure 4.4: The population size throughout 150 generations

From the graph, it shows that the most critical part of the optimization process is between the first stage of iterations. At dyn_{mean}, the size of ants reduced almost 50%, and it keeps decreasing linearly with increasing in iterations until it reaches a minimum of ants to ensure smoother change.

B. Single Dimension Tuning Heuristic (SDT)

This heuristic helps to recover the current best solution s_1 through sampling with proper deviation for the optimization of a single dimension out of its *n* components. For a continuous variable, a newly created ant x_{sdt}^i for every $i \leq n_{cont}$ can be expressed as follows:

$$x_{sdt}^i = s_1^i + \frac{\left(x_u^i - x_l^i\right) . \; x_{rand}^i}{\#iteration} \tag{4.24}$$

where x_{rand}^i is a vector of component n with a random number between [0,1].

For integer variables, the current integer values are sampled with random numbers between 0 and 1, which increased or decreased by one unit and written as follows:

$$x_{sdt}^i = s_1^i + \begin{Bmatrix} 1, & if\ x_{rand}^i \geq \frac{1}{2} \\ -1, & if\ x_{rand}^i \leq \frac{1}{2} \end{Bmatrix} \tag{4.25}$$

The advantage of this heuristics is the improvements to the high dimension and full-range problem, especially for the case of mixed-integer optimization problems. This gives benefit to the algorithm to be flexible with the number of integer variables.

C. Weighted Average Best Ant Heuristic (WABA)

For this heuristic, its purposes are to improve all solution using the information saved in *SA.* By using previous weight *w*, the weighted average best ant (WABA) x_{waba}^i is created out of the *k* solutions s_l saved in SA and calculated as follows:

$$x_{waba}^i = \sum_{l=1}^{k} w_l^i * s_l^i \tag{4.26}$$

where dimension *i* is referred to the dimension of the optimization variable. The value of x_{waba}^i is rounded to the next integer for case *i* referring to an integer variable. There is only one additional function evaluation for each of the iteration to be performed, which causes this heuristic to be low in computational cost.

D. Final Stage Heuristic

The local solvers are called frequently to solve around the present best solution when the algorithm reaches the "final stage" mode. The ACOmi detects its final stage by monitoring the fitness of ants. In the whole process, there are two different successive generations of ants that are computed, namely, maximum, dc_{max} and average $dc_{average}$ values. The final stage criterion is expressed as Equation (4.27) below:

$$stage_{final} = \begin{cases} 1, & if \quad dc_{average} < \dfrac{dc_{max}}{W_{final}} \quad \left(W_{final} \epsilon N^{+}\right) \\ 0, & else \end{cases} \tag{4.27}$$

where W_{final} acts as a weight to compare with dc_{max} and $dc_{average}$.

If there is no feasible solution found between two different successive generations of ant, it will then be reset to avoid the solution from being stuck in that "current best solution." A local solver will be called frequently during second ACO search process after every *freq*-th iteration for a given frequency $freq \epsilon N^{+}$.

The implementation of MIDACO is categorized into two main stages known as Stage 1: *ACOmain* and Stage 2: *ACOfinal*. Figure 4.5 illustrates the flowchart throughout the optimization process in MIDACO.

First is initializing the pheromones in random. For Stage 1, *ACOmain* starts its simple ACO search process in which the number of ants is not fixed. This allows additional ants to be used throughout the process.

On every generation, two additional heuristics are calculated, starting with single dimension tuning and then *WABA*. From the current best solution, both of these heuristics are used to improve the solution before they are saved in *SA*. At the end-stage generation in *ACOmain*, a stopping criterion is considered after every iteration, where the flag of $stage_{final}$ will change the algorithm to the *ACOfinal*.

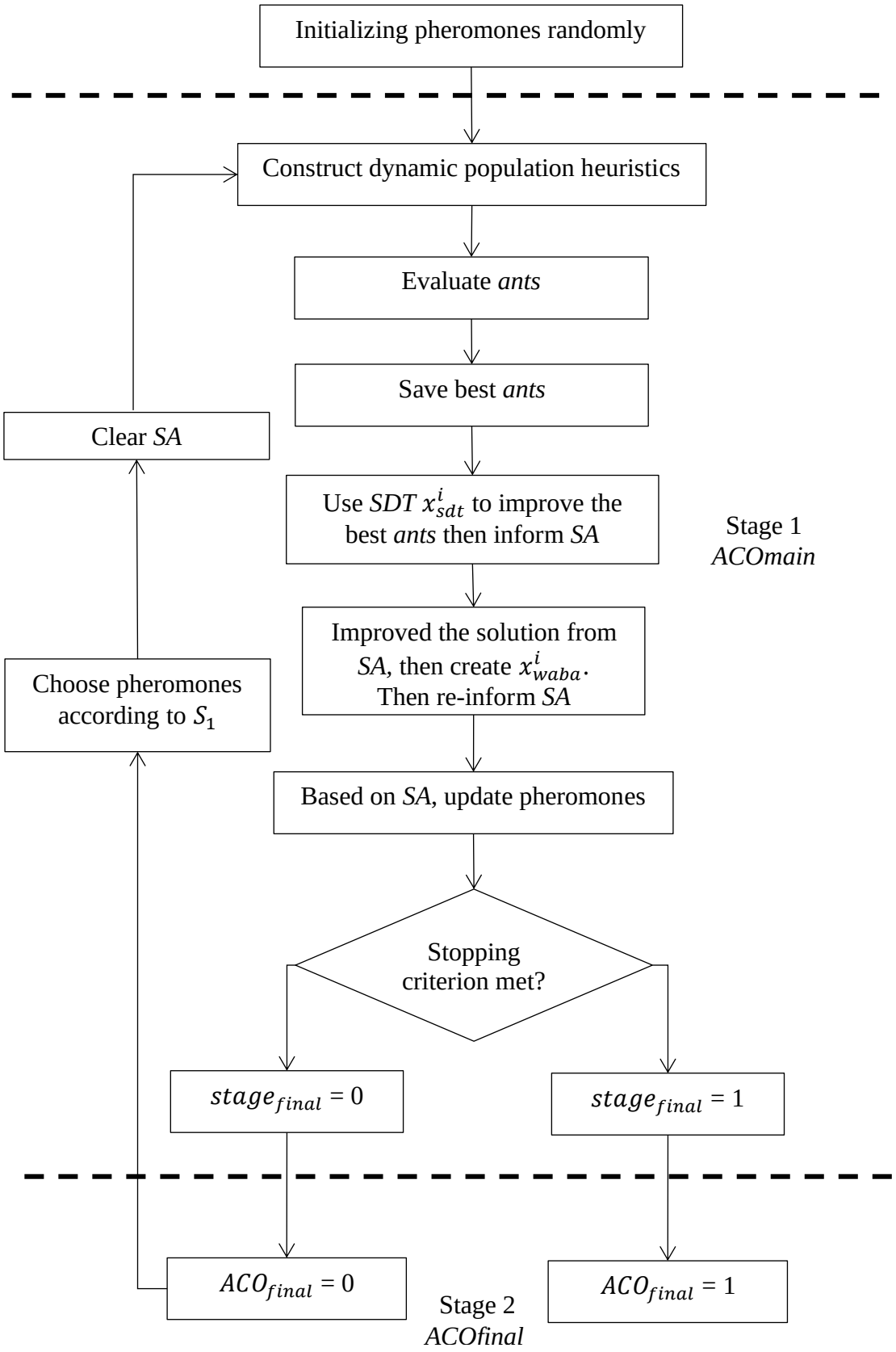

Figure 4.5: The flowchart implementation of ACOmi

There are three conditions of stopping criteria considered in this research:

- The function evaluations that reach the maximum limit (*MAXEVAL*)
- A CPU time to reach the maximum limit (*MAXTIME*)
- The feasible solution achieved with the F(X) $\leq fex$

If the stopping criterion is not met, the first step of Stage 1 will be repeated in which the selected pheromones are initialized according to s_1. To avoid getting stuck in the same s_1, *SA* will be cleared, but the best solution is represented in the pheromones in the hope that the solution will be sampled around the best solution and biased with the solution in *SA*.

4.4 Multi-objective Optimization

The multiobjective optimization problem is when the simulation considers more than one objective function to be optimized at the same time. In contrast to the single-objective optimization, which usually results in a single solution as global optimum, multiobjective optimization results to the set of nondominated solutions or known as Pareto-optimal, which represents a trade-off curve (Pareto front) between the individual objectives. In MIDACO, the presented algorithm is based on a combination of a decomposition of the original multiobjective problem into a series of single-objective problem.

The decomposition approach considered here is based on Utopia–nadir–balance concept [198]. By comparing this concept with previous traditional multiobjective approaches, the most significant advantage of Utopia–nadir–balance concept in MIDACO is that the objective function will fully automatically scale or measure the amount of weighting factor for its internal algorithmic process. The utopia U_i information is defined in Equation (4.28) as follows:

$$U_i = \min \left\{ f_i(x) \forall\, x \in \mathcal{F} \right\} \tag{4.28}$$

where $f_i(x)$ is an individual objective that denotes the global minimum of the respective objective among all solutions x. $\mathcal{F}$ is the set of all x's that satisfy the feasibility constraints.

The nadir N_i information can be described as shown in Equation (4.29) below.

$$N_i = \max \left\{ f_i(x) \forall\, x : \ni\, k \neq U_k \right\} \tag{4.29}$$

where N_i represents the worst respective objective $f_i(x)$ among all solutions x, which correspond to an U_k of any other objective $f_k(x)$.

Additionally, the most significant of MIDACO is the ability of this algorithm to freely choose to focus the algorithmic search effort on a particular area of the Pareto front. Therefore, MIDACO introduced scalar function based on the information given in Equations (4.28) and (4.29), where this function acts as an indicator for the balance of a solution *x*. Refer to Figure 4.6 for the graphical illustration of the concept of Utopia–nadir–balance in MIDACO.

Now, the concept of Utopia–nadir–balance decomposition is defined in detail. According to the balance, $B_j(x)$ can be defined as below.

$$B_j(x) = \sum_{i=1}^{M} \left| d_i^j(x) - D_j(x) \right| \tag{4.30}$$

where $B_j(x)$ refers to the balance of a solution *x* to a subproblem *j*. From Equation (4.30), the parameter $d_i^j(x)$ and $D_j(x)$ are the given weighted distance and average distance, respectively, and can be described as follows:

$$d_i^j(x) = w_i^j \frac{f_i(x) - U_i}{N_i - U_i} \tag{4.31}$$

$$D_j(x) = \frac{\sum_{i=1}^{M} d_i^j(x)}{M} \tag{4.32}$$

By the given information that U_i and N_i are globally available among subproblems, d_i^j is calculated for a solution *x* in each $f_i(x)$ to subproblem *j*. Let *S* be the integer value that denotes the amount of single-objective subproblems in which the original multiobjective problem is decomposed into. That weight w_i^j be a matrix of size O × *S* is bounded to the interval [0,1].

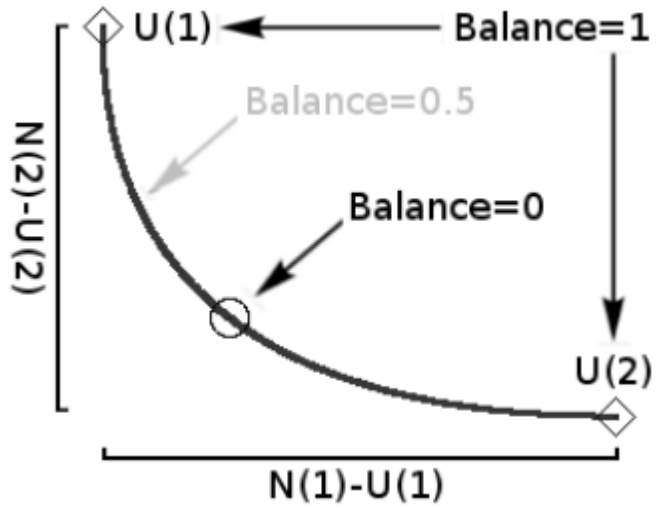

Figure 4.6: Graphical illustration of *Utopia-Nadir-Balance* decomposition with balance concept [198].

The *target* function is defined based on $B_j(x)$, U_i , N_i, and w_i^j for each of subproblem j.

$$T_j(x) = \sum_{i=1}^{M} w_i^j \frac{f_i(x) - U_i}{N_i - U_i} + B_j(x) \tag{4.33}$$

where the set of single-objective function T problem is given by $T_1, \ldots, T_M$, which therefore decomposes the multiobjective problem.

The equation for the initial *target* function is given as below.

$$\check{\mathrm{T}}_j(x) = \sum_{i=1}^{M} w_i^j f_i(x) \tag{4.34}$$

where there is no information for U_i and N_i for the first execution. Therefore, the first initial execution will replace the *target* function by a simple weighted sum w_i^j over $f_i(x)$ for all $j = 1, \ldots, S$

4.5 Parameter Selection

The proposed method compromises several parameters to be tuned in order to modify the performance and behavior of the algorithm. For every problem, this method requires precise tuning because of the optimal values as these parameters are problem-specific. The detailed descriptions for every parameter are deliberated as follows:

A. ACCURACY

This parameter has a substantial impact on the performance of the constraint problem, where it defines the accuracy tolerance for the constraint violation.

- Equality constraints: the solution is feasible if $G(X) \leq \text{ACCURACY}$.
- Inequality constraints: the solution is feasible if $G(X) \geq -\text{ACCURACY}$.

It is recommended to start the test with less accuracy, for example, ACCURACY = 0.1 or 0.05 and increase the accuracy to 0.0001 or 0.00001 afterward to be more precise.

B. SEED

The initial SEED for the internal pseudorandom numbers is defined by this parameter in which the sequence number is sampled by the generator. The main advantage of using this method is that this parameter allows MIDACO runs to be 100% reproducible if it set with the same random SEED.

The SEED parameter must be set to a number of an integer equal to or greater than 0, where the impact varies with the intricacy problematic. Therefore, it is advisable to execute several runs of MIDACO by utilizing different SEED rather than performing it using one number for a very long run, especially for severe problems.

C. FSTOP

The *FSTOP* parameter is used to enable stopping criterion in MIDACO. The *FSTOP* will be assigned if it is set with a number greater than zero, where the simulation stops until the feasible solution reaches with objective function $\leq FSTOP$. This parameter was not used during the simulation of this research.

D. ALGOSTOP

The parameter is enabled if assigned with a positive integer value where the algorithm that calculates the maximal number of internal ACO restarts without improvement of the objective function. Besides, this parameter has some drawbacks, where it usually needs many function evaluations that can result in expensive CPU-time evaluations. However, it is the most advanced as an indicator of global optimality. In this research, this parameter also was disabled because of the times taken to tune this parameter.

E. EVALSTOP

This parameter works similarly with the criteria when using *ALGOSTOP*, but the difference lies in the stopping criteria, which is based on the evaluation of individual function without improvement of the objective function. It aims to provide stopping criteria that are not as expensive in CPU time as *ALGOSTOP*, nonetheless, is based on the algorithm measure. It is recommended to experience this parameter with a low number of function evaluation, such as 500 or 1000 to feel the effect of run time on a specific application in order to achieve optimal global solutions. In this research, this parameter was also disabled because MIDACO used hard limit criteria (*MAXEVAL* and *MAXTIME*) instead of algorithmic criteria (*FSTOP*, *ALGOSTOP*, and *EVALSTOP*) to stop the optimization process. Hard limit criteria are the process, where MIDACO will be stopped by setting the maximum number function evaluation, *MAXEVAL*, and maximal budget of CPU time, *MAXTIME*.

F. FOCUS

FOCUS is the utmost influential parameter, which is especially used for MIDACO to focus on its search process on the current best solution. This parameter must be set with an integer number in which it is recommended to test the first runs with smaller values without any specific starting point (e.g., 10 or 100). In contrast, more considerable value (e.g., 10,000 or 100,000) is typically used for improvement runs with a given specific solution as a starting point.

G. ANTS

This parameter allows MIDACO to fix the number of ants or iterates within one generation. The performance can be decreased when tuning this parameter, although it

is sometimes promising for specific problems especially large-scale problem or intensive CPU time application.

H. KERNEL

This parameter allows MIDACO to fix the number of the kernel within MIDACO's multikernel Gauss PDF. This parameter with a combination of *ANTS* must be used together where tuning both of them is very much for precise problems.

A large number of the kernel will result in expensive CPU time per generation compared to the small number of the kernel, which results in the fast convergence of solutions. However, a small number of kernels increase will increase the chance of MIDACO trapped in local solution. In contrast, a higher number of kernels give the advantage to reach the optimal global solution.

I. ORACLE

The *Oracle* tunes with only one parameter known as Ω, which uses penalty function in MIDACO to solve constrained problems. In this research, the initial Oracle used is 0 or 10^9. Besides, this research also proves that this parameter will only affect the movement of the axis and will and will not affect the optimal solution.

J. PARETOMAX

In this thesis, the *PARETOMAX* is used explicitly to solve multiobjective problems where the effects of changing this parameter are presented in Chapter 6. This parameter defines the maximum Pareto points stored in *SA*. The high number of *PARETOMAX* will require more memory and slow down the internal calculation time due to the increasing Pareto filtering efforts.

K. EPSILON

This parameter is used in combination with *PARETOMAX* for the multiobjective problem. The precision used by MIDACO for its multiobjective dominance filter is defined by this parameter, where it has a big influence on the stored Pareto point and the internal calculation time. The lower value of *EPSILON* will increase the chance of the new solution to be introduced into the Pareto front. Most applications suggest using

EPSILON = 0.001 and *EPSILON* = 0.01 for two objectives and three objectives problems or more, respectively.

L. CHARACTER

This parameter allows the user to activate the internal parameter settings in MIDACO. There are three settings of *CHARACTER* offered by MIDACO, which are 1, 2, and 3 for the internal parameters for the continuous problem, combinatorial problem, and all-different problem types, respectively. For the thesis, only continuous variables are used, and thus this parameter was set to 0 (default). By setting the parameter to 0, MIDACO will decide its internal parameters between continuous or combinatorial problem by itself.

4.6 MIDACO Advantages and Disadvantages

MIDACO acts as a black box optimizer where it allows the objective function and constraints to be represented and formulated in maximum possible freedom without any restrictions. Therefore, the advantages and drawbacks of MIDACO are described as follows:

1. The capability to solve the large-scale problem with up to 100,000 variables, thousands of constraints, and hundreds of objectives
2. MIDACO has no requirement to try different values of initial conditions. This is because MIDACO is a global optimization algorithm
3. MIDACO has smooth implementation and fast sampling time
4. Fast local convergence because MIDACO is internally hybridized with backtracking line search
5. A single Gaussian function can only focus on one mean, incapable of defining conditions with more disjoints area of the search domain. However, the weighted Gaussian PDFs, $G^i(x)$ given in Equation (4.8) is used to overcome the drawback.

4.7 Summary

This chapter explains the inventiveness of ACO and the implementation of an extension to the ACO metaheuristics in MIDACO with a combination of Oracle penalty method for constraints handling. Besides, four new heuristic methods to develop the global competency of the ACO algorithm in MIDACO are also elaborated in this chapter. Furthermore, the concept of Utopia–nadir–balance has been explained where this concept is specifically used to solve the multiobjective problem. Besides, several parameters, including the non compulsory parameters that can be tuned, are briefly explained to understand the influence of each parameter toward the performance and behavior of the algorithm. Lastly, this chapter ends by explaining the advantages and disadvantages of MIDACO

Chapter 5

Optimal Undamped Single Tuned Filter Design

5.1 Introduction

It is suggested to understand single tuned filter with least damping. Thus, the simulated and analysis of the results for the best design of filter without dissipation energy from the resistor in the single tuned filter is presented in this chapter. The analytic start with the equivalent system circuit, all the mathematical formulations involved were carefully presented in this chapter in which the main components of the undamped filter, namely inductance and capacitance are obtained based on the four objective functions. The primary intention of the filter design mainly considered the harmonics amplification problem caused as the parallel resonance frequencies are located at, or close to the eliminated harmonics. The application of IEEE 519 limit the voltage total harmonic distortion, at least minimum of 90% of the power factor and the standard of capacitors following IEEE 18 standard [22], [122], [199]. Four cased were studied and simulated, in which the performances of each case were investigated and compared to each other. The simulated results are also compared between the proposed method with GA, PSO and other published journals. Apart from that, the efficiency and significant contributions of the proposed method will be highlighted in this category.

5.2 Problem Demonstration and Equations

5.2.1 Objective Functions

In this research, the circuit consists of single-tuned filter, linear and non-linear load that are connected in shunt, where the filter placement in the circuit network performs as small impedance path. This filter allows harmonic current to go through the impedance which overall, will further reduce the voltage distortion [187], [200]. Refer to Fig. 5.1(a) and 5.1 (b) to see the equivalent circuits for uncompensated and compensated system, respectively.

The utility supply and harmonic current source are written as Equation (5.1) and (5.2), while represented as V_{THK} and I_{LK} respectively.

$$v_{th}(t) = \sum_{K} v_{thk}(t) \tag{5.1}$$

$$i_{lk}(t) = \sum_{K} i_{lk}(t) \tag{5.2}$$

The *K*th harmonic of Thevenin and load impedance is shown in the Equation (5.3) and (5.4) and formulated as

$$Z_{THK} = R_{THK} + jX_{THK} \tag{5.3}$$

$$Z_{LK} = R_{LK} + jX_{LK} \tag{5.4}$$

After some complex analysis of mathematical modelling, I_{SK} and V_{LK} which represented the current source and load voltage at harmonic number *K* can be determined through the calculation as below.

$$I_{SK} = \frac{V_{THK}}{Z_T} + \frac{I_{LK}Z_{CLK}}{Z_T} \tag{5.5}$$

$$V_{LK} = V_{THK} - I_{SK}Z_{THK} \tag{5.6}$$

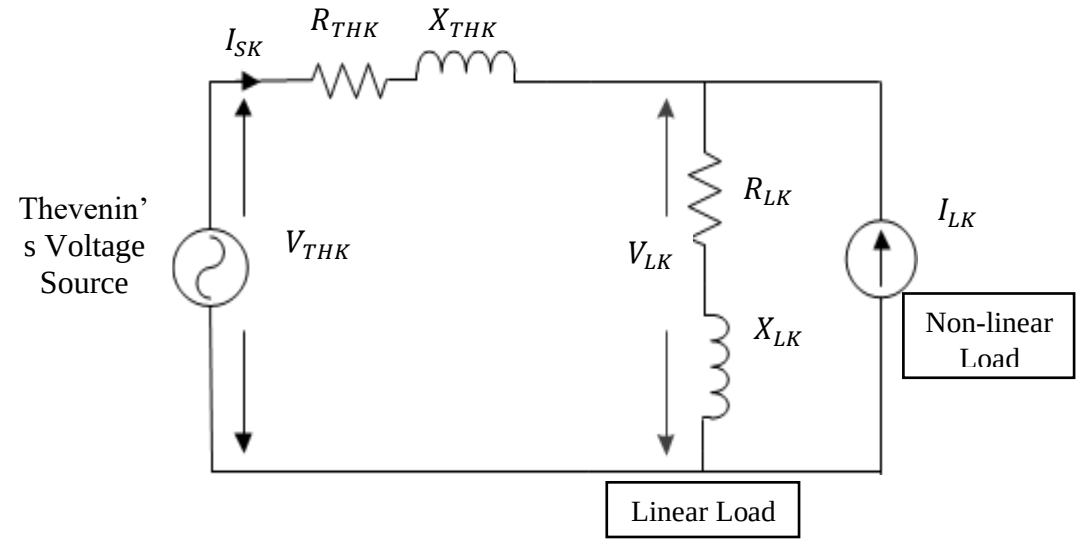

(a)

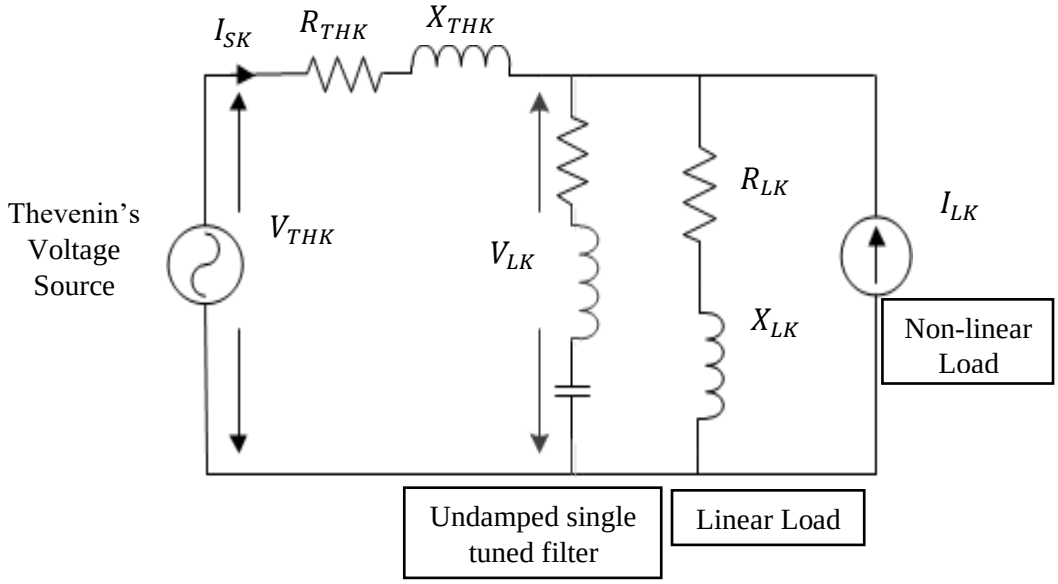

(b)

Figure 5.1: System equivalent circuit, (a) uncompensated system, (b) compensated system

Given Z_{CLK} is where Z_{FK} in parallel with Z_{LK} and can be written as

$$Z_{CLK} = \frac{Z_{FK}Z_{LK}}{Z_{FK} + Z_{LK}} \tag{5.7}$$

$$Z_T = Z_{THK} + Z_{CLK} \tag{5.8}$$

So that Z_{FK} is the total undamped filter impedance specified as

$$Z_{FK} = j\left(KX_{LU} - \frac{X_{CU}}{K}\right) \tag{5.9}$$

For I_{SK} in amperes (A) and V_{LK} in volts (V) given in Equations (5.5) and (5.6) are expressed as in the Equation (5.10) and (5.11) below.

$$I_S = \sqrt{\sum_{K=1}^{13} I_{SK}^2} \tag{5.10}$$

$$V_L = \sqrt{\sum_{K=1}^{13} V_{LK}^2} \tag{5.11}$$

The system performance based on Fig. 5.1 is analyzed using Equation (5.12) until (5.15) and expressed as follows:

The total harmonic voltage distortion, THD_V can be written as

$$THD_V = \frac{\sqrt{\sum_{K=2}^{13} V_{LK}^2}}{V_{L1}} \tag{5.12}$$

The load power factor, PF can be defined according to

$$PF = \frac{P_L}{I_S V_L} = \frac{\sum V_{LK} I_{SK} \cos(\theta_K - \phi_K)}{\sqrt{\sum I_{SK}^2 \sum V_{LK}^2}} \tag{5.13}$$

Then, the transmission efficiency, η is given as

$$\eta = \frac{P_L}{P_S} = \frac{\sum V_{LK} I_{SK} \cos(\theta_K - \phi_K)}{\sum V_{LK} I_{SK} \cos(\theta_K - \phi_K) + \sum I_{SK}^2 R_{THK}} \tag{5.14}$$

Additionally, the losses in the Thevenin resistor, P_{LOSS} describes as

$$P_{LOSS} = \sum_K I_{SK}^2 R_{THK} \tag{5.15}$$

5.2.2 Constraints

a) Practical Capacitor Compliance with IEEE Standard.

In designing the capacitor, the specifications are selected from the industrial values of reactive power and voltage rating, as according to established IEEE Std. 18-2012. From the IEEE standard, it shows that the typical capacitor voltage of 2400V terminal to terminal has reactive power ratings of 50, 100, 150, 200 and 400kVAR [199]. Consequently, the capacitor intends to operate below the following limitation for its continuous operation:

- 135% of nominal current, I_C (in rms), so that

$$I_C = \sqrt{\sum_K I_{CK}^2} \tag{5.16}$$

By substituting Equation (5.6) and (5.7) into Equation (5.16), the value of *K*th harmonic of capacitor current, I_{CK} is given as

$$I_{CK} = \frac{V_{LK}}{Z_{CLK}} \tag{5.17}$$

- 110% of capacitor voltage, V_C(in rms), so that

$$V_C = \sqrt{\sum_K V_{CK}^2} \tag{5.18}$$

Where V_{CK} is *K*th harmonic of capacitor voltage and can be expressed as

$$V_{CK} = I_{CK}\frac{X_C}{K} \tag{5.19}$$

- 120% of rated peak capacitor voltage, V_{CP}.

$$V_{CP} = \sum_K I_{CK}\frac{X_C}{K} \tag{5.20}$$

- 135% of the reactive power of capacitor, Q_C.

$$Q_C = I_C V_C \tag{5.21}$$

Based on the explanations in IEEE Std. 18-2012, the capacitor unit voltage is increased when the capacitor associated with the reactor in series. Therefore, a higher rating of voltage is recommended for the protection during switching, sudden loss of load and voltage upsurge for the case beyond the standard limit. Besides, the tolerance value of the capacitor considers in this research is 1.05 [201].

b) Design to Avoid Resonance.

The nonlinear loads create harmonic currents, which is injected all over the system. This harmonic resonance is typically known as series and parallel resonance. In series or parallel *RLC* circuit, there will be a crossover point known as resonant frequency point, f_r for any power system that consists of the capacitor, where X_L is equal to X_C.

In parallel resonance, the occurrence of the resonance can happen in the condition known as a parallel resonant circuit, in which the total of load bus impedance, Z_{CLK} in Equation (5.7) is parallel with source Thevenin's impedance, Z_{THK} in Equation (5.3) and given as

$$Z_{PARALLEL} = \frac{Z_{THK} Z_{CLK}}{Z_{THK} + Z_{CLK}} \tag{5.22}$$

At this point, the parallel resonance can happen in which the voltage reaches maximum while the admittance is at a minimum, hence, consequently limiting the circuit currents. Refer to Figure 5.2 to see the impedance response of the parallel resonant circuit where the impedance is at maximum [202].

In contrast, the impedance at a minimum for the series resonance can be risky due to the small value of resistance at resonance, which will result in the current flowing through the circuit to be dangerously high. Refer to Figure 5.3 to see the impedance response of the series resonant circuit where the impedance is at a minimum. The series resonance circuit can be obtained where the series resonance impedance in Equation (5.23) is equal to the total impedance, Z_T in Equation (5.8) and described as

$$Z_{SERIES} = Z_T \tag{5.23}$$

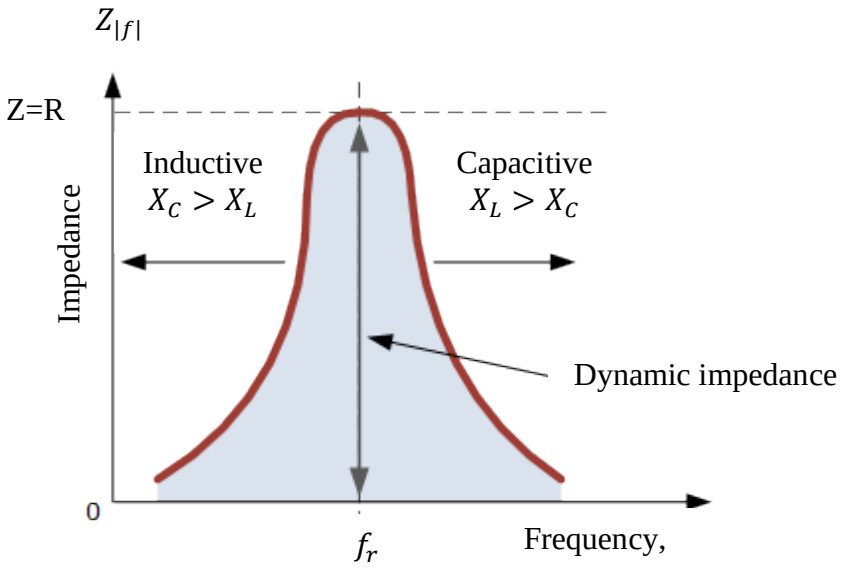

Figure 5.2: Impedance response in the parallel circuit [202]

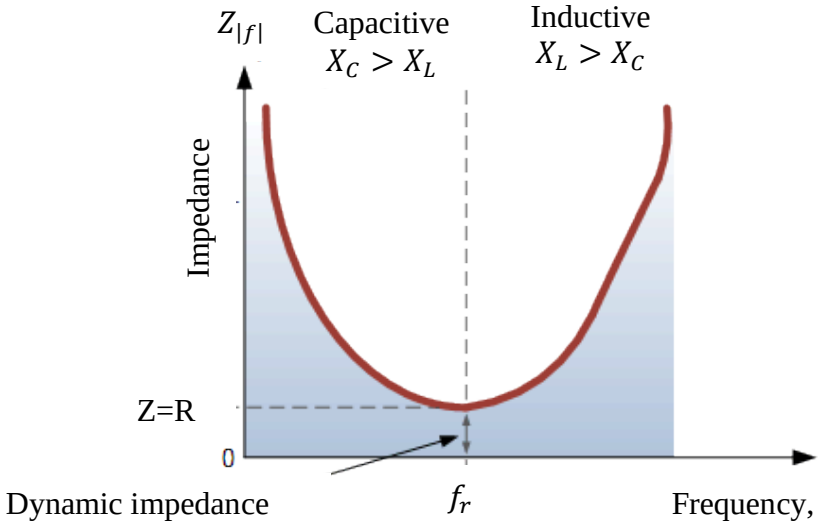

Figure 5.3: Series resonance impedance response [203]

The harmonic order activating resonance h_r can be expressed in Equation (5.24) as below.

$$h_r = \sqrt{\frac{X_C}{X_L + X_{TH1}}} \tag{5.24}$$

One approach to solving the harmonic resonances problem is by applying the de-tuned harmonic filter. Therefore, the constraints will consider the harmonic order in Equation (3.6) to be tuned 9% from the desired harmonic frequency to be eliminated and the harmonic order value which is always higher than the harmonic order activating resonance, h_r given in Equation (5.24) above.

c) Additional Constraints

For the facility has loaded with poor power factor, a higher current will be supplied by the utility. Hence, the current-carrying component in the power system, such as cables, generators and transformers must be able to carry the total of higher current. In utilities, they are paid based on the energy consumed (kWh) where the current component is not registered by that. Thus, most of the utilities impose a penalty for power factor when delivering power to the customers to receive income, as well as to encourage efficient use of electricity. The established power factor imposed is as low as 0.85 to 0.95. With the increasing rate of energy and concerns to the power delivery efficiency, this research considered achieving at least a minimum of 90% of established *PF*.

The voltage usually consists of fundamental and harmonics, whereas the harmonic voltage generated from the source increases with the increasing distance of the voltage measurement from the source power. This is due to the increasing number of impedances that needs to be passed by the harmonics current, which must flow through resulted in the higher generation of harmonic voltage. The distorted current that flows through the system is caused by the nonlinear loads that initiated them, and it is becoming more severe because of the increasing current, which can result in overheating. The total harmonic current distortion is described below.

$$THD_i = \frac{\sqrt{\sum_{k=2}^{k_{max}} I_{SK}^2}}{I_{S1}} \tag{5.25}$$

For $k = 2,3,4,\ldots k_{max}$ and I_{S1} is the RMS source current at fundamental. While I_{SK} is refer to the source current at *k*-th harmonic number.

Other necessary consequences of current distortion are that it will cause the distortion of voltage distortion formed. It is becoming essential to limit the current distortion from the nonlinear loads at the PCC in order to avoid excessive voltage limits. Therefore, the practices and requirement for harmonics control recommended by IEEE 519 have been taken into consideration, which is imposed after the filter placement in the network. The IEEE 519 total harmonic voltage is given in Equation (5.12) must be equal or below to 5%.

There four objective functions are presented as X_{CU} and X_{LU} functions using Equations (5.12) until (5.15). The parameter of X_{CU} and X_{LU} which refer to the value of capacitance and inductance, respectively are the decision variables to be optimized in this problem. In MIDACO, the definition of the mixed-integer term is referring to the type of the decision variables which is either continuous, discrete or combination of both. In this thesis, the value of decision variables X_{CU} and X_{LU} contains continuous variables only. After formulating the objective functions and constraints involved, the maximization and minimization for each of the objective functions are formulated as below:

Objective 1: Minimize $THD_V(X_{CU}, X_{LU})$

Subject to:

$$
\begin{aligned}
G(1) \quad & I_C = 1.35 \times I_{C(rated)} \\
& V_C = 1.1 \times V_{C(rated)} \\
& V_{CP} = 1.2 \times \sqrt{2} \times V_{C(rated)} \\
& Q_C = 1.35 \times Q_{C(rated)} \\
G(2) &= h \leq 0.9 * f_n \\
G(3) &= h > h_r \\
G(4) &= 0 \leq VTHD \leq 5\% \\
G(5) &= 90\% \leq PF \leq 100\%
\end{aligned}
\tag{5.26}
$$

Objective 2: Maximize $PF(X_{CU}, X_{LU})$

Subject to:

$$
\begin{aligned}
G(1) \quad & I_C = 1.35 \times I_{C(rated)} \\
& V_C = 1.1 \times V_{C(rated)} \\
& V_{CP} = 1.2 \times \sqrt{2} \times V_{C(rated)} \\
& Q_C = 1.35 \times Q_{C(rated)} \\
G(2) &= h \leq 0.9 * f_n \\
G(3) &= h > h_r \\
G(4) &= 0 \leq VTHD \leq 5\% \\
G(5) &= 90\% \leq PF \leq 100\%
\end{aligned}
\tag{5.27}
$$

Objective 3: Maximize $\eta(X_{CU}, X_{LU})$

Subject to:

$$G(1) \quad I_C = 1.35 \times I_{C(rated)}$$
$$V_C = 1.1 \times V_{C(rated)}$$
$$V_{CP} = 1.2 \times \sqrt{2} \times V_{C(rated)}$$
$$Q_C = 1.35 \times Q_{C(rated)}$$
$$G(2) = h \leq 0.9 * f_n$$
$$G(3) = h > h_r$$
$$G(4) = 0 \leq VTHD \leq 5\%$$
$$G(5) = 90\% \leq PF \leq 100\% \tag{5.28}$$

Objective 4: Minimize $P_{LOSS}(X_{CU}, X_{LU})$

Subject to:

$$G(1) \quad I_C = 1.35 \times I_{C(rated)}$$
$$V_C = 1.1 \times V_{C(rated)}$$
$$V_{CP} = 1.2 \times \sqrt{2} \times V_{C(rated)}$$
$$Q_C = 1.35 \times Q_{C(rated)}$$
$$G(2) = h \leq 0.9 * f_n$$
$$G(3) = h > h_r$$
$$G(4) = 0 \leq VTHD \leq 5\%$$
$$G(5) = 90\% \leq PF \leq 100\% \tag{5.29}$$

For the problem formulation, there is no practical standard that needs to be followed when finding the optimal value of inductance, X_{LU}. However, the value of X_{LU} be selected to achieve the desired tuning so that the filter is resonant at the desired frequency. Therefore, the constraints for h given in $G(2)$ in the equations above which represents the values of X_{CU} and X_{LU} is given to find optimal inductance at the desired tuning frequency which can be calculated using Equation (3.6) given in Chapter 3. The value of f_n can be calculated by the multiplied value of h in Equations (3.6) with fundamental frequency as shown in the Equations (3.5).

5.3 System Under Study

There are four industrial plants with random harmonics that have been studied, in which the examples of the calculation for short circuit parameters are adopted from the IEEE 519-1992 system. A 60Hz fundamental frequency supply bus voltage determined at 4.16kV (line-to-line). Based on the system given in Figure 5.1, the settings for three-phase load power is set to 5100kW and three-phase load reactive power is set to 4965kVAR. Then, the calculations to find the short circuit and load parameters are performed and presented in Table 5.1.

Table 5.1: The input parameters and harmonic sources for simulation

Parameters & Harmonics	I	II	III	IV
MVA_{SC}	150	150	80	80
$R_{TH1}(\text{ohm})$	0.01154	0.01154	0.02163	0.02163
$X_{TH1}(\text{ohm})$	0.1154	0.1154	0.2163	0.2163
$R_{L1}(\text{ohm})$	1.742	1.742	1.742	1.742
$X_{L1}(\text{ohm})$	1.696	1.696	1.696	1.696
$V_{S1}(\text{Volts})$	2400	2400	2400	2400
$V_{S5}(\%V_{S1})$	5	7	5	7
$V_{S7}(\%V_{S1})$	3	4	3	4
$V_{S11}(\%V_{S1})$	2	2	2	2
$V_{S13}(\%V_{S1})$	1	1	1	1
$I_{L5}(\text{Ampere})$	33	33	33	33
$I_{L7}(\text{Ampere})$	25	25	25	25
$I_{L11}(\text{Ampere})$	8	8	8	8
$I_{L13}(\text{Ampere})$	9	9	9	9

For the first two rows in the Table 5.1 above show different power system parameters, following with the parameters of the load and then the following rows show the related source and load harmonics. For Case I and II, the system represents a system which has high short-circuit capacity which is 150MVA while Case III and IV represent the system with low short-circuit capacity which is 80 MVA. For the first scenario, such as Case I and II or Case III and IV, represents the system with the same short capacity and current harmonic distortion ($I_{L5} = 33A, I_{L7} = 25\text{A}, I_{L11} = 8\text{A}, I_{L13} = 9\text{A}$) but with different harmonics voltage supply ($V_{S5} = 120V, V_{S7} = 72\text{V}, V_{S11} = 48\text{V}, V_{S13} = 24\text{V}$) and ($V_{S5} = 168V, V_{S7} = 96\text{V}, V_{S11} = 48\text{V}, V_{S13} = 24\text{V}$), respectively.

For the second scenario, such as Case I and III or Case II and IV, represents the system with different short capacity but the same current harmonic distortion and harmonics voltage supply. The probabilistic of the harmonics voltage source and generated harmonic currents are randomly designated for all cases.

5.4 Simulated Results

5.4.1 Analysis of Simulated Results for Constrained Without Practical Values of Capacitor

In this research, four cases have been studied and simulated and the results for each case were compared. In addition to that, the performance when the system has a different short circuit with same voltage source harmonics and the effects on the performance for additional voltage source harmonics with the same short circuit capacity is analysed. Table 5.2 below is included to show the results performed for the uncompensated system and for the comparison purpose.

Table 5.2: The system performance before installing any filter

No. of Cases	I	II	III	IV
PF (%)	71.72	71.71	71.71	71.71
η (%)	99.34	99.34	98.78	98.78
P_{LOSS} (kW)	10.48	10.48	18.45	18.45
THD_V (%)	6.20	8.22	6.38	8.29
I_S (A)	953.03	953.17	923.58	923.71
dpf (%)	71.65	71.65	71.65	71.65
V_L (V)	2318.88	2322.26	2247.59	2355.48

Table 5.3 shows the simulated results for single-objective function considering all constraints, however, without the practical value of the capacitor. There are four objectives involved where problems of the objective functions is expressed as below:

Objective 1: Minimize $THD_V(X_{CU}, X_{LU})$

Subject to:

$G(1) = h \leq 0.9 * f_n$

$G(2) = h > h_r$

$G(3) = 0 \leq THD_V \leq 5\%$

$G(4) = 90\% \leq PF \leq 100\%$

Objective 2: Maximize $PF(X_{CU}, X_{LU})$

Subject to:

$G(1) = h \leq 0.9 * f_n$

$G(2) = h > h_r$

$G(3) = 0 \leq THD_V \leq 5\%$

$G(4) = 90\% \leq PF \leq 100\%$

Objective 3: Maximize $\eta(X_{CU}, X_{LU})$

Subject to:

$G(1) = h \leq 0.9 * f_n$

$G(2) = h > h_r$

$G(3) = 0 \leq THD_V \leq 5\%$

$G(4) = 90\% \leq PF \leq 100\%$

Objective 4: Minimize $P_{LOSS}(X_{CU}, X_{LU})$

Subject to:

$G(1) = h \leq 0.9 * f_n$

$G(2) = h > h_r$

$G(3) = 0 \leq THD_V \leq 5\%$

$G(4) = 90\% \leq PF \leq 100\%$

In this simulation, the settings for controlling parameter of MIDACO were set to 1) n_{pop} will change dynamically for every generation; 2) k is fixed to 100 and 3) $\Omega = 0$. From Table 5.3, the results show the impact of the designed filter on the different optimal solutions for each criterion are achieved subject to the constraints involved. When comparing Table 5.3 with Table 5.2, satisfying results are showing greatest improvement in the PF, η, P_{LOSS} and THD_V. It can be noticed that for Case I, PF is improved from 71.72%, to 95.30%, 95.21%, 97.16% and 96.04%, η is increased from 99.34% to 99.63%, 99.63%, 99.64% and 99.63%, P_{LOSS} is decreased from 10.48kW to 6.30kW, 6.28kW, 6.07kW and 6.15kW, THD_V is also reduced from 6.20% to 1.63%, 1.77%, 2.17% and 2.42%, respectively. For Case II, PF is improved from 71.71%, to 95.16%, 94.88%, 94.15% and 94.88%, η is increased from 99.34% to 99.62%, 99.62%, 99.62% and 99.62%, P_{LOSS} is decreased from 10.48kW to 6.51kW, 6.38kW, 6.45kW

and 6.37kW, THD_V is also reduced from 8.22% to 2.49%, 2.75%, 2.57% and 2.77%, respectively. For Case III, *PF* is improved from 71.71%, to 98.78%, 98.75%, 98.63% and 98.93%, η is increased from 98.78% to 99.35%, 99.35%, 99.35% and 99.35%, P_{LOSS} is decreased from 18.45kW to 10.98kW, 11.02kW, 10.92kW and 10.88kW, THD_V is reduced from 6.38% to 1.43%, 1.56%, 1.23% and 1.52%, respectively. For Case IV, *PF* is improved from 71.71%, to 97.04%, 97.91%, 97.14% and 97.91%, η is increased from 98.78% to 99.33%, 99.34%, 99.33% and 99.34%, P_{LOSS} is decreased from 18.45kW to 11.39kW, 11.01kW, 11.29kW and 11.08kW, THD_V is also reduced from 8.29% to 1.23%, 1.98%, 1.28% and 1.82%, respectively. Overall, the results proved that better performance is achieved subject to the constraints involved where all the resultant value of THD_V below 5%, as suggested in IEEE 519 standards and the *PF* is greater than 90% with the employment of the undamped single tuned filter.

Table 5.3: Simulated results without considering IEEE 18-2012 standards.

No. of Cases	X_{CU} (Ω)	X_{LU} (Ω)	*PF* (%)	η (%)	P_{LOSS} (kW)	THD_V (%)	I_S (A)	dpf (%)	V_L (V)
Minimize THD_V									
Case I	3.74	0.1459	95.30	99.63	6.30	1.63	738.74	99.95	2388.38
Case II	3.40	0.1615	95.16	99.62	6.51	2.49	750.91	99.72	2397.26
Case III	3.48	0.1607	98.78	99.35	10.98	1.43	712.61	99.88	2387.57
Case IV	3.42	0.1271	97.04	99.33	11.39	1.23	725.54	99.84	2388.77
Maximize *PF*									
Case I	4.11	0.1663	95.21	99.63	6.28	1.77	737.48	99.37	2381.83
Case II	3.62	0.1777	94.88	99.62	6.38	2.75	743.78	99.99	2392.49
Case III	3.42	0.1686	98.75	99.35	11.02	1.56	713.88	99.75	2390.91
Case IV	3.88	0.1880	97.91	99.34	11.01	1.98	715.50	99.85	2372.28
Maximize η									
Case I	3.71	0.1783	97.16	99.64	6.07	2.17	725.48	99.99	2390.10
Case II	3.91	0.1811	94.15	99.62	6.45	2.57	747.53	99.80	2386.16
Case III	3.72	0.1492	98.63	99.35	10.92	1.23	710.38	99.88	2376.89
Case IV	3.60	0.1328	97.14	99.33	11.29	1.28	722.47	99.99	2381.17
Minimize P_{LOSS}									
Case I	4.45	0.2150	96.04	99.63	6.15	2.42	730.02	98.53	2377.30
Case II	3.71	0.1817	94.88	99.62	6.37	2.77	743.11	99.99	2390.39
Case III	3.67	0.1719	98.93	99.35	10.88	1.52	709.30	99.99	2379.90
Case IV	3.77	0.1766	97.91	99.34	11.08	1.82	715.65	99.96	2376.22

From Table 5.3 above, the improvement to the value of THD_V in the compensated system has proved that the quality of the load voltage also heightened for all cases. Therefore, the results in the table indicate that V_L is increased from 2318.88V to 2388.38V, 2381.83V, 2390.10V and 2377.30V for Case I, from 2322.26V to 2397.26V, 2392.49V, 2386.16V and 2390.39V for Case II, from 2247.59V to 2387.57V, 2390.91V, 2376.89V and 2379.90V for Case III and lastly from 2355.48V to 2388.77V, 2372.28V, 2381.17V and 2376.22V for Case IV, respectively.

Next, the results also show that the compensated system leads to the reduction in the rms value of supply current where I_s is decreased from 953.03A to 738.74A, 737.48A, 725.48A and 730.02A for Case I, while from 953.17A to 750.91A, 743.78A, 747.53A and 743.11A for Case II, accordingly. For Case III, the I_s is reduced from 923.58A to 712.61A, 713.88A, 710.38A and 709.30A and from 923.17A to 725.54A, 715.50A, 722.47A and 725.65A for Case IV, respectively. This is because the system has become more linear after added the filter, which results in the reduction to the line current.

Additionally, the results also proved that dpf is increased for the compensated system from 71.65% to 99.95%, 99.37%, 99.99 and 98.53% for Case II, from 71.65% to 99.88%, 99.75%, 99.88 and 99.99% for Case II, from 71.65% to 99.88%, 99.75%, 99.88 and 99.99% for Case III and from 71.65% to 99.84%, 99.85%, 99.99 and 99.96% for Case IV, respectively. Overall, it is expected that the value of *PF* is lower than dpf because of the effects of the harmonic is excluded in the calculation of dpf which therefore has no direct effects to the results.

5.4.2 Analysis of Simulated Results for Constrained with Practical Values of Capacitor

The capacitor produced from the optimal solution presented in Table 5.3 does not lie within the practical standard. Therefore, it is recommended to consider IEEE-18 for power shunt capacitors in order to solve the optimal solutions.

Table 5.4 summarised simulated results while including the actual value of the capacitor in the constraints. The objective functions and all constraints involved are based on the formulation in Equation (5.12)-(5.15). For this simulation, the MIDACO controlling parameters are remaining constant. However, for each objective, the algorithm was run

with 100 different SEED parameters and the best solution out of a reasonable number of runs was chosen. From Table 5.4, the results show that different SEED values will results in different optimal filter solutions obtained for each of the objective functions. This is because of the highly sensitive nature of the internal random number generator which impies to different results.

Table 5.4: Simulated results considering all the constraints involved.

No. of Cases	SEED	X_{CU} (Ω)	X_{LU} (Ω)	PF (%)	η (%)	P_{LOSS} (kW)	THD_V (%)	I_S (A)	dpf (%)
Minimize THD_V									
Case I	7	3.32	0.1513	96.27	99.6342	6.230	1.865	723.81	99.89
Case II	25	3.40	0.1615	94.16	99.6176	6.506	2.485	750.91	99.72
Case III	27	3.48	0.1607	98.78	99.3507	10.984	1.428	734.73	99.54
Case IV	45	3.48	0.1654	97.85	99.3382	11.201	1.764	750.91	99.72
Maximize *PF*									
Case I	11	3.85	0.1900	97.28	99.6417	6.045	2.315	724.72	99.99
Case II	44	3.85	0.1889	94.91	99.6236	6.354	2.850	742.04	99.90
Case III	55	3.48	0.1699	98.85	99.3516	10.974	1.559	723.81	99.89
Case IV	25	3.65	0.1805	98.09	99.3414	11.083	1.962	742.04	99.90
Maximize η									
Case I	35	3.65	0.1805	97.32	99.6419	6.061	2.248	723.96	99.76
Case II	70	3.95	0.1951	94.91	99.6235	6.345	2.923	741.50	99.76
Case III	55	3.75	0.1829	98.97	99.3531	10.847	1.642	724.72	99.99
Case IV	8	3.95	0.1950	97.89	99.3387	11.028	2.073	741.50	99.76
Minimize P_{LOSS}									
Case I	67	3.95	0.1951	97.18	99.6409	6.048	2.350	734.73	99.54
Case II	49	3.85	0.1900	94.98	99.6241	6.345	2.880	741.55	99.90
Case III	22	4.18	0.1922	98.27	99.3439	10.868	1.682	723.96	99.76
Case IV	91	4.06	0.1980	97.67	99.3358	11.042	2.068	741.55	99.90

By referring to Table 5.3 and 5.4, the results for the same values of Thevenin's impedance with different harmonics, such as Case I and II, will reduce the power factor of the cases that have additional harmonics. By comparing the results Case I with Case II in Table 5.4, *PF* is reduced from 96.27% to 94.16% for Min THD_V, from 97.28% to 94.91% for Max *PF*, from 97.32% to 94.91% for Max η and from 97.18% to 94.98% for Min P_{LOSS}. This is predictable because extra harmonics will result in an increasing number of compensated line current across the load. Therefore, the increasing

compensated line current will increase the THD_V, causing more losses in the impedance at the source and reduce the efficiency of transmission. This is shown in the results of Case I and II in Table 5.4, THD_V is increased from 1.865% to 2.485% for Min THD_V, from 2.315% to 2.850% for Max *PF*, from 2.248% to 2.923% for Max η and from 2.350% to 2.880% for Min P_{LOSS}. Besides, P_{LOSS} also increased from 6.230% to 6.506% for Min THD_V, from 6.045% to 6.354% for Max *PF*, from 6.061% to 6.345% for Max η and from 6.048% to 6.345% for Min P_{LOSS}. Therefore, η is reduced from 99.6342% to 99.6176% for Min THD_V, from 99.6417% to 99.6236% for Max *PF*, from 99.6419% to 99.6235% for Max η and from 99.6409% to 99.6241% for Min P_{LOSS}. Overall, the additional harmonics affect the performance of the circuit.

For the cases in which harmonics condition is identical but different short circuit, such as Case I and III, higher transmission impedance will increase of the power factor. By comparing the results Case I with Case III in Table 5.4, *PF* is increased from 96.27% to 98.78% for Min THD_V, from 97.28% to 98.85% for Max *PF*, from 97.32% to 98.97% for Max η and from 97.18% to 98.27% for Min P_{LOSS}. Conversely, low short circuit capacity has bigger Thevenin impedance where overall the results to lower THD_V, more losses in the source and hence degrade the efficiency. From Table 5.4, the comparison of results between Case I and III show that THD_V is increased from 1.865% to 1.428% for Min THD_V, from 2.315% to 1.559% for Max *PF*, from 2.248% to 1.642% for Max η and from 2.350% to 1.682% for Min P_{LOSS}. Besides, P_{LOSS} also increased from 6.230% to 10.984% for Min THD_V, from 6.045% to 10.974% for Max *PF*, from 6.061% to 10.847% for Max η and from 6.048% to 10.868% for Min P_{LOSS}. Therefore, η is reduced from 99.6342% to 99.3507% for Min THD_V, from 99.6417% to 99.3516% for Max *PF*, from 99.6419% to 99.3531% for Max η and from 99.6409% to 99.3439 % for Min P_{LOSS}. Generally, the resultants of THD_V values for all cases are not exceeding the standard limitation and the value of the capacitor can be attained from the real market as well. When comparing Table 5.4 with Table 5.3, the results proved that the size of the capacitor has no consequence to the result of the optimal solutions.

Table 5.5 shows the simulated results when controlling parameters Ants and Kernel when the objectives maximize *PF*.

Table 5.5: Simulated results with different setting of ants and kernel

Setting	Parameters		THD_V (%)			
	Ants	Kernel	I	II	III	IV
1	2	2	2.46	3.09	1.84	1.98
2	30	5	2.11	3.32	2.15	3.07
3	500	10	2.13	2.65	1.55	4.95
4	100	50	3.01	2.87	3.78	2.40
5	0	100	2.32	2.85	1.56	1.96
Setting	Parameters		*PF* (%)			
	Ants	Kernel	I	II	III	IV
1	2	2	96.19	93.68	98.07	97.32
2	30	5	95.45	92.06	93.97	88.88
3	500	10	93.41	92.61	98.15	89.84
4	100	50	90.12	93.61	95.51	93.09
5	0	100	97.28	94.91	98.85	98.09
Setting	Parameters		η (%)			
	Ants	Kernel	I	II	III	IV
1	2	2	99.63	99.61	99.34	97.33
2	30	5	99.63	99.60	99.28	99.20
3	500	10	99.61	99.60	99.34	99.22
4	100	50	99.58	99.61	99.31	99.27
5	0	100	99.64	99.62	99.35	99.34
Setting	Parameters		P_{LOSS} (kW)			
	Ants	Kernel	I	II	III	IV
1	2	2	6.13	6.46	10.89	11.09
2	30	5	6.22	6.65	11.58	12.72
3	500	10	6.46	6.61	10.89	12.65
4	100	50	6.87	6.48	11.47	11.80
5	0	100	6.05	6.35	10.97	11.08

From Table 5.5, the results have shown that tuning the parameters of Ants and Kernel will reduce the chance of getting the best solutions for the results from getting the best solutions. From the table, it shows a small kernel, as Setting 1, will result in the solutions trapped in the local solution. With increasing the size of kernel correspondingly, the chance of the solutions to reach the global optimum also increases. However, the optimal solutions cannot be reached without proper adjustment of both parameters if the sizes of ants are changed.

Next, the impact of changing the Oracle parameter on the optimal solutions is shown in Table 5.6. For this test, the simulation is based on maximizing *PF*, given that only the Oracle parameter is changed while other parameters remain the same. As mentioned in the previous chapter, this parameter will select equal or slightly better optimal (feasible) solutions. Therefore, from the table, the results proved that changing the Oracle parameter would not affect the optimal solution.

Table 5.6: Simulated results with a different Oracle parameter for all cases

Parameters	THD_V (%)			
Oracle	I	II	III	IV
1	2.32	2.85	1.56	1.96
3	2.32	2.85	1.56	1.96
6	2.32	2.85	1.56	1.96
Parameters	*PF* (%)			
Oracle	I	II	III	IV
1	97.28	94.91	98.85	98.09
3	97.28	94.91	98.85	98.09
6	97.28	94.91	98.85	98.09
Parameters	η (%)			
Oracle	I	II	III	IV
1	99.64	99.62	99.35	99.34
3	99.64	99.62	99.35	99.34
6	99.64	99.62	99.35	99.34
Parameters	P_{LOSS} (kW)			
Oracle	I	II	III	IV
1	6.05	6.35	10.97	11.08
3	6.05	6.35	10.97	11.08
6	6.05	6.35	10.97	11.08

Table 5.7 showed the effects on the results of THD_V, *PF*, η and P_{LOSS} when the total of iterations is increased for the optimisation when the objective was maximizing *PF*. From the table, it also pointed out that there is a higher chance to obtain optimal solutions when hard limit criteria of maximum function evaluation are increased.

Table 5.7: Simulated results when increasing number of iterations

Parameters	THD_V (%)			
Number of iterations	I	II	III	IV
1000	8.67	12.16	1.54	3.99
5000	3.66	3.40	1.42	1.68
10000	2.32	3.52	1.22	1.88
Parameters	*PF* (%)			
Number of iterations	I	II	III	IV
1000	80.34	76.41	96.79	82.07
5000	83.75	86.36	96.87	95.88
10000	97.28	91.18	97.33	98.02
Parameters	η (%)			
Number of iterations	I	II	III	IV
1000	99.48	99.43	99.32	99.06
5000	99.52	99.55	99.33	99.31
10000	99.64	99.59	99.33	99.34
Parameters	P_{LOSS} (kW)			
Number of iterations	I	II	III	IV
1000	8.48	9.30	11.56	14.58
5000	7.85	7.45	11.54	11.41
10000	6.05	6.75	11.41	1.88

Thus, Figure 5.4 is also added for a clear explanation of the convergence rate. From Figure 5.4a, the results show that the objective function for THD_V at 1000th iterations is 10.82% can reduce down to 1.45% when the iterations reach 20000. While the graph of objective function when maximize *PF* is shown in Figure 5.4b, where the objective is 82.65% at 1000th iterations and is increased up to 96.83% when the iterations reached to its maximum. Based on Figure 5.4c, the results show that the objective function for maximizing η at 1000th iterations is 99.53 % can increased up to 99.63% when the objective function reach up 20000 of maximum function evaluations. Lastly, Figure 5.4d shows that the objective function reduced from 7620.11kW to 6119.89kW when the iterations increased from 1000 and reached to 20000 number of iterations. Overall, the results proved that there would be a chance for the objective function to reach its optimality by increasing the hard limit criteria of maximum function evaluation.

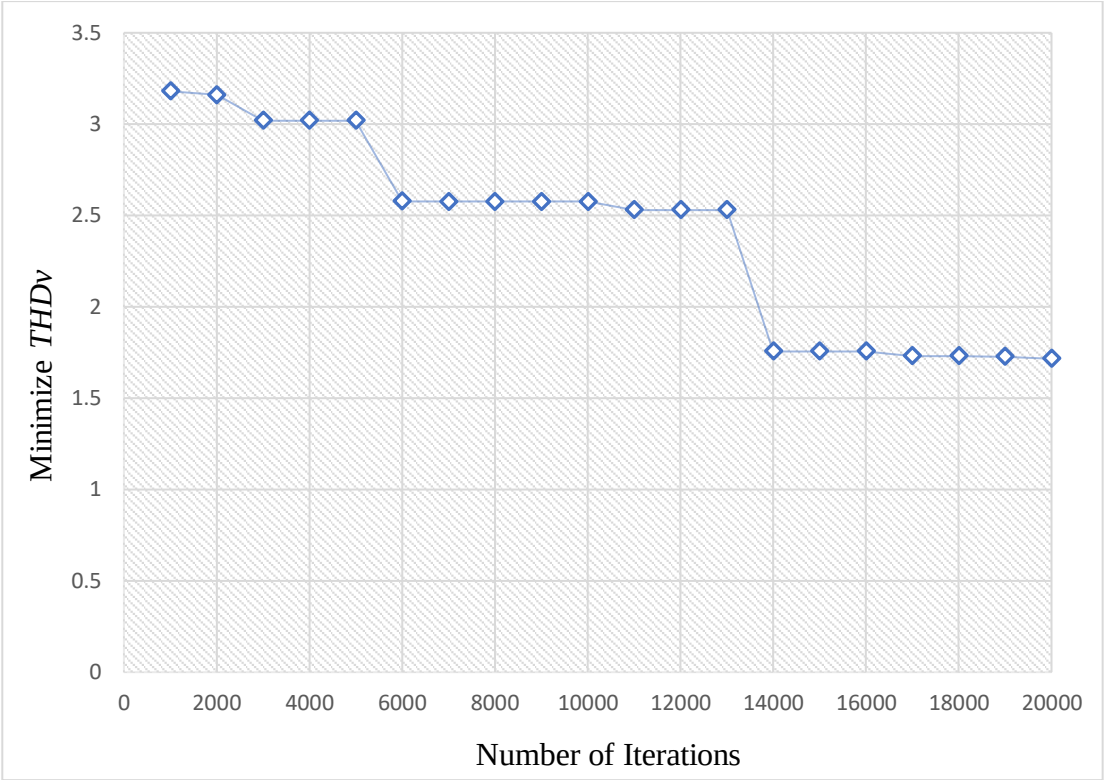

a) Objective 1

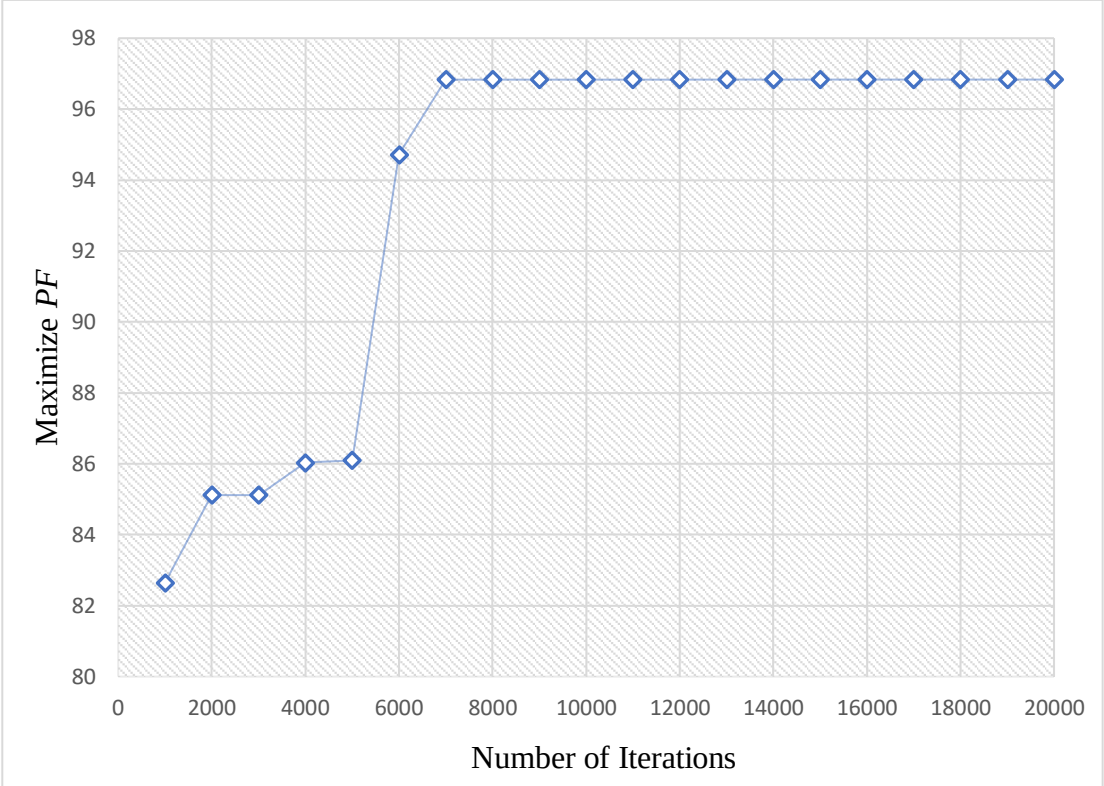

b) Objective 2

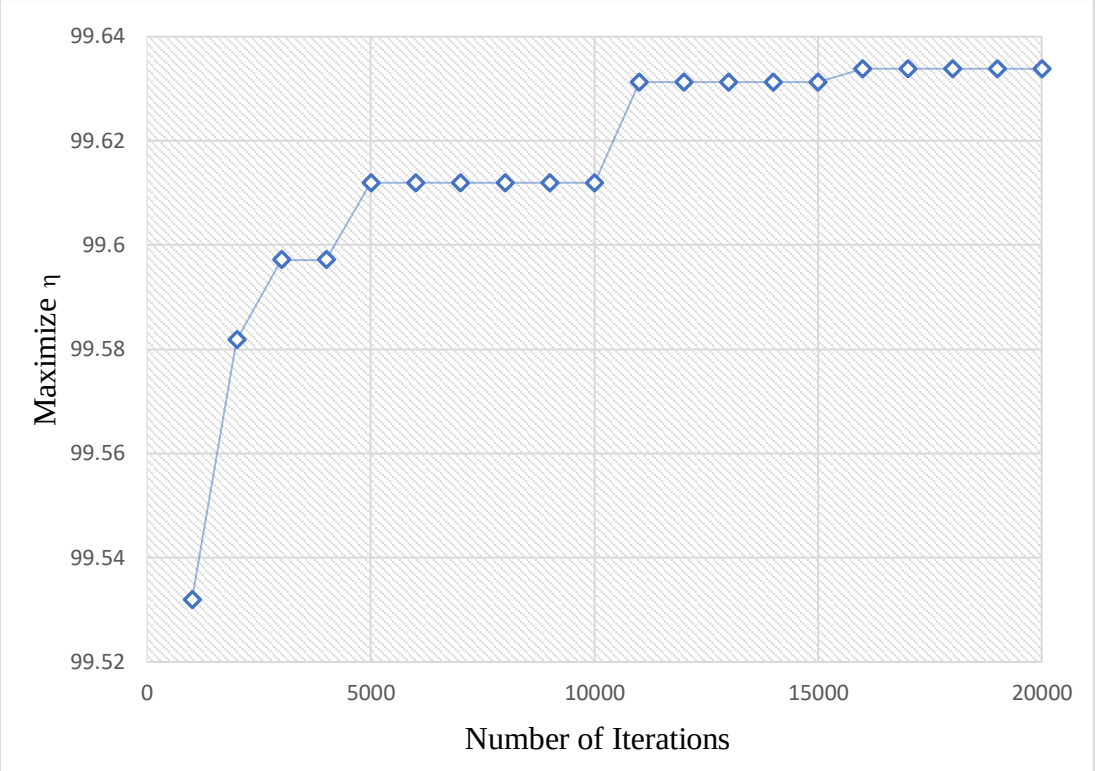

c) Objective 3

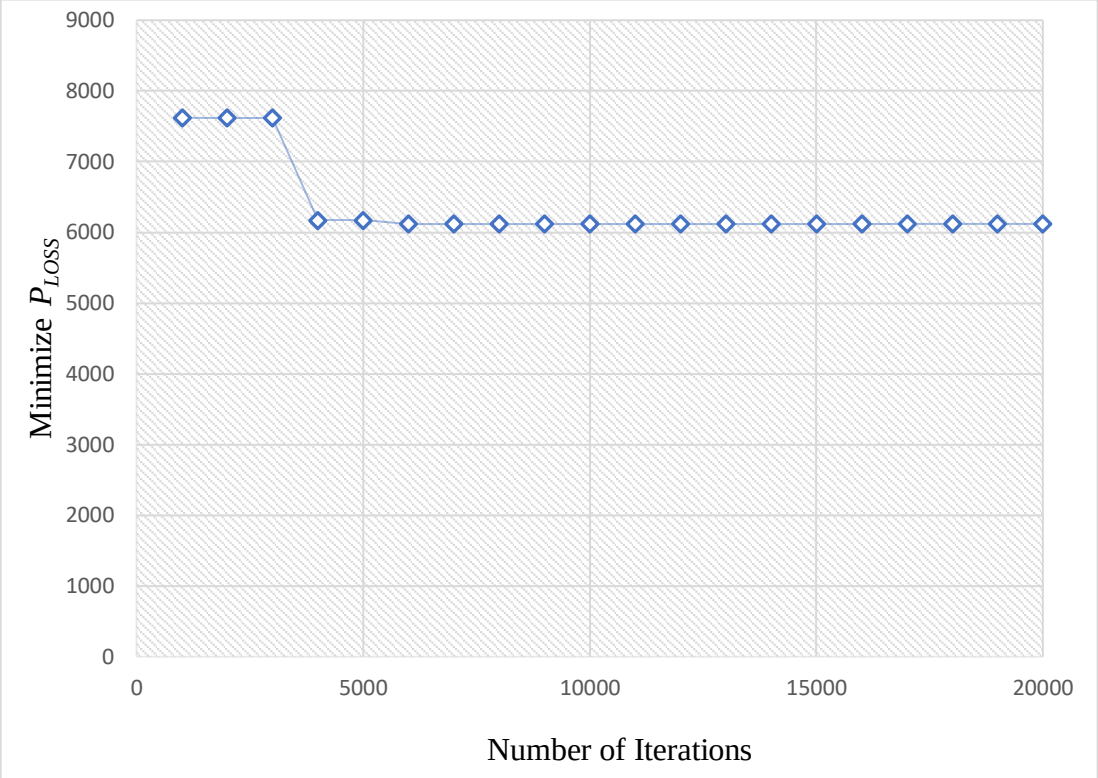

d) Objective 4

Figure 5.4: The convergence graph for Case 1 a) min THD_V b) max PF, c) max η, and d) min P_{LOSS}

Table 5.8 presents the results for the current source and load voltage for individual harmonics. From the table, the results showed that harmonic current I_{SK} is higher in the case that has the same values of Thevenin's impedance with extra supply voltage harmonic, such as Case III and IV. The increasing value I_{SK} will also result in the high value of V_{LK} which consequently gain more power source to be supplied to the load. On the other hand, small values of I_{SK} are supplied for a power system that has large values of Thevenin's impedance. Overall, this will result to lower V_{LK} as well as the load power consumption.

Table 5.8: The results for current source and load voltage for individual harmonics

Harmonic order, K	Minimize THD_V		Maximize PF		Maximize η		Minimize P_{LOSS}	
	I_{SK} (%)	V_{LK} (%)	I_{SK} (%)	V_{LK} (%)	I_{SK} (%)	V_{LK} (%)	I_{SK} (%)	V_{LK} (%)
Case I								
5	25.29	0.69	22.62	1.19	22.87	1.14	22.50	1.21
7	7.57	1.27	6.86	1.49	6.99	1.45	6.79	1.50
11	2.72	1.02	2.47	1.14	2.52	1.12	2.44	1.15
13	1.28	0.59	1.22	0.65	1.24	0.64	1.22	0.66
Case II								
5	33.75	1.26	31.87	1.62	31.46	1.69	31.65	1.66
7	9.68	1.76	9.06	1.94	8.92	1.98	9.02	1.95
11	2.65	1.06	2.48	1.14	2.44	1.15	2.47	1.14
13	1.26	0.61	1.23	0.65	1.22	0.66	1.22	0.65
Case III								
5	14.35	0.47	13.83	0.64	13.79	0.68	13.93	0.64
7	4.95	0.96	4.84	1.02	4.78	1.08	4.72	1.12
11	1.88	0.78	1.84	0.81	1.81	0.85	1.77	0.89
13	0.90	0.54	0.89	0.57	0.90	0.59	0.89	0.62
Case IV								
5	18.98	0.79	19.49	0.86	21.56	0.12	19.12	0.99
7	5.58	1.66	6.36	1.33	6.39	1.29	6.17	1.44
11	1.57	1.03	1.83	0.83	1.78	0.86	1.77	0.89
13	0.85	0.72	0.90	0.58	0.88	0.61	0.89	0.62

Meanwhile, Table 5.9 is added to ensure that the proposed capacitor is intended to operate without exceeding the limit suggested by IEEE 18-2012 [199]. From the table, the results show that the values of V_{CP}, V_C, I_C and Q_C for all of the cases are below the recommended standard limit.

Table 5.9: The recommended limit for the power shunt capacitor

Objective Function	V_{CP} (%)	V_C (%)	I_C (%)	Q_C (%)
Case I				
Minimize THD_V	68.01	90.82	98.14	87.44
Maximize PF	68.02	90.76	98.16	87.34
Maximize η	67.99	90.90	98.10	87.55
Minimize P_{LOSS}	68.04	90.68	98.20	87.24
Standard	120	110	135	135
Case II				
Minimize THD_V	69.33	91.03	100.51	88.50
Maximize PF	69.45	90.83	100.86	88.30
Maximize η	69.48	90.79	100.95	88.27
Minimize P_{LOSS}	69.42	90.86	100.80	88.33
Standard	120	110	135	135
Case III				
Minimize THD_V	66.35	90.40	95.99	86.12
Maximize PF	66.44	90.66	96.18	86.60
Maximize η	66.29	90.25	95.89	85.85
Minimize P_{LOSS}	66.09	89.56	95.46	84.63
Standard	120	110	135	135
Case IV				
Minimize THD_V	67.35	88.11	97.73	83.06
Maximize PF	67.14	90.36	96.89	86.33
Maximize η	67.17	88.50	97.18	83.49
Minimize P_{LOSS}	67.05	89.88	96.74	85.52
Standard	120	110	135	135

Finally, the filter must be tuned below the harmonic frequency to be eliminated when adding the filter into the power circuit. Therefore, Figure 5.5 is added to illustrate the impedance resonance for Case I, which has been recommended in this research in order to avoid any series or parallel resonance. The graph of the response is assessed and evaluated as follows:

1) The series or parallel resonance can happen because of the interaction between the impedance at the source and the loads.
2) The impedance is at the lowest point when the reactance of inductance is equal to the capacitance for the series resonance, thus canceling each other out. However, the impedance is at maximum for parallel resonance.
3) For both resonances, the frequencies after the tuning are increased along with the impedance.
4) It is vital to consider detuning effects when designing this type of filter. This is clearly shown in the sharp increase of in impedance in Figure 5.5 where the parallel resonance causes a sudden increase in voltage.
5) This can also happen to series resonance where the small value of resistance at resonance wills results in the current flowing through the circuit to be dangerously high.
6) Overall, the design of a de-tuned filter to avoid series or parallel resonance is very important to protect the circuit from damage.

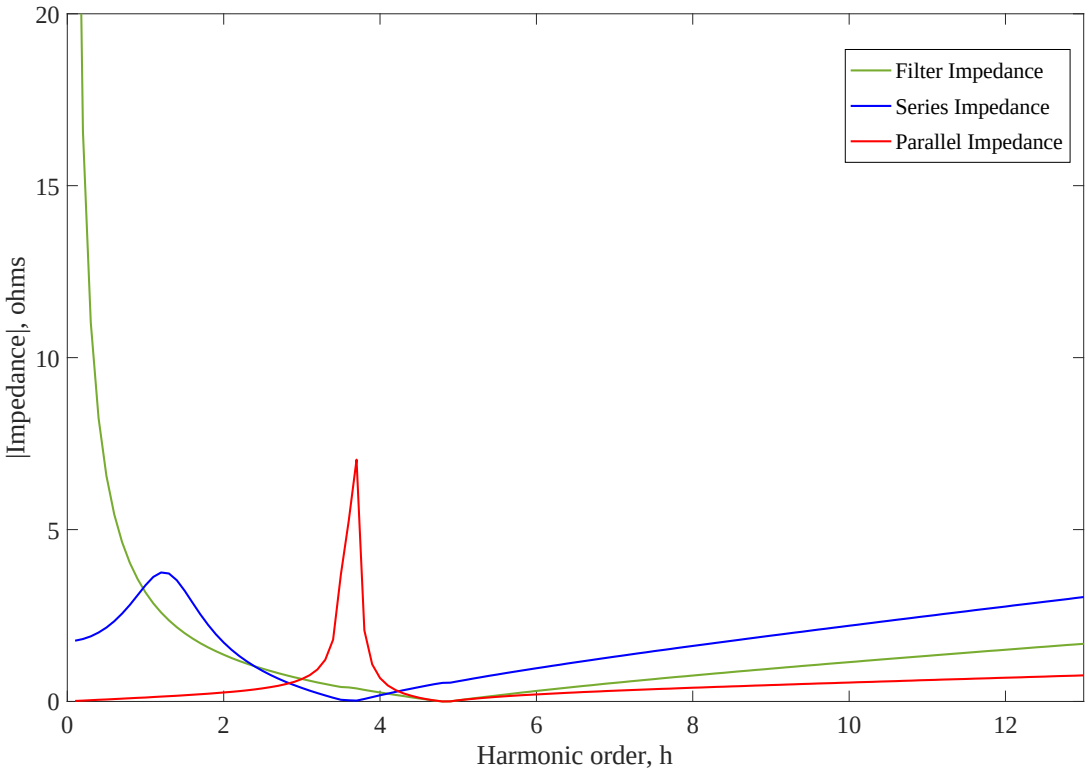

a) Minimize THD_V

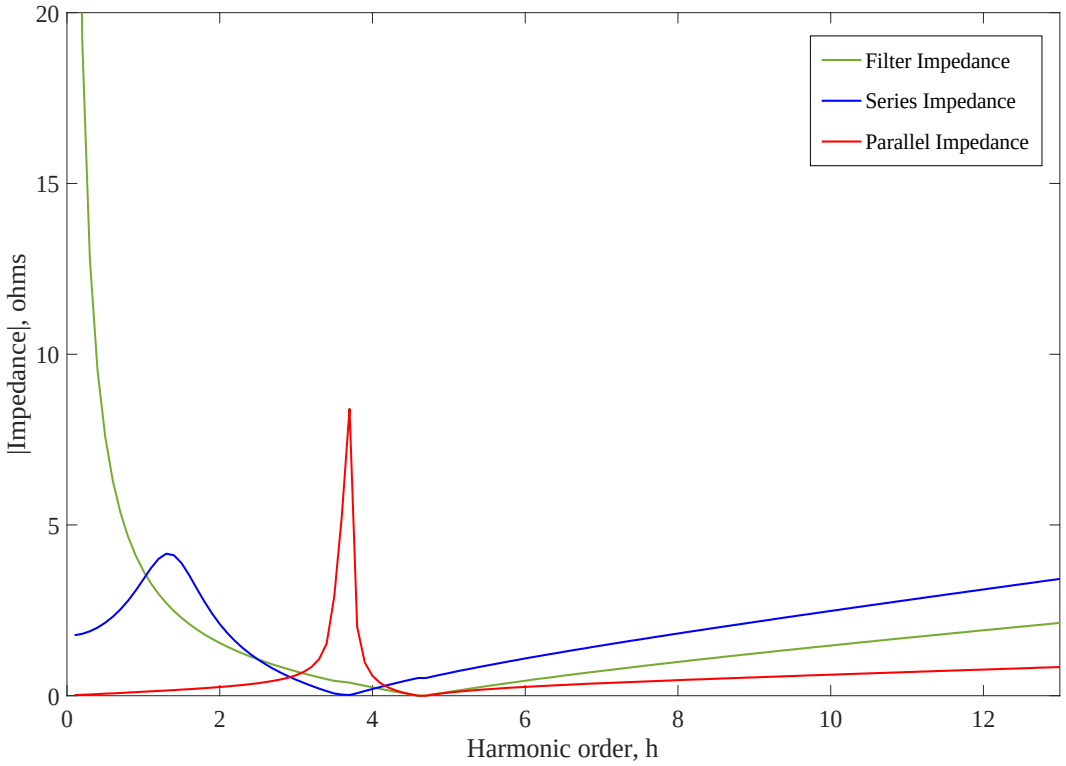

b) Maximize *PF*

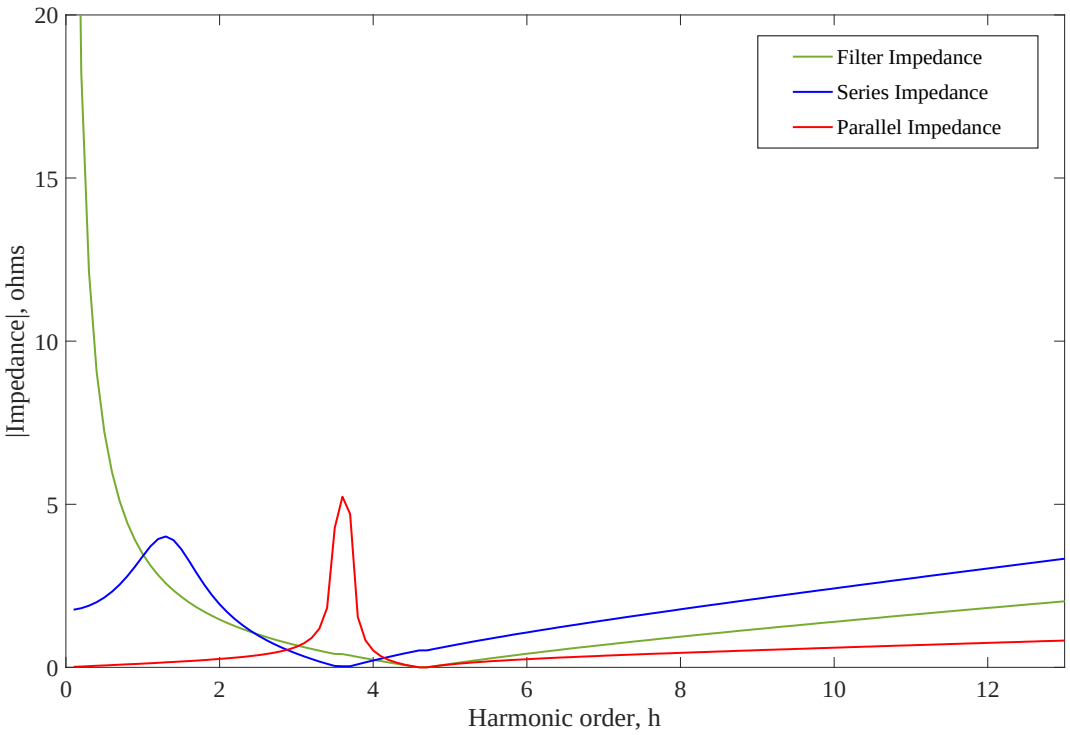

c) Maximize η

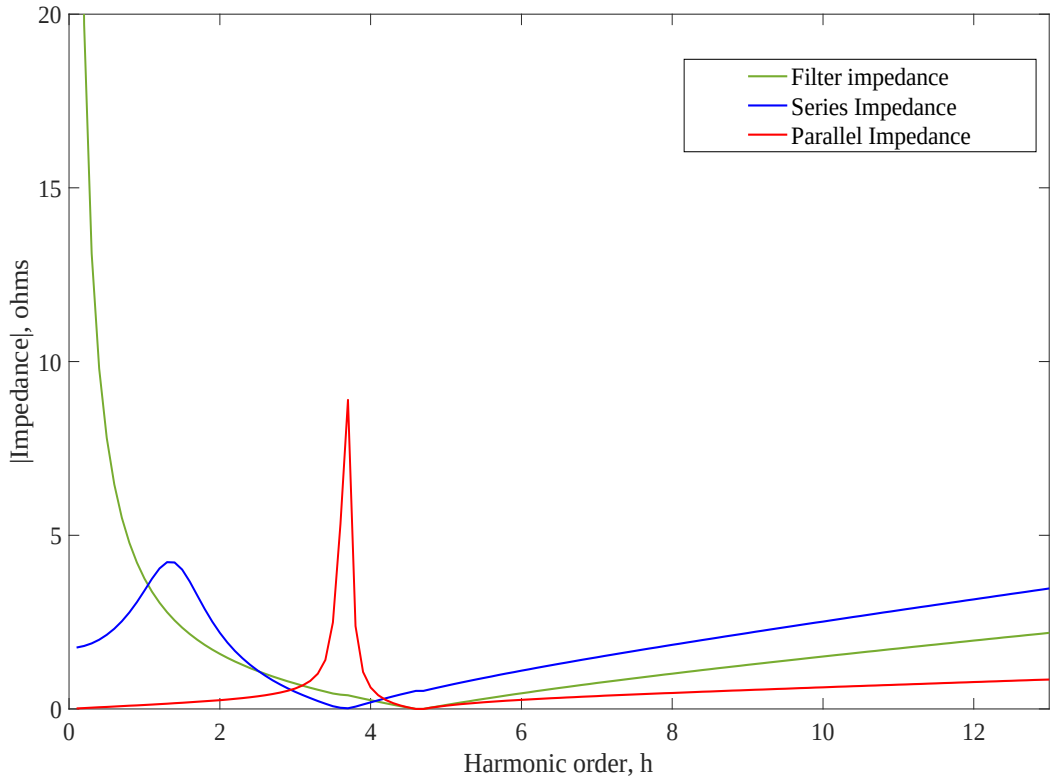

d) Minimize P_{LOSS}

Figure 5.5: The filter, series and parallel impedance resonance for Case I based on four objectives

5.5 Comparison of Results with Other Published Techniques

In this study, the capability of the suggested technique is compared with other two evolutionary computation optimizers [204], [205]. There are three objectives involved in this comparison which are maximizes *PF*, η and Minimize P_{LOSS}.

In GA, the optimization is inspired by relying on bio-inspired operators [204]. After generating a random initial population, then GA will select group of individuals (parents) from the current population who contributes their genes to produce children, in order to form the next generation [206].

Table 5.10 shows the outcome of the result when simulated using GA based on the problem formulation in Equation (5.26). For GA, the crossover rate, mutation probability, and population size are set to 0.8, 0.001 and 50 respectively.

Table 5.10: The simulation outcomes when using GA

Objective Function	X_{CU} (Ω)	X_{LU} (Ω)	*PF* (%)	η (%)	P_{LOSS} (kW)	THD_V (%)
Maximize *PF*						
Case I	4.18	0.2062	96.83	99.64	6.07	2.42
Case II	4.87	0.2406	93.14	99.61	6.51	2.99
Case III	4.18	0.2062	98.36	99.35	10.85	1.80
Case IV	4.18	0.2062	97.49	99.33	11.05	2.16
Maximize η						
Case I	5.41	0.2673	93.49	99.61	6.43	2.77
Case II	6.09	0.3008	90.07	99.58	6.90	2.88
Case III	4.87	0.2406	96.38	99.32	11.13	1.99
Case IV	4.71	0.2328	96.06	99.31	11.25	2.34
Minimize P_{LOSS}						
Case I	4.87	0.2406	95.07	99.62	6.25	2.63
Case II	5.22	0.2577	92.25	99.60	6.62	3.23
Case III	4.87	0.2406	96.38	99.32	11.14	1.99
Case IV	5.04	0.2489	95.07	99.30	11.42	2.45

When comparing Table 5.10 with Table 5.4, the results show that the proposed method has improved the overall performance when compared to the consequences for GA in

Case I and II. Apart from that, the proposed method might also have several benefits over GA for the cases that have additional of losses with high Thevenin's impedance, such as Case III and IV. Overall, the results showed that the results of THD_V is higher than the proposed method, which ultimately proves that the proposed technique has a better performance.

PSO algorithm initialises with random initial population and updated generations in order to search for optima. The population members which is referred to by the term "particles" will change the accelerations and velocities, where small volume results in an enhanced direction of behaviour [147], [205]. From modified velocity, the particles will update their positions.

In PSO, the searching procedure is based on modified velocity, V_i^{k+i} and position updates, X_i^{k+1} where *Pbest* and *Gbest.* will be updated first before continuing the searching which can be described as below:

$$V_i^{k+i} = \omega_0 V_i^k + C_1 rand_1 \times \left(Pbest_i^k - X_i^k\right) + C_2 rand_2 \times \left(Gbest_i^k - X_i^k\right) \quad (5.27)$$

$$X_i^{k+1} = X_i^k + V_i^{k+i} \quad (5.28)$$

Where $\omega_0 =$ An inertia weight (ranging between 0 to 1)

C_1 and $C_2 =$ Cognitive and social attraction (range $0 < C_1 + C_2 < 4$)

$rand_1$ and $rand_2 =$ Two random sequences (ranging between 0 to 1)

$X_i^k =$ Current position of individual *i* at iteration *k*

$V_i^k =$ Current velocity of individual *i* at iteration *k*

$Pbest =$ Fitness best solution tracked in the population

$Gbest =$ Fitness best value tracked in the population

PSO also possesses an excellent memory, which is the key advantage of this algorithm. However, the disadvantage of PSO which depending on the initial point and parameters make it difficult for the algorithm to find their optimal solution.

Table 5.11 shows the simulation results based on the problem in Equation (5.26) when using PSO. For PSO simulation, some limitations are requiring to be set as follows:

a) Cognitive and social attraction, C_1 and $C_2 = 1.0$
b) Inertia weight, $0.4 \leq C_0 \leq 0.9$
c) Population size, $n = 50$
d) Maximum iterations, $iter_{max} = 200$

Table 5.11: The simulation outcomes when using PSO

Objective Function	X_{CU} (Ω)	X_{LU} (Ω)	PF (%)	η (%)	P_{LOSS} (kW)	THD_V (%)
Maximize PF						
Case I	3.95	0.3587	99.28	99.66	5.82	4.09
Case II	3.95	0.3006	98.01	99.65	5.97	4.83
Case III	3.65	0.4098	99.48	99.36	10.88	3.63
Case IV	3.74	0.3843	99.33	99.36	10.97	4.48
Maximize η						
Case I	5.04	0.2562	94.77	99.62	6.28	2.79
Case II	4.06	0.2418	96.53	99.64	6.13	3.91
Case III	5.22	0.3030	95.64	99.31	11.88	2.59
Case IV	4.55	0.2437	94.99	99.30	11.43	2.36
Minimize P_{LOSS}						
Case I	4.18	0.4060	99.19	99.66	5.81	4.30
Case II	4.06	0.4486	99.06	99.65	5.85	5.91
Case III	4.30	0.4310	99.28	99.36	10.70	3.67
Case IV	4.30	0.4272	98.97	99.35	10.77	4.69

The results from the between Table 5.3 with Table 5.10 and 5.11, has shown that tuning of the initial condition of the inductance and capacitance will affect the effective solutions. Besides, the table also showed that the PSO is less accurate since the value of the filter's inductance is large compared to the proposed method and GA for all three objectives in all cases. Besides, the results for Case II also showed that the PSO optimiser is not satisfied with the involved constraints where the value of THD_V is beyond 5% as suggested by the IEEE 519 standard.

Table 5.12 shows the estimation between the maximum number of evaluations and the time taken to complete simulations for each objective for all cases. From the results, the proposed method has shown that it has the shortest computation time, it can complete

the simulations within 17s to 18s when optimising up to 20 000 function evaluation. The second fastest is PSO where it can process up to 50 iterations within 7s to 11s while GA is the slowest where it will take up to 120s to process a maximum of 8 iterations.

Table 5.12: The computation time up to the maximum function evaluation

Objective Function	Running Time, t/s			Function Evaluation		
	Proposed	GA	PSO	Proposed	GA	PSO
Case I						
Maximize *PF*	21	54.21	7.53	20 000	3	50
Maximize η	21	67.49	7.12	20 000	6	50
Minimize P_{LOSS}	22	33.98	8.31	20 000	4	50
Case II						
Maximize *PF*	21	69.27	10.50	20 000	4	50
Maximize η	21	84.58	9.12	20 000	5	50
Minimize P_{LOSS}	22	38.02	8.76	20 000	4	50
Case III						
Maximize *PF*	22	43.68	7.92	20 000	5	50
Maximize η	22	86.17	6.93	20 000	8	50
Minimize P_{LOSS}	22	23.94	9.13	20 000	4	50
Case IV						
Maximize *PF*	21	36.47	7.81	20 000	5	50
Maximize η	22	119.29	7.34	20 000	8	50
Minimize P_{LOSS}	22	35.67	8.51	20 000	4	50

Table 5.13 shows the comparison of statistical test based on the objective function when maximizing *PF* for all methods. From Table 5.13, it is observable that the proposed method has a significant standard deviation, followed by GA and PSO respectively. This is beneficial especially during the existence of resonance because it is essential to return different values to avoid resonances. Unlike GA and PSO, the methods have small variants which are challenging to differentiate visually.

Table 5.13: The statistical tests based on Objective 2

Techniques	Maximize *PF*				
	Minimum	Maximum	Mean	Middle	Standard Deviation
Case I					
Proposed	82.6462	96.8334	93.7704	96.8334	5.2531
GA	96.9612	97.8850	97.3013	97.0578	0.5078
PSO	98.8990	98.8993	98.8992	98.8992	0.0001
Case II					
Proposed	79.4589	94.3707	91.1680	93.3035	4.6314
GA	96.5421	94.2012	94.5491	94.2021	0.8841
PSO	98.0259	98.0336	98.0311	98.0319	0.0019
Case III					
Proposed	85.9370	97.1883	94.7749	93.8998	4.8013
GA	99.0107	99.0549	99.0200	99.0110	0.0195
PSO	99.4066	99.4146	99.4143	99.4145	0.0013
Case IV					
Proposed	84.7486	97.0741	95.1597	96.9988	4.2046
GA	98.0911	98.2382	98.1220	98.0938	0.0650
PSO	98.9253	98.9397	98.9393	98.9397	0.0023

Table 5.14 shows the comparison of harmonic tuning order for the proposed method with other techniques. From Table 5.15, the results showed that the optimal filter satisfied the resonance constraints that have been considered in this study. In contrast, all the harmonic order is below the desired harmonic to be eliminated. Besides, the results also showed that the value of h_r is always lower than h. The design gives advantages to the system where it provides sufficient harmonic filtering action to avoid detuning effects.

Table 5.14: Comparison of tuning harmonic order for all methods

Objective Function	Proposed		GA		PSO	
	h	h_r	h	h_r	h	h_r
I						
Maximize *PF*	4.50	3.55	4.50	3.60	3.32	2.89
Maximize η	4.50	3.51	4.50	3.76	4.43	3.68
Minimize P_{LOSS}	4.50	3.95	4.50	3.70	3.21	2.83
II						
Maximize *PF*	4.51	3.56	4.50	3.70	3.62	3.08
Maximize η	4.50	3.57	4.50	3.83	4.10	3.37
Minimize P_{LOSS}	4.50	3.55	4.50	3.74	3.01	2.68
III						
Maximize *PF*	4.53	3.00	4.50	3.14	2.99	2.42
Maximize η	4.53	3.01	4.50	3.27	4.15	3.17
Minimize P_{LOSS}	4.60	3.18	4.50	3.27	3.16	2.58
IV						
Maximize *PF*	4.50	3.03	4.50	3.14	3.12	2.50
Maximize η	4.50	3.10	4.50	3.24	4.55	3.31
Minimize P_{LOSS}	4.53	3.13	4.50	3.29	3.17	2.58

5.6 Comparison of Results with Other Published Paper

To show the validity of this research, the proposed method is also compared to other published journals using the golden section search method. The most significant advantage of this algorithm is that the requirements only need several steps and function evaluations in order for it to reach the optimal solution.

Figure 5.6 shows the chart comparison of THD_V results between the suggested method with the method in [15].

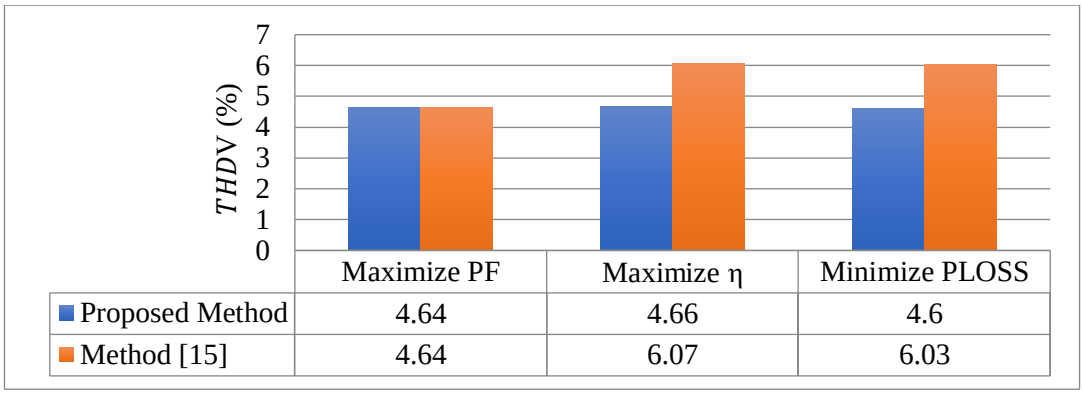

	Maximize PF	Maximize η	Minimize PLOSS
Proposed Method	4.64	4.66	4.6
Method [15]	4.64	6.07	6.03

a) Case I

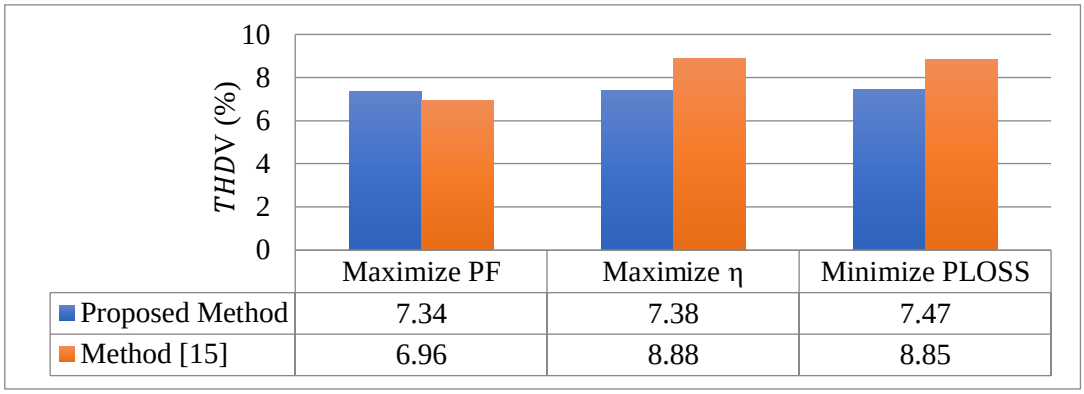

	Maximize PF	Maximize η	Minimize PLOSS
Proposed Method	7.34	7.38	7.47
Method [15]	6.96	8.88	8.85

b) Case II

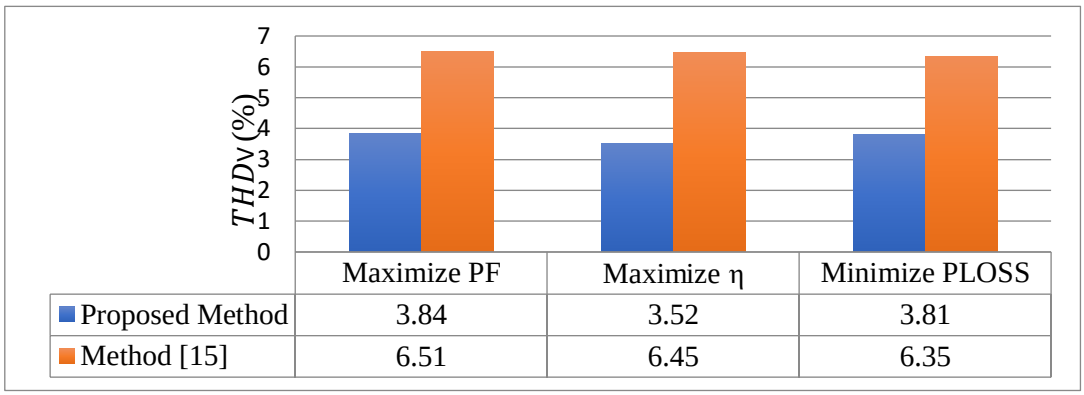

	Maximize PF	Maximize η	Minimize PLOSS
Proposed Method	3.84	3.52	3.81
Method [15]	6.51	6.45	6.35

c) Case III

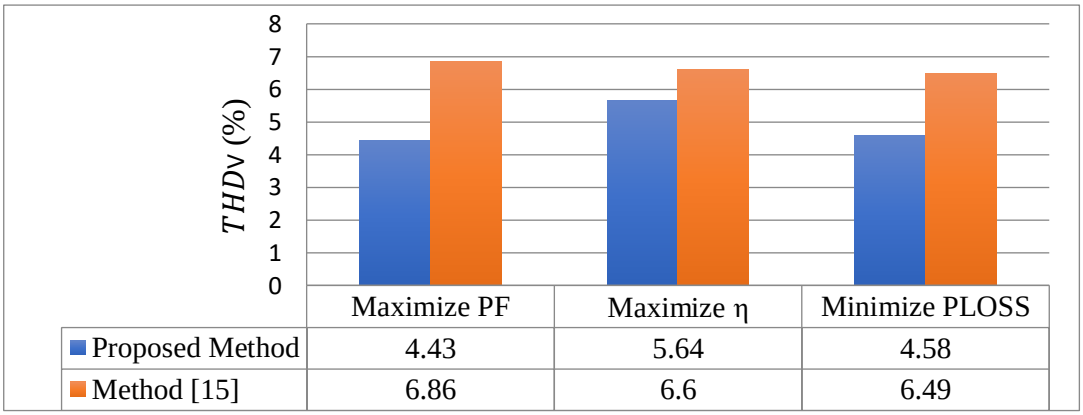

	Maximize PF	Maximize η	Minimize PLOSS
Proposed Method	4.43	5.64	4.58
Method [15]	6.86	6.6	6.49

d) Case IV

Figure 5.6: The comparison of THD_V results between the proposed method with method [15].

The optimization problems are expressed based on the objective functions and constraints formulation [15].

Objective 1: Maximize $PF(X_{CU}, X_{LU})$

Subject to:

$$G(1) \quad I_C = 1.35 \times I_{C(rated)}$$
$$V_C = 1.1 \times V_{C(rated)}$$
$$V_{CP} = 1.2 \times \sqrt{2} \times V_{C(rated)}$$
$$Q_C = 1.35 \times Q_{C(rated)}$$
$$G(2) \quad h > h_r$$

Objective 2: Maximize $\eta(X_{CU}, X_{LU})$

Subject to:

$$G(1) \quad I_C = 1.35 \times I_{C(rated)}$$
$$V_C = 1.1 \times V_{C(rated)}$$
$$V_{CP} = 1.2 \times \sqrt{2} \times V_{C(rated)}$$
$$Q_C = 1.35 \times Q_{C(rated)}$$
$$G(2) \quad h > h_r$$

Objective 3: Minimize $P_{LOSS}(X_{CU}, X_{LU})$

Subject to:

$$G(1) \quad I_C = 1.35 \times I_{C(rated)}$$
$$V_C = 1.1 \times V_{C(rated)}$$
$$V_{CP} = 1.2 \times \sqrt{2} \times V_{C(rated)}$$
$$Q_C = 1.35 \times Q_{C(rated)}$$
$$G(2) \quad h > h_r$$

Figure 5.6 shows the chart comparison of THD_V results between the suggested methods with the method in [15] are higher than the proposed method and far beyond the standard limit. Hence, it is becoming essential to limit the current distortion from the non-linear loads at the PCC in order to avoid excessive voltage limits. In a power system, voltage distortion can be found mainly in the transformer due to the flowing harmonic currents across its secondary terminal. These days, the phase-shifting

transformer with low impedance has been proposed for modifications to limit the harmonic currents while providing small impedance.

5.7 Summary

This chapter proposed MIDACO as the new approach in filter design. In this research, four cases that have been studied where each of the undamped filter designs is aimed to attain the best solution for all of the four single objectives that satisfy all the constraints involved. For each of the cases, the proposed method successfully found the best filter considering that the constraints for the power factor are greater than 90%, to avoid the series and parallel resonance problem which happen because of the interaction between the impedance at the source and the loads, all of the capacitors are following IEEE Std. 18-2012 standard and the voltage total harmonic distortion below its limitation following IEEE Std. 519-2014. The overall performance and all the consequences of the performances were compared with other published approaches and journals to highlights the effectiveness and robustness of using MIDACO.

Chapter 6

Optimal Damped Single Tuned Filter Design

6.1 Introduction

From the previous chapter, this research is continued with the concern of energy losses in the single tuned filter which must be considered because it certainly affects the performance of the system. Practically, there are low internal losses in the capacitor that are insignificant while inductor has reasonable resistance and other losses which cannot be neglected. Therefore, in this chapter, the simulation is carried out by considering the losses in the inductor. The research is then aimed at the optimisation of the capacitance, inductance and resistor based on four objectives. Besides, the design considers whether the constraints satisfy the performance of the filter, the values of a filter to avoid resonances, the range of power factor to ensure efficiency, as well as voltage total harmonic distortion and practical standard of capacitor following IEEE standards. Four cases based on the examples adopted in Chapter 5 were studied in which the performances of the proposed method are compared and analysed from the numerical results performances. Additionally, the performances of the results simulated by the proposed method are also compared with Genetic Algorithm (GA) and Particle Swarm Optimization (PSO). The comparative study to emphasise the advantages and disadvantages of damping over an undamped filter are also presented in this chapter.

Additionally, this chapter also studies the multi-objective optimisation considering two objectives to be minimized which are total harmonics voltage distortion and the losses of the Thevenin's resistor. The performance of the simulated results for all cases was studied and analysed where the studies highlighted the effects of changing the parameters of MIDACO and the advantage of multi-objective optimisation over the results of single-objective optimisation.

6.2 Problem Demonstration and Equations

6.2.1 Objective Functions

Figure 6.1 below shows a single line diagram for the 3-phase harmonic circuit. The circuit is combining linear load, which deliberated as impedance and non-linear loads that act as the harmonic current source. A damped single tuned filter is connected in shunt and assumed to provide small impedance where the resistor, R_{DF} is responsible for preventing the harmonic current from going to the source and confining the harmonic current to flow across the filter.

The total impedance for a damped single tuned filter, Z_F can be written as

$$Z_F = R_{DF} + j(X_{LF} - X_{CF}) \tag{6.1}$$

After some complex mathematical modeling equations from (5.1) until (5.11) in Chapter 5, the objective functions are described as following:

The total harmonic voltage distortion, THD_V can be written as

$$THD_V = \frac{\sqrt{\sum_{K=2}^{13} V_{LFK}^2}}{V_{LF1}} \tag{6.2}$$

The load power factor, PF can be defined according to

$$PF = \frac{P_L}{I_S V_L} = \frac{\sum V_{LFK} I_{SFK} \cos(\theta_K - \phi_K)}{\sqrt{\sum I_{SFK}^2 \sum V_{LFK}^2}} \tag{6.3}$$

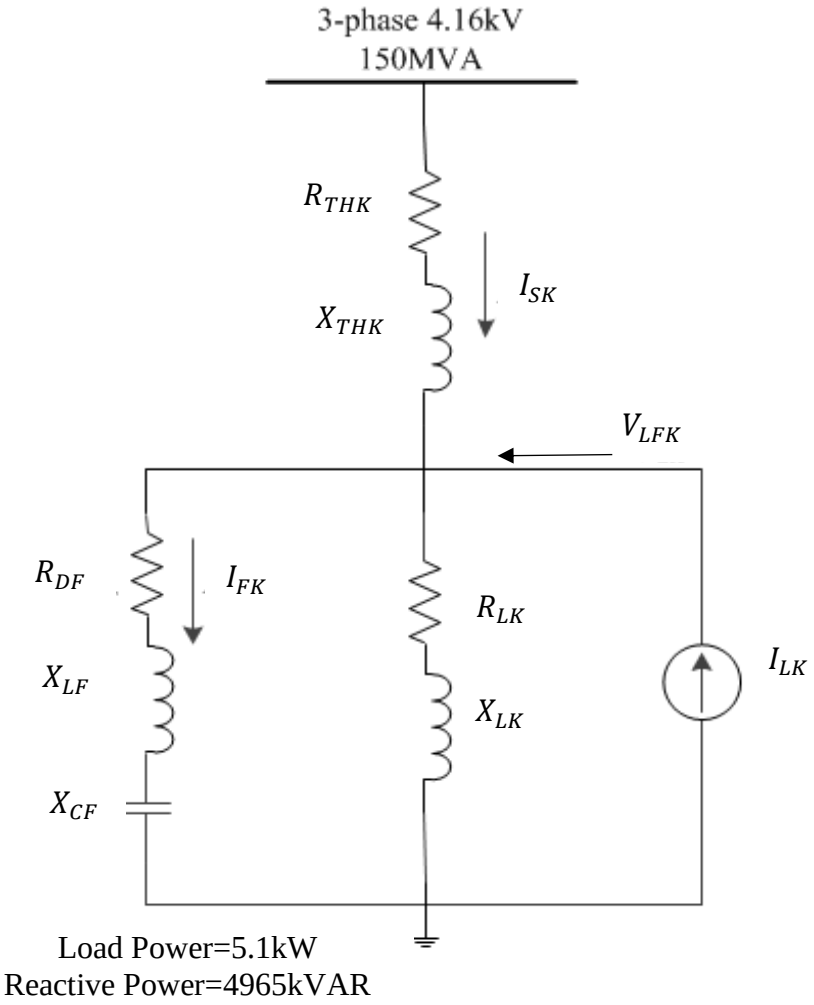

Figure 6.1: The single line diagram for a compensated system

Then, the transmission efficiency, η is given as

$$\eta = \frac{P_L}{P_S} = \frac{\sum V_{LFK} I_{SFK} \cos(\theta_K - \phi_K)}{\sum I_{SFK} V_{LFK} \cos(\theta_K - \phi_K) + \sum I_{SFK}^2 R_{THK}} \tag{6.4}$$

Additionally, the losses in the Thevenin resistor, P_{LOSS} describes as

$$P_{LOSS} = \sum_K I_{SFK}^2 R_{THK} \tag{6.5}$$

6.2.2 Constraints

In this case, there is an additional constraint that is added to the constraints involved when designing an undamped single tuned filter in the previous chapter, known as a quality factor. The quality factor value defines the energy losses, which consequently

explain the performance of the filter from the minimum or maximum value of intrinsic resistance of the inductance in the filter. A high value of resistance will result in the low value of Q_F, hence, it is essential to measure this value irregular for filtering action.

Higher Q_F the value indicates a sharper peak for the resonance, thus resulting in higher frequency selectivity and enhanced harmonic attenuation. Therefore, it is essential to set limitations for the value of Q_F, where the recommended standard restriction is usually set in the middle of 20 to 100. Thus, the problem formulation for simulation can be written as:

Objective 1: Minimize $THD_V(X_{DF}, X_{CF}, X_{LF})$

Subject to:

$$
\begin{aligned}
G(1) \quad & I_C = 1.35 \times I_{C(rated)} \\
& V_C = 1.1 \times V_{C(rated)} \\
& V_{CP} = 1.2 \times \sqrt{2} \times V_{C(rated)} \\
& Q_C = 1.35 \times Q_{C(rated)} \\
G(2) &= 20 \leq Q_F \leq 100 \\
G(3) &= h_{DF} \leq 0.9 f_n \\
G(4) &= h_{DF} > h_{DFr} \\
G(5) &= THD_V \leq 5\% \\
G(6) &= PF \geq 90\%
\end{aligned}
\tag{6.6}
$$

Objective 2: Maximize $PF(X_{DF}, X_{CF}, X_{LF})$

Subject to:

$$
\begin{aligned}
G(1) \quad & I_C = 1.35 \times I_{C(rated)} \\
& V_C = 1.1 \times V_{C(rated)} \\
& V_{CP} = 1.2 \times \sqrt{2} \times V_{C(rated)} \\
& Q_C = 1.35 \times Q_{C(rated)} \\
G(2) &= 20 \leq Q_F \leq 100 \\
G(3) &= h_{DF} \leq 0.9 f_n \\
G(4) &= h_{DF} > h_{DFr} \\
G(5) &= THD_V \leq 5\% \\
G(6) &= PF \geq 90\%
\end{aligned}
\tag{6.7}
$$

Objective 3: Maximize $\eta(X_{DF}, X_{CF}, X_{LF})$

Subject to:

$$
\begin{aligned}
G(1) \quad & I_C = 1.35 \times I_{C(rated)} \\
& V_C = 1.1 \times V_{C(rated)} \\
& V_{CP} = 1.2 \times \sqrt{2} \times V_{C(rated)} \\
& Q_C = 1.35 \times Q_{C(rated)} \\
G(2) &= 20 \leq Q_F \leq 100 \\
G(3) &= h_{DF} \leq 0.9 f_n \\
G(4) &= h_{DF} > h_{DFr} \\
G(5) &= THD_V \leq 5\% \\
G(6) &= PF \geq 90\%
\end{aligned}
\tag{6.8}
$$

Objective 4: Minimize $P_{LOSS}(X_{DF}, X_{CF}, X_{LF})$

Subject to:

$$
\begin{aligned}
G(1) \quad & I_C = 1.35 \times I_{C(rated)} \\
& V_C = 1.1 \times V_{C(rated)} \\
& V_{CP} = 1.2 \times \sqrt{2} \times V_{C(rated)} \\
& Q_C = 1.35 \times Q_{C(rated)} \\
G(2) &= 20 \leq Q_F \leq 100 \\
G(3) &= h_{DF} \leq 0.9 f_n \\
G(4) &= h_{DF} > h_{DFr} \\
G(5) &= THD_V \leq 5\% \\
G(6) &= PF \geq 90\%
\end{aligned}
\tag{6.9}
$$

6.3 Simulated Results

In this case, the same utilities which have been explained in the previous chapter were simulated when designing this filter, in which all the parameters are kept constant and presented in Table 5.1 in Chapter 5. The inductive load and reactive power as well as supply bus voltage, remain the same which, are set to 5100kW, 4965kVAR and 4.16kV (line to line), respectively. Besides, all the source and load harmonics are also kept constant.

Table 6.1 shows the simulated performance for the uncompensated system. From the table, it showed that the system has very poor power quality with high harmonics distortions before the passive filter was added into the system.

Table 6.1: The numerical results for uncompensated system

No. of cases	I	II	III	IV
PF (%)	71.72	71.71	71.71	71.71
η (%)	99.34	99.34	98.78	98.78
P_{LOSS} (kW)	10.48	10.48	18.45	18.45
THD_V (%)	6.20	8.22	6.38	8.29
I_S (A)	953.03	953.17	923.58	923.71
dpf (%)	71.65	71.65	71.65	71.65

Table 6.2 summarised the simulated results after including damped single tuned filter into the system. The best value of R_{DF}, X_{CF} and X_{LF} were found by using the proposed method in which these results will be used for evaluating the overall performance. In this simulation, the controlling parameters of MIDACO were set to: 1) n_{pop} will change dynamically for every generation; 2) k is fixed to 100 and 3) $\Omega = 0$. For each objective, the algorithm was run with 100 different SEED parameter and the best solution out of a reasonable number of runs was chosen.

From Table 6.2, the results showed that the optimal filter obtained proved the validity and effectiveness of this proposed solver with an enhancement in the power factor and transmission efficiency as the losses in the resistor of Thevenin impedance and total harmonic voltage distortion reduced.

It can be noticed that for Case I, PF is improved from 71.72%, to 95.74% 97.12%, 97.06% and 97.05%, η is increased from 99.34% to 99.62876625%, 99.63592182%, 99.63860524% and 99.63906499%, P_{LOSS} is decreased from 10.48kW to 6.31kW, 6.27kW, 6.17kW and 6.15kW, THD_V is also reduced from 6.20% to 1.63%, 2.18%, 2.17% and 2.17%, respectively. For Case II, PF is improved from 71.71%, to 93.00%, 95.13%, 95.53% and 95.03%,η is increased from 99.34% to 99.60697930%, 99.62067483%, 99.61155946% and 99.62352366%. P_{LOSS} is decreased from 10.48kW to 6.74kW, 6.49kW, 6.51kW and 6.38kW, THD_V is also reduced from 8.22% to 2.20%, 2.85%, 3.00% and 2.84%, respectively.

Table 6.2: The numerical results using MIDACO

No. of Cases	*SEED*	X_{CF} (Ω)	R_{DF} (Ω)	X_{LF} (Ω)	*PF* (%)	η (%)	P_{LOSS} (kW)	THD_V (%)	I_S (A)
Minimize THD_V									
Case I	74	3.54	0.1431	0.0121	95.74	99.62876625	6.31	1.63	739.70
Case II	70	3.18	0.1451	0.0068	93.00	99.60697930	6.74	2.20	764.07
Case III	6	3.04	0.1251	0.0062	97.06	99.32601203	11.63	1.09	733.37
Case IV	88	3.48	0.1447	0.0071	97.49	99.33200995	11.32	1.39	723.42
Maximize *PF*									
Case I	8	3.43	0.1694	0.0381	97.12	99.63592182	6.27	2.18	736.97
Case II	32	3.75	0.1846	0.0415	95.13	99.62067483	6.49	2.85	750.07
Case III	47	3.95	0.1867	0.0134	98.72	99.34767025	10.91	1.62	710.09
Case IV	92	3.95	0.1940	0.0437	97.94	99.33211438	11.26	2.07	721.12
Maximize η									
Case I	26	3.43	0.1693	0.0120	97.06	99.63860524	6.17	2.17	731.08
Case II	4	4.57	0.2188	0.0104	95.53	99.61155946	6.51	3.00	750.96
Case III	72	3.95	0.1951	0.0088	98.80	99.34942015	10.87	1.74	708.86
Case IV	45	3.95	0.1951	0.0119	97.91	99.33701020	11.09	2.08	716.02
Minimize P_{LOSS}									
Case I	13	3.43	0.1694	0.0077	97.05	99.63906499	6.15	2.17	730.10
Case II	38	3.75	0.1851	0.0085	95.03	99.62352366	6.38	2.84	743.64
Case III	55	4.06	0.1762	0.0121	98.34	99.34309933	10.94	1.45	711.12
Case IV	48	3.85	0.1807	0.0084	97.87	99.33700710	11.11	1.86	716.69

For Case III, *PF* is improved from 71.71% to 97.06%, 98.72%, 98.80% and 98.34%, η is increased from 98.78% to 99.32601203%, 99.34767025%, 99.34942015% and 99.34309933%, P_{LOSS} is decreased from 18.45kW to 11.63kW 10.91kW, 10.87kW and 10.94kW, THD_V is reduced from 6.38% to 1.9%, 1.63%, 1.74% and 1.45%, respectively. For Case IV, *PF* is improved from 71.71% to 97.49%, 97.94%, 97.91% and 97.87% , η is increased from 98.78% to 99.33200995%, 99.33211438%, 99.33601020, and 99.33700710%, P_{LOSS} is decreased from 18.45kW to 11.32kW, 11.26kW, 11.09kW and 11.11kW, THD_V is also reduced from 8.29% to 1.39%, 2.07%, 2.08% and 1.86%, respectively. Overall, the results proved that the proposed filter showed satisfactory improvement in the entire performances. Furthermore, the results for all cases also showed that the value of THD_V satisfied with the constraints, where

the value is reduce below 5% as suggested by IEEE519-2014 and *PF* is always greater than 90%.

Besides, the reduction in short circuit capacity has a higher value of Thevenin impedance. The increasing number of resistors in the Thevenin impedance and losses, are also increasing, which results in the decrease of transmission efficiency. Nevertheless, the power factor is increased because less harmonic current will flow to the source system which also results in improvement of the THD_V. Please refer to the results for Case I and III in Table 6.2.

In contrast, the same value of Thevenin' impedance with additional supply voltage harmonics in the system will reduce the power factor, which results in increasing value of THD_V because of the additional line current passes through the source. Due to the increasing number of the line current, the losses in the source impedance and the voltage drop will increase while the transmission efficiency will decrease. Refer the results for Case I and II in Table 6.2.

Next, Table 6.3 displays the effect of tuning the parameter of ants and kernel when the objective maximizing *PF*. Only these two parameters are varying in five different settings, while other parameters are set with the same setting.

From Table 6.3, the results showed that the optimal value of a solution could be reached by increasing the number of the kernel. This confirms that a large kernel provides the solution for the proposed method from getting stuck in local optimum and provides a higher chance for it to reach its global optimum. However, tuning the ants and kernel parameters might significantly reduce the performance. Overall, the result showed that Setting 5, which was the setting used for the base case is the best setting for ant and kernel to get the best solutions.

Table 6.3: The effect of changing n_{pop} and k parameters based on Objective 2

Setting	Parameters		THD_V (%)			
	Ants, n_{pop}	Kernel, k	I	II	III	IV
1	2	2	1.63	2.72	1.95	2.10
2	30	5	2.18	2.98	1.37	1.88
3	500	10	1.78	2.48	1.08	2.34
4	100	50	1.38	2.26	1.30	1.81
5	0	100	2.18	2.85	1.62	2.07
Setting	Parameters		PF (%)			
	Ants, n_{pop}	Kernel, k	I	II	III	IV
1	2	2	94.80	92.88	96.92	96.80
2	30	5	97.12	93.96	98.26	95.61
3	500	10	95.55	91.61	98.29	96.14
4	100	50	90.97	89.63	98.12	93.92
5	0	100	97.12	95.13	98.72	97.94
Setting	Parameters		η (%)			
	Ants, n_{pop}	Kernel, k	I	II	III	IV
1	2	2	99.62	99.60	99.32	99.32
2	30	5	99.64	99.61	99.34	99.30
3	500	10	99.62	99.59	99.34	99.31
4	100	50	99.59	99.57	99.34	99.28
5	0	100	99.64	99.62	99.35	99.33
Setting	Parameters		P_{LOSS} (kW)			
	Ants, n_{pop}	Kernel, k	I	II	III	IV
1	2	2	6.64	6.65	11.24	11.35
2	30	5	6.27	6.56	11.08	11.43
3	500	10	6.52	6.87	11.33	11.44
4	100	50	7.18	7.17	11.23	11.87
5	0	100	6.27	6.49	10.91	11.26

Meanwhile, Table 6.4 shows the effect of tuning the Oracle parameter while others are kept constant. From the results collected, it is proven that the different **Ω** does not affect the obtained optimal solutions as explained in Chapter 4, Section 4.4.

Table 6.4: Effects of tuning Oracle parameter only

Setting	Parameters	THD_V (%)			
	Oracle	I	II	III	IV
1	1	2.18	2.85	1.62	2.07
2	3	2.18	2.85	1.62	2.07
3	6	2.18	2.85	1.62	2.07
Setting	Parameters	*PF* (%)			
	Oracle	I	II	III	IV
1	1	97.12	95.13	98.72	97.94
2	3	97.12	95.13	98.72	97.94
3	6	97.12	95.13	98.72	97.94
Setting	Parameters	η (%)			
	Oracle	I	II	III	IV
1	1	6.27	99.62	99.35	99.33
2	3	6.27	99.62	99.35	99.33
3	6	6.27	99.62	99.35	99.33
Setting	Parameters	P_{LOSS} (kW)			
	Oracle	I	II	III	IV
1	1	99.64	6.49	10.91	11.26
2	3	99.64	6.49	10.91	11.26
3	6	99.64	6.49	10.91	11.26

Table 6.5 shows the resultant individual voltage and current harmonic distortions for all the cases based on the objective maximize *PF*.

From Table 6.5, the results showed that there is more current that passes through the system for Case I compared to Case III, as the system has a small value of Thevenin resistance in the same harmonics condition. These will increase the load voltage, which overall increases the load power feeding to the power system. However, an additional supply of voltage harmonics to the same system will cause more current source for Case II compared to Case I supplied to the load, which will also reduce the load voltage. Hence, these also benefit to the higher power source as well.

Table 6.5: Simulated results for each of individual harmonic current and voltage

Number of harmonic order, K	Minimize THD_V		Maximize PF		Maximize η		Minimize P_{LOSS}	
	I_{SFK} (A)	V_{LFK} (V)	I_{SFK} (A)	V_{LFK} (V)	I_{SFK} (A)	V_{LFK} (V)	I_{SFK} (A)	V_{LFK} (V)
Case I								
5	29.08	0.12	22.99	1.12	23.07	1.09	23.07	1.09
7	8.07	1.16	7.12	1.40	7.13	1.40	7.13	1.40
11	2.84	0.98	2.57	1.08	2.58	1.08	2.58	1.08
13	1.31	0.57	1.24	0.62	1.24	0.62	1.25	0.62
Case II								
5	35.21	0.94	31.78	1.65	31.28	1.67	31.82	1.63
7	10.08	1.63	9.12	1.92	8.48	2.07	9.11	1.92
11	2.75	0.99	2.49	1.13	2.29	1.21	2.49	1.13
13	1.28	0.58	1.23	0.65	1.18	0.69	1.23	0.65
Case III								
5	15.12	0.08	18.65	0.95	13.59	0.76	14.90	0.32
7	5.20	0.74	5.80	0.52	4.70	1.13	4.94	0.99
11	1.97	0.65	2.12	0.58	1.77	0.88	1.84	0.82
13	0.90	0.46	0.94	0.42	0.89	0.61	0.90	0.58
Case IV								
5	21.50	0.18	19.03	1.04	18.99	1.04	19.76	0.79
7	6.85	1.06	6.19	1.43	6.18	1.44	6.37	1.34
11	1.95	0.72	1.77	0.88	1.77	0.88	1.82	0.84
13	0.91	0.51	0.89	0.61	0.89	0.61	0.90	0.59

Table 6.6 indicates the limitations of the proposed main capacitors in the filter to follow the IEEE Std. 18. From the table, the results showed that all capacitors are capable of operating below the standard limitation.

Table 6.6: The capacitor limitation

Objective Function	V_{CFP} (%)	V_{CF} (%)	I_{CF} (%)	Q_{CF} (%)
Case I				
Minimize THD_V	78.85	104.07	114.06	115.38
Maximize PF	78.42	105.11	113.14	116.97
Maximize η	78.43	105.12	113.17	116.99
Minimize P_{LOSS}	78.43	105.12	113.17	117.00
Standard	120	110	135	135
Case II				
Minimize THD_V	69.32	91.06	100.46	88.54
Maximize PF	69.37	90.90	100.66	88.34
Maximize η	69.93	90.35	102.38	88.03
Minimize P_{LOSS}	69.38	90.92	100.67	88.39
Standard	120	110	135	135
Case III				
Minimize THD_V	66.47	90.71	96.23	86.68
Maximize PF	66.16	89.82	95.61	85.09
Maximize η	66.22	90.03	95.74	85.46
Minimize P_{LOSS}	66.04	89.32	95.35	84.22
Standard	120	110	135	135
Case IV				
Minimize THD_V	67.08	89.98	96.78	85.69
Maximize PF	67.03	90.03	96.75	85.76
Maximize η	67.07	90.07	96.78	85.84
Minimize P_{LOSS}	67.06	89.97	96.76	85.67
Standard	120	110	135	135

The filter impedance in the resonant circuit and the effects of the resonance peak for different values of Q_F for four objective functions in case I are shown in Figure 6.2, where the characteristics of the filter responses are evaluated and explained as follows:

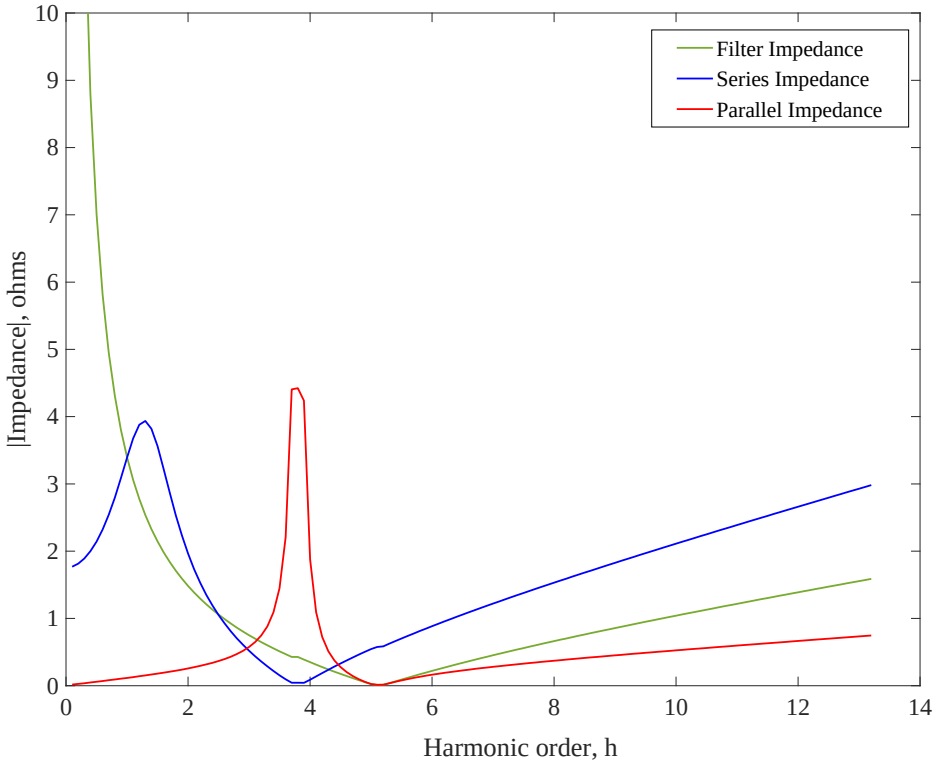

a) Objective 1

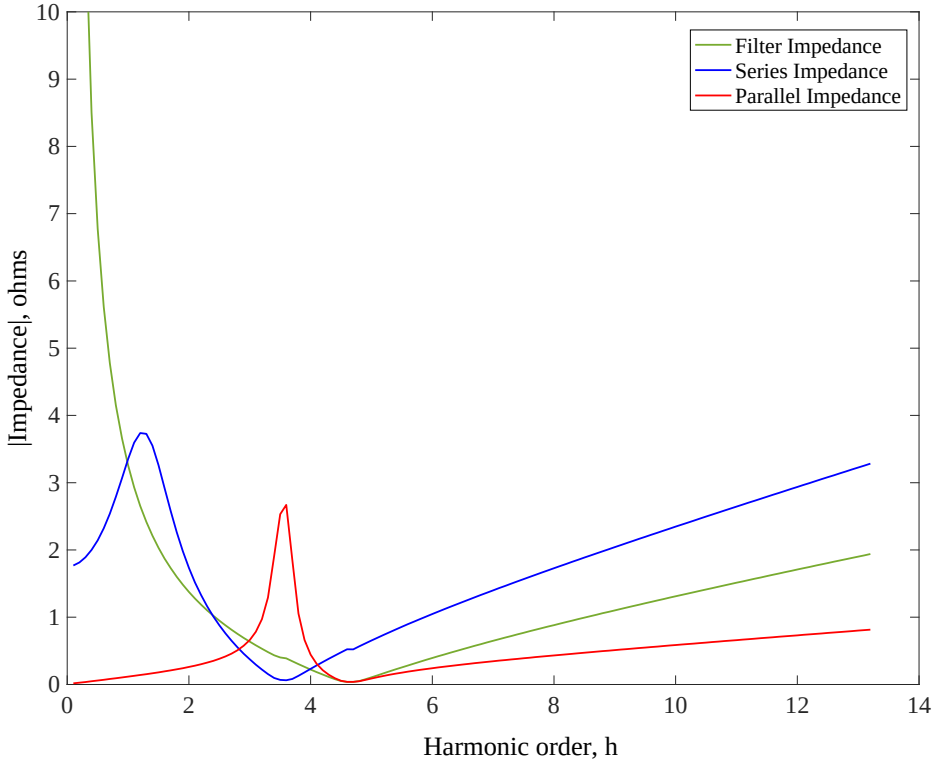

b) Objective 2

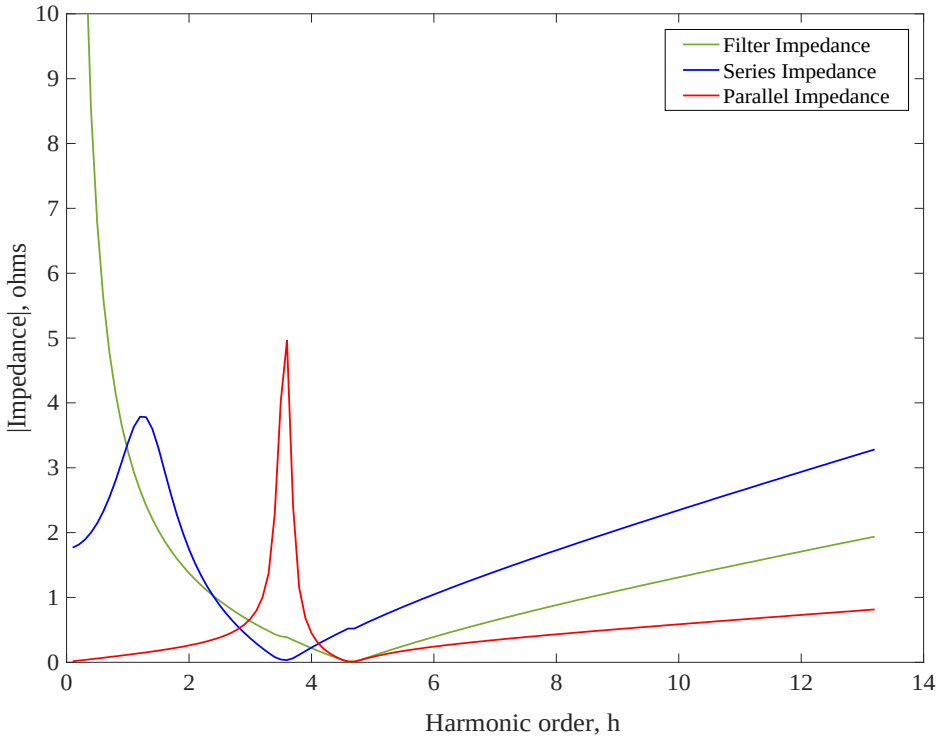

c) Objective 3

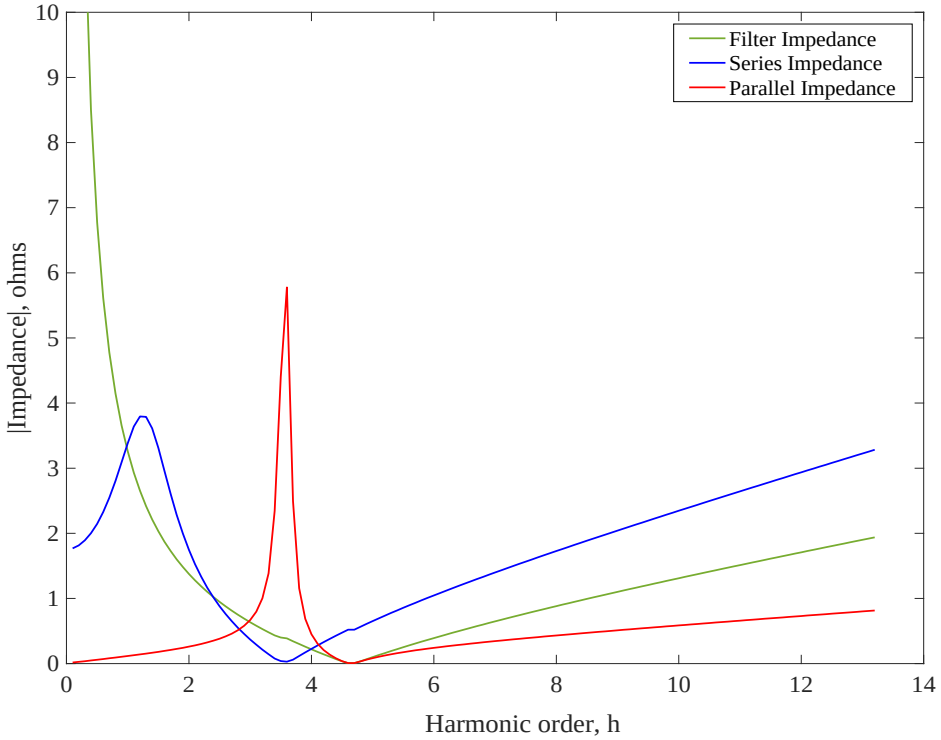

d) Objective 4

Figure 6.2: Graphs of impedance resonance for case I for four different objective functions

1. Adding the single tuned filter into the system can result in the occurrences of series and parallel resonance. This can happen because of the interaction between the impedance at the source and the compensated load.
2. For series resonance, the value of inductance and capacitance reactance is equal, thus allowing the resistance to reach the local minimum at resonant. In contrast, the resistance is at a local maximum for parallel resonance.
3. The value of *R* determines the resonant peak. A lower value of *R* results in a higher value of Q_F where the resonant peak becomes sharp. This results in high-frequency selectivity and better harmonic attenuation. However, the passband is reduced with higher Q_F.
4. It is recommended to always tuned the filter below the harmonic to be filtered in order to avoid resonance.

6.4 Comparison of Results with Other Published Techniques

In this chapter, the same system is also tested with two conventional optimisers in power quality areas which are GA and PSO.

Table 6.7 show simulated results when using GA. In this test, three parameters are used, where crossover rate, mutation probability, and population size are set to 0.8, 0.001 and 50, respectively.

Table 6.8 show the results when simulated using PSO. The learning factors which are a cognitive attraction and social attraction are set to 1 and 1.5, respectively. During iterations, the inertia weight is decreases from 0.9 to 0.1.

From Table 6.7 and 6.8, GA and PSO showed that the method caused very high THD_V satisfied the constraints and came out well below the standard limit. From Table 6.7 and 6.8, GA and PSO showed that the method caused very high THD_V for all the cases and exceeded the standard limits for the cases that have additional voltage harmonics in the power system, such as Case II and IV.

Table 6.7: Simulated results using GA to design damped tuned filter

Objective Function	X_{CF} (Ω)	R_{DF} (Ω)	X_{LF} (Ω)	PF (%)	η (%)	P_{LOSS} (kW)	THD_V (%)
Maximize PF							
Case I	4.18	0.018	0.370	99.01	99.65	5.88	4.12
Case II	3.85	0.025	0.502	99.24	99.65	5.94	6.16
Case III	4.30	0.017	0.347	98.96	99.35	10.82	3.18
Case IV	4.18	0.020	0.414	99.17	99.35	10.87	4.62
Maximize η							
Case I	4.06	0.017	0.337	99.03	99.65	5.88	3.94
Case II	3.95	0.021	0.418	99.02	99.65	5.93	5.77
Case III	3.32	0.032	0.641	96.01	99.30	12.37	4.35
Case IV	3.40	0.030	0.609	97.01	99.32	12.01	5.55
Minimize P_{LOSS}							
Case I	3.40	0.023	0.603	97.11	99.64	6.36	4.88
Case II	3.48	0.029	0.577	97.62	99.64	6.24	6.40
Case III	3.75	0.027	0.536	99.50	99.35	11.08	4.11
Case IV	3.40	0.030	0.611	96.99	99.32	12.02	5.56

Table 6.8: Simulated results using PSO to design damped tuned filter

Criteria	X_{CF} (Ω)	R_{DF} (Ω)	X_{LF} (Ω)	PF (%)	η (%)	P_{LOSS} (kW)	THD_V (%)
Maximize PF							
Case I	3.85	0.020	0.406	99.48	99.66	5.88	4.34
Case II	3.65	0.020	0.464	98.85	99.65	6.00	6.03
Case III	3.48	0.027	0.657	97.45	99.33	11.83	4.39
Case IV	4.30	0.022	0.429	98.99	99.35	10.87	4.70
Maximize η							
Case I	3.11	0.022	0.627	93.07	99.60	6.98	4.91
Case II	3.85	0.023	0.620	99.23	99.65	5.96	6.51
Case III	3.11	0.024	0.631	93.09	99.26	13.29	4.32
Case IV	3.65	0.024	0.650	98.58	11.41	99.34	5.67
Minimize P_{LOSS}							
Case I	3.65	0.023	0.557	99.01	99.65	6.01	4.80
Case II	3.48	0.026	0.650	97.23	99.64	6.31	6.57
Case III	3.65	0.025	0.618	98.88	99.35	11.32	4.32
Case IV	3.56	0.026	0.699	97.70	11.74	99.33	5.79

Table 6.9 shows the running time up until maximum iterations are reached for all methods. The comparison of the proposed method with other techniques proved that this method has the shortest running time over GA and PSO, as it can process a thousand iterations within a few seconds. From the table, the results also proved the disadvantage of GA as mentioned in Chapter 2, where it consumed the longest time when compared to PSO, hence, degrading the efficiency of GA.

Table 6.9: The convergence time up until maximum iterations are reached

Criteria	Running Time, t/s			No. of Function Evaluation		
	Proposed	GA	PSO	Proposed	GA	PSO
Case I						
Maximize *PF*	22.00	21.10	8.22	20 000	3	62
Maximize η	20.00	30.83	11.27	20 000	5	57
Minimize P_{LOSS}	21.00	28.43	12.93	20 000	6	88
Case II						
Maximize *PF*	20.00	26.23	8.83	20 000	3	62
Maximize η	21.00	48.31	11.53	20 000	5	59
Minimize P_{LOSS}	21.00	39.18	6.83	20 000	6	63
Case III						
Maximize *PF*	21..00	27.57	8.22	20 000	3	57
Maximize η	21.00	60.51	8.22	20 000	5	59
Minimize P_{LOSS}	20.00	33.15	15.00	20 000	5	103
Case IV						
Maximize *PF*	21.00	21.37	8.54	20 000	3	58
Maximize η	19.00	39.02	7.49	20 000	6	55
Minimize P_{LOSS}	19.00	29.91	11.42	20 000	4	60

Table 6.10 presents the statistical test results for all methods at their best run when the objective function is based on Objective 2, where the objective maximizes *PF*. From the table, the proposed method proved that it has a high standard deviation for *PF* values compared to GA and PSO. Therefore, the proposed method will have a more significant opportunity to the extent of getting the best solution up until the hard limit of *MAVEVAL* achieved. Due to the critical fact that the existence of resonance can be avoided with different returned values, this ultimately benefited to the proposed method. However, GA and PSO have minimal variants of standard deviation which are challenging to tell apart from the minimum to maximum of optimal solution visually.

Table 6.10: The statistical measurement based on objective 2 (maximize *PF*)

Optimization Tool	*PF*				
	Minimum	Maximum	Mean	Middle	Standard Deviation
Case I					
Proposed	97.4173	97.2736	97.2713	97.2692	0.0411
GA	99.6827	99.7239	99.7117	99.7175	0.0148
PSO	99.2157	99.2164	99.2162	99.2162	0.0001
Case II					
Proposed	89.7608	94.3214	93.2128	92.8802	1.0262
GA	99.3513	99.4848	99.4612	99.4829	0.0442
PSO	98.2808	98.7809	98.7809	98.7809	0.0001
Case III					
Proposed	94.3264	98.6867	97.3919	98.6863	1.9881
GA	99.4642	99.8360	99.7594	99.8348	0.1485
PSO	99.6648	99.6650	99.6649	99.6649	0.0001
Case IV					
Proposed	96.3828	97.8815	97.3940	97.7322	0.6298
GA	99.3924	99.6656	99.5970	99.6651	0.1364
PSO	99.3656	99.4423	99.4384	99.4409	0.0111

Table 6.11 shows the series and parallel resonance harmonic tuning order for all cases. From the table, the results showed that the optimal filter satisfied the resonance constraints that are considered in this study. In contrast, the harmonic order is less than the desired harmonic that need to be eliminated. Besides, the results also showed that the value of h_{DFr} is always lower than h_{DF} . Apart from that, the designs give advantages to the system, in which it provides sufficient harmonic filtering action to avoid detuning as explained in the Chapter 5.

Table 6.11: Harmonic tuning orders for series and parallel resonance

Criteria	Proposed Method		GA		PSO	
	h_{DF}	h_{DFr}	h_{DF}	h_{DFr}	h_{DF}	h_{DFr}
Case I						
Maximize *PF*	4.50	3.47	3.36	2.93	3.75	3.26
Maximize η	4.50	3.47	3.47	2.99	3.58	2.99
Minimize P_{LOSS}	4.50	3.47	2.37	2.18	3.89	3.15
Case II						
Maximize *PF*	4.51	3.53	2.77	2.50	3.61	3.17
Maximize η	4.57	3.70	3.07	2.72	4.07	3.31
Minimize P_{LOSS}	4.50	3.53	2.46	2.24	3.60	2.98
Case III						
Maximize *PF*	4.60	3.13	3.52	2.76	3.95	3.08
Maximize η	4.50	3.10	2.28	1.97	3.07	2.36
Minimize P_{LOSS}	4.80	3.22	2.64	2.23	3.86	2.75
Case IV						
Maximize *PF*	4.51	3.10	3.18	2.57	3.57	2.85
Maximize η	4.50	3.10	2.36	2.03	4.04	2.90
Minimize P_{LOSS}	4.61	3.11	2.36	2.03	4.21	3.02

Table 6.12 shows the comparison results of R and Q_F for all cases. From Table 6.12, the dissimilar value of R proved that it has a different value of Q_F. Thus, the higher the value of Q_F, the sharper the peak, which consequently resulted in high-frequency selectivity of the circuit.

Table 6.12: The quality factor for all cases

Objective Function	Proposed Method		GA		PSO	
	R	Q_F	R	Q_F	R	Q_F
Case I						
Maximize *PF*	0.0381	20.02	0.0182	68.09	0.0202	61.89
Maximize η	0.0120	63.70	0.0166	70.28	0.0216	64.81
Minimize P_{LOSS}	0.0077	99.50	0.0298	48.09	0.0231	61.73
Case II						
Maximize *PF*	0.0415	20.04	0.0248	56.04	0.0201	64.78
Maximize η	0.0104	96.11	0.0206	62.26	0.0232	66.67
Minimize P_{LOSS}	0.0085	98.28	0.0285	49.74	0.0262	57.42
Case III						
Maximize *PF*	0.0134	64.20	0.0171	71.33	0.0270	55.93
Maximize η	0.0088	99.98	0.0317	46.08	0.0241	58.15
Minimize P_{LOSS}	0.0121	70.16	0.0265	53.52	0.0246	61.00
Case IV						
Maximize *PF*	0.0437	20.02	0.0204	64.36	0.0217	62.72
Maximize η	0.0119	73.91	0.0301	47.84	0.0236	65.30
Minimize P_{LOSS}	0.0084	98.67	0.0302	47.72	0.0262	60.35

6.5 A Comparison Study of Undamped and Damped Single Tuned Filter

In this section, the comparison between damped and undamped filter is discussed to give a better understanding of the effects of damping resistor. Table 6.13 shows the simulated results for damped and undamped filter based on Objective 2 when maximizing *PF* for all cases. From the table, the results proved that additional damping, namely R_{DF} in the filter would increase of the power losses in the filer, which consequently reduced the system performance. The comparison results in Table 6.13 illustrated that the damped filter overall has weak *PF,* low η, increase P_{LOSS} as well as THD_V.

Table 6.13: Simulated results of the damped and undamped filter when the objective maximize *PF*

Type of filter	Damped filter				Undamped filter			
No. of cases	I	II	III	IV	I	II	III	IV
$X_{CF}, X_{CU}(\Omega)$	3.43	3.75	3.95	3.95	3.85	3.85	3.48	3.65
R_{DF} (Ω)	0.0381	0.0085	0.0134	0.0437	-	-	-	-
$X_{LF}X_{LU}(\Omega)$	0.1694	0.1851	0.1867	0.1940	0.1900	0.1889	0.1699	0.1805
THD_V (%)	2.18	2.84	1.62	2.07	2.32	2.85	1.56	1.96
PF (%)	97.12	95.13	98.72	97.94	97.28	94.91	98.85	98.09
η(%)	99.64	99.62	99.34	99.33	99.64	99.62	99.35	99.34
P_{LOSS} (kW)	6.15	6.38	10.91	11.26	6.05	6.35	10.97	11.08
h_{DF}, h	4.50	4.50	4.60	4.51	4.50	4.51	4.53	4.50
h_{DFR}, h_r	3.47	3.53	3.13	3.10	3.55	3.56	3.00	3.03
$I_{SF,}\ I_S$ (A)	730.10	743.64	710.09	721.46	723.81	742.04	712.29	715.83

Besides, the results also showed that the harmonic tuning order is closer to the fifth harmonics; therefore, it seems that the undamped filter needs high ratings of reactor current and capacitor voltage. In consequences, the total value of the filter bank will increase. Nevertheless, the additional of R_{DF} will cause high maintenance requirements because of added the number of components.

Besides, more current supply will be supplied to the power system which is equipped with a damped filter instead of the undamped filter. This is because the damping resistance provides additional impedance that results to increase current supply when added with damped filter, compared to the undamped filter.

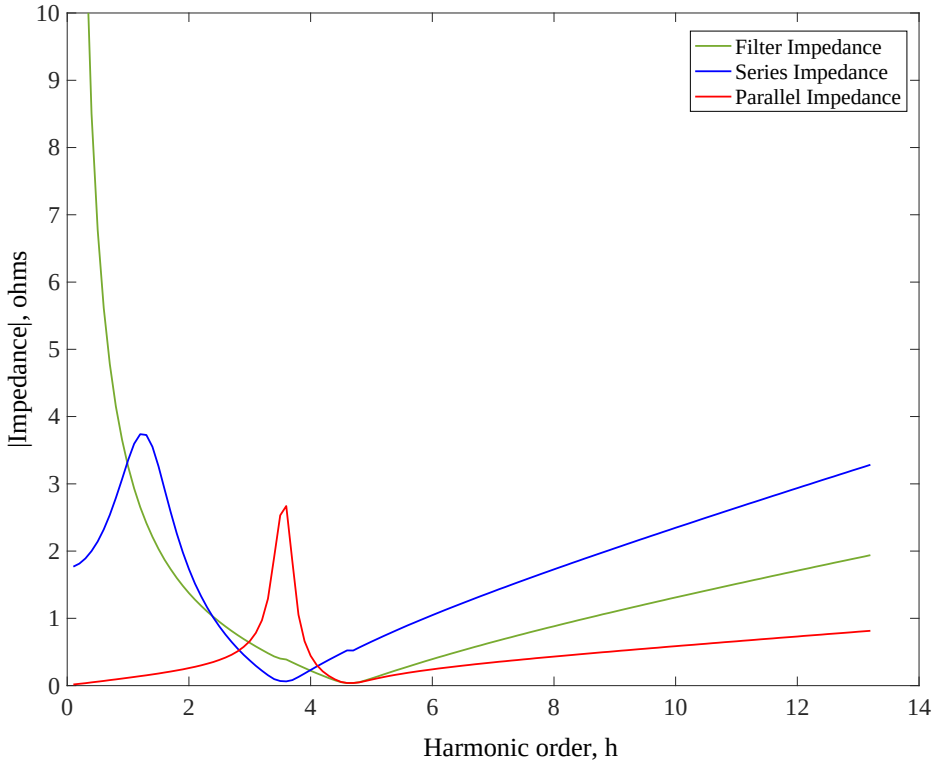

a) Damped single tuned filter

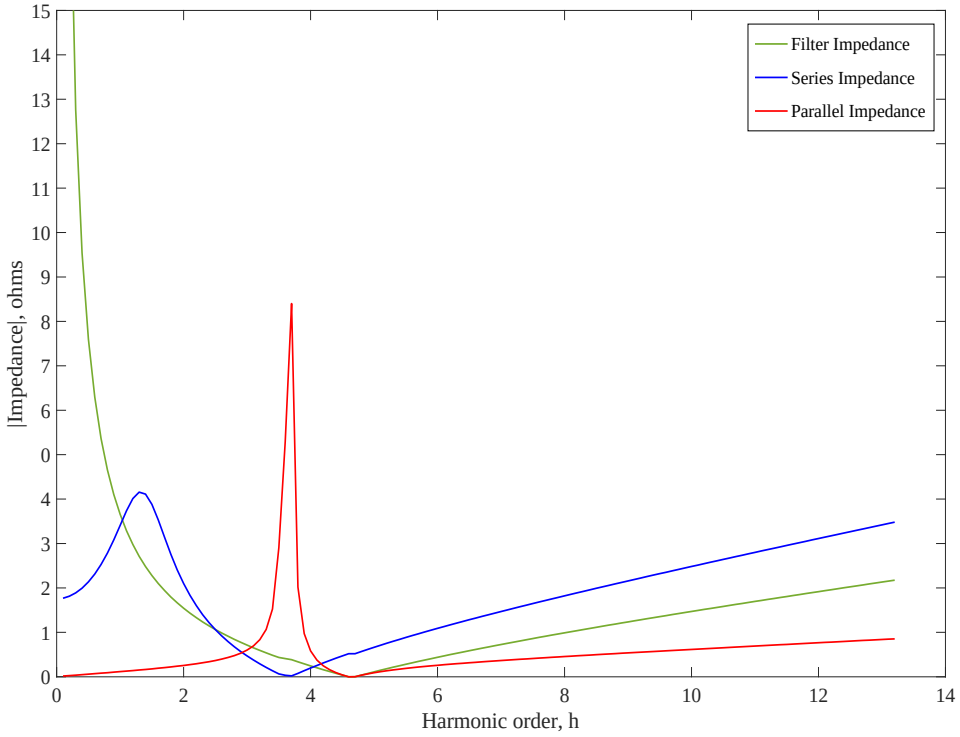

b) Undamped single tuned filter

Figure 6.3: Comparison of impedance resonance Case I

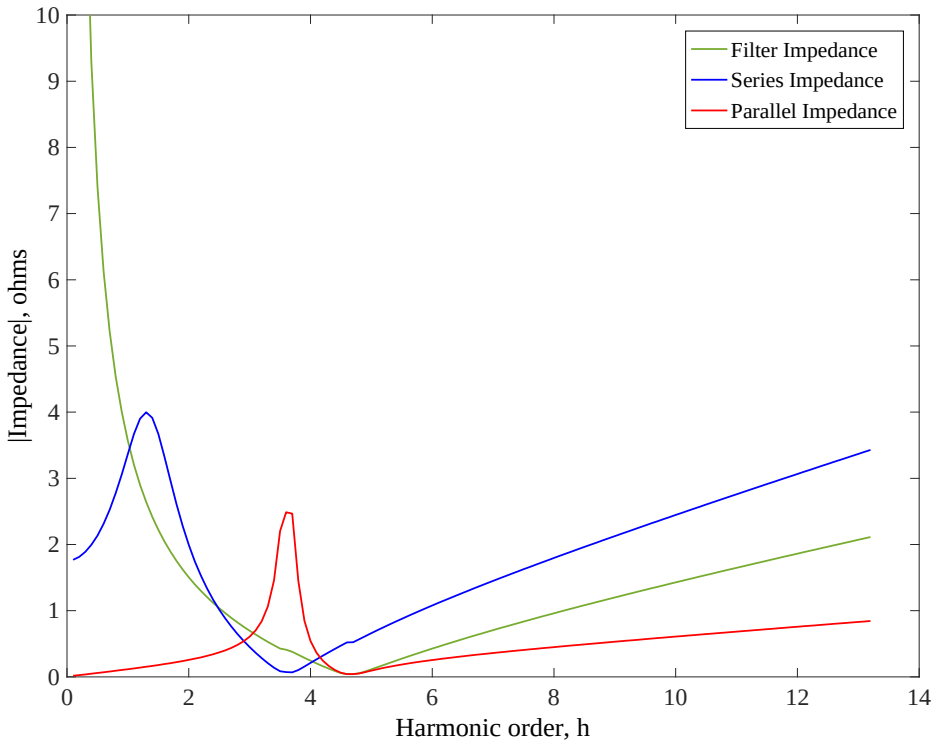

a) Damped single tuned filter

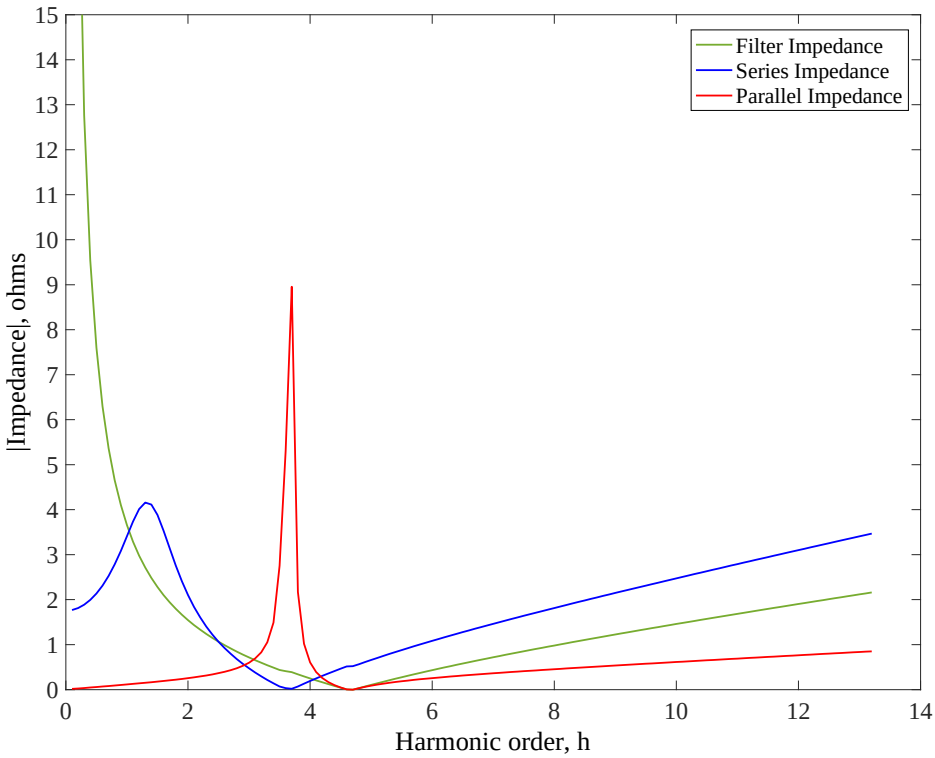

b) Undamped single tuned filter

Figure 6.4: Comparison of impedance resonance Case II

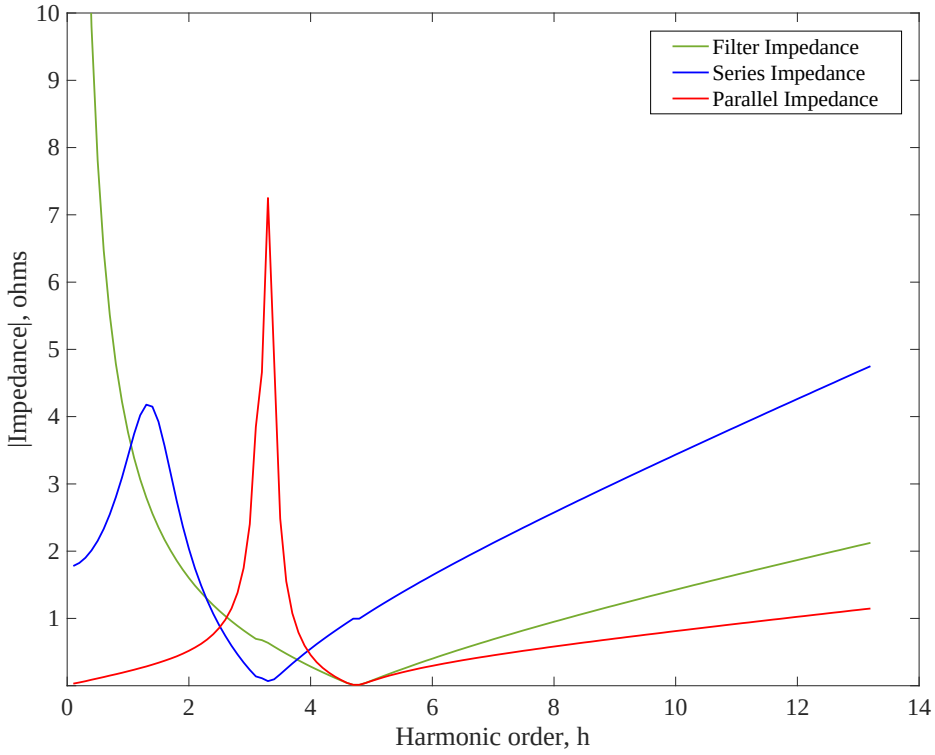

a) Damped single tuned filter

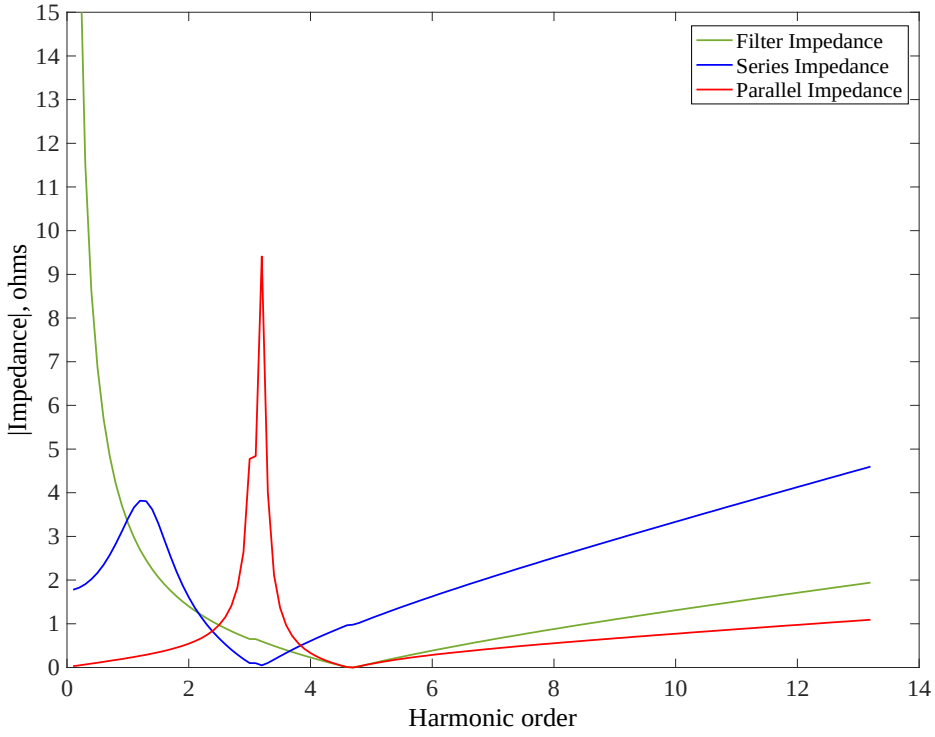

b) Undamped single tuned filter

Figure 6.5: Comparison of impedance resonance Case III

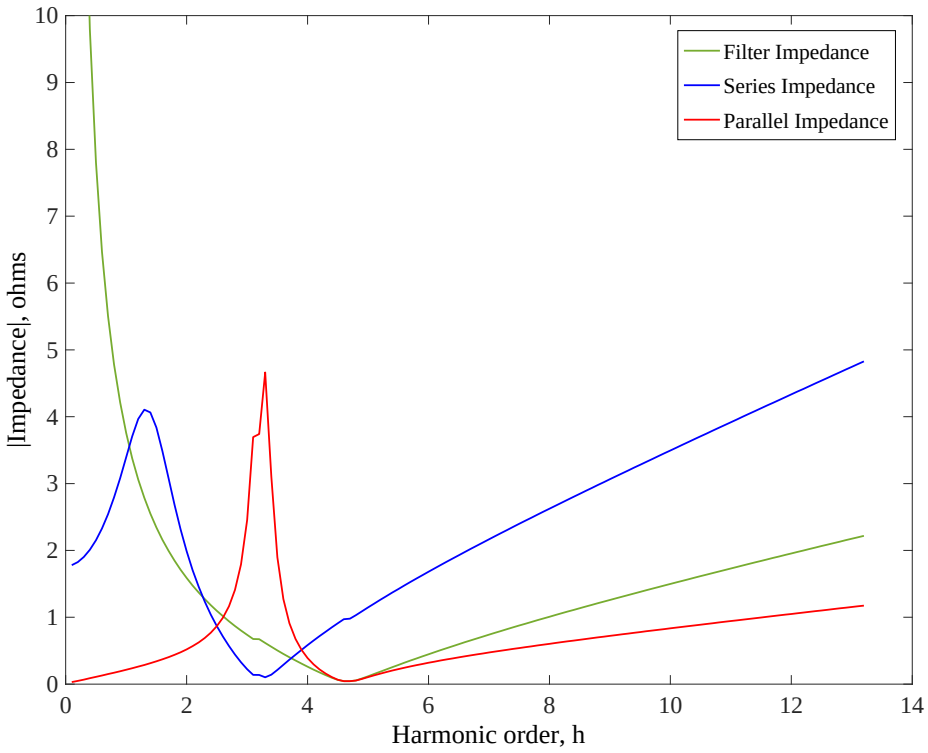

a) Damped single tuned filter

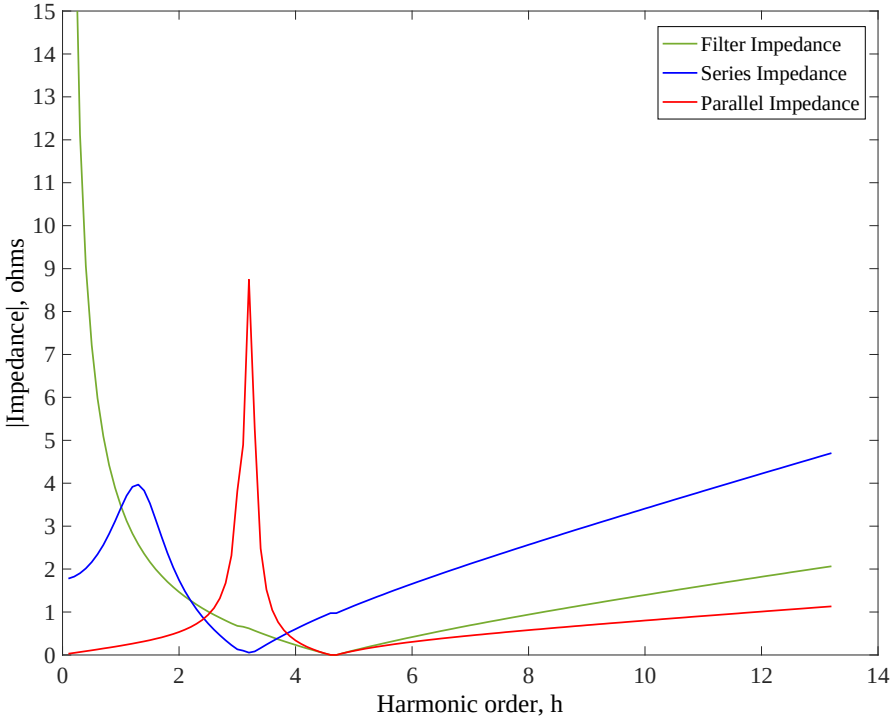

b) Undamped single tuned filter

Figure 6.6: Comparison of impedance resonance Case IV

Based on Figure 6.3 until 6.6, it is evident that resistance does not affect the resonance frequency but affect the circuit bandwidth. The resistor in a parallel resonant circuit has a damping effect, which made the circuit to have wide band instead of narrowband and overall making the circuit less selective for a damped filter.

A comparative investigation between the advantages and the disadvantages of the damped and undamped filter crucial to the engineers and manufacturers, as the damping resistor must be taken into concern when designing this type of passive filter.

6.6 Multi-objective Optimisation of Damped Single Tuned Filter

In this section, the simulation presents the numerical results achieved by the proposed algorithm when the simulation considers more than one objective to be optimized concurrently. For this task, the simulations are based on two out of four objective functions given from the previous section in this chapter. There are two objective functions to be minimized simultaneously. First is the total harmonic voltage distortion and second, the losses in the Thevenin's resistor to find the optimal damped single tuned filter subjects to the same constraints involved when simulating single-objective optimization for the damped filter in the previous section. Thus, the multi-objective problem is formulated as below:

Objective 1: Minimize $THD_V(R_{DF}, X_{CF}, X_{LF})$
Objective 2: Minimize $P_{LOSS}(R_{DF}, X_{CF}, X_{LF})$
Subject to:

$G(1) =$ Capacitor is lower than 135% of I_{CF}, 110% of V_{CF}, 120% of V_{CFP} and 135% of Q_{CF}

$G(2) = 20 \leq Q_F \leq 100$

$G(3) = h_{DF} \leq 0.9 f_n$

$G(4) = h_{DF} > h_{DFr}$

$G(5) = THD_V \leq 5\%$

$G(6) = PF \geq 90\%$ (6.10)

Table 6.14 summarized the simulated results for the multi-objective problem given in Equation (6.10) after including damped single tuned filter into the system. The best

value of R_{DF}, X_{LF} and X_{CF} was found by using the proposed method in which these results will be used for evaluating the overall performance. In this simulation, the controlling parameter of MIDACO was set to: 1) n_{pop} will change dynamically for every generation; 2) k is fixed to 100 and 3) $\Omega = 0$. For each of every objective, the algorithm was run with 100 different SEED parameter and the best solution out of a reasonable number of runs was chosen. The setting for the adjustable parameter of multi-objective problem were set to default setting where PARATEMOX=1000 and EPSILON=0.001. In this simulation, MIDACO will focus its search effort on the part of the Pareto front, which offers a best equally balanced trade-off between all objectives by setting the parameter BALANCE=0.

Table 6.14: The simulated results for multi-objective problem

No. of Cases	*SEED*	X_{CF} (Ω)	R_{DF} (Ω)	X_{LF} (Ω)	PF (%)	η (%)	P_{LOSS} (kW)	THD_V (%)	I_S (A)
Case I	91	3.78	0.0083	0.1802	97.09	99.64	6.10	2.17	727.16
Case II	99	4.06	0.0090	0.1982	94.67	99.62	6.39	2.91	744.40
Case III	50	3.78	0.0083	0.1827	98.94	99.35	10.89	1.63	709.55
Case IV	65	3.92	0.0087	0.1902	97.89	99.34	11.08	2.00	715.87

From Table 6.14, the results show that the ideal damped filter is successfully obtained while considering two objective functions concurrently subject to the constraints involved. By comparing Table 6.14 with the results of single-objective optimization in Table 6.2, the overall performance of the multi-objective optimization is satisfied with providing enhanced to the power factor, transmission efficiency as well as the losses in the resistor of Thevenin impedance.

It can be noticed that for Case I, PF is improved to 97.09% for multi-objective optimization from 95.74% and 97.05% for the single-objective optimization of the THD_V and P_{LOSS}, respectively. For Case II, PF is improved to 94.67% for multi-objective optimization compare to 93.00% and 95.03% for the single-objective optimization of the THD_V and P_{LOSS}, correspondingly. While for Case III, PF is improved to 98.94% for multi-objective optimization from 97.06% and 98.34% for the single-objective optimization of the THD_V and P_{LOSS}, individually. For Case IV, PF is improved to 97.89% for multi-objective optimization from 97.49% and 97.87% for the single-objective optimization of the THD_V and P_{LOSS}, consistently.

The increasing value of *PF* will result in an increased value of η as well. It is shown in Case I, the multi-objective optimization results to η increased to 99.64% from 99.62876625% when the objective minimize THD_V and 99.63906499% when the objective minimize P_{LOSS}. For Case II, the multi-objective optimization results to η increased to 99.62% from 99.60697930% when the objective minimize THD_V and 99.62352366% when the objective minimize P_{LOSS}. For Case III, the multi-objective optimization results to η increased to 99.35% from 99.32601203% when the objective minimize THD_V and 99.34309933% when the objective minimize P_{LOSS}. For Case IV, the multi-objective optimization results to η increased to 99.34% from 99.33200995% when the objective minimize THD_V and 99.33700710% when the objective minimize P_{LOSS}.

While the increasing value of *PF* will result from the increasing value of η which overall decrease the P_{LOSS}. Furthermore, the results show there is an improvement in the results of P_{LOSS} between multi-objective optimization and single-objective optimization. As shown in Table 6.14 and Table 6.2, the results of P_{LOSS} when solving multi-objective optimization in Case I is 6.10kW which is lower compared to the objective when solving individual optimization for THD_V and P_{LOSS} which is 6.31kW and 6.15kW. For Case II, the results for solving multi-objective optimization is 6.39kW which is better than solving individual optimization for THD_V and P_{LOSS} which is 6.74kW and 6.38kW. For Case III, the results for solving multi-objective optimization is 10.89kW which is better than solving single optimization for THD_V and P_{LOSS} which is 11.63kW and 10.94kW. For Case IV, the results for P_{LOSS} also lower for multi-objective optimization which is 11.08kW comparing to 11.32kW and 11.11kW when the simulation optimize single objective of THD_V and P_{LOSS}, respectively.

When compare the results of THD_V in Table 6.14 with Table 6.2, the results show that the value of THD_V is slightly higher for multi-objective optimization comparing to the single-objective problem. Because of the objective when maximizing THD_V is conflicting with the objective when minimizing P_{LOSS}. Thus, improvement of P_{LOSS} results to worsening THD_V. It is shown in Case I, the results for THD_V for multi-objective optimization slightly higher which is 2.17% compare to 1.63% when the objective minimize THD_V and 2.17% when the objective minimize P_{LOSS}. For Case II, the results for THD_V for multi-objective optimization is 2.91% which is higher when

compare to single-objective optimization of THD_V and P_{LOSS} which is 2.20% and 2.84%, respectively. For Case III, the multi-objective optimization results to THD_V increased to 1.63% from 1.09% when the objective minimize THD_V and 1.45% when the objective minimizes P_{LOSS}. For Case IV, the multi-objective optimization results to THD_V increased to 2.00% from 1.39% when the objective minimize THD_V and 1.86% when the objective minimizes P_{LOSS}. However, although there is a slight increase in the results of THD_V, but overall THD_V is still below than 5% which is below than suggested standard by IEEE.

In table 6.14 also shows the performance of the proposed filter to the current source, I_S for multi-objective problem where for a Case I, Case II, Case III and Case IV, the results for the I_S is 727.16A, 744.40A, 709.55A and 715.87A, respectively. Generally, the value of I_S for multi-objective is lower than the value of I_S for single-objective optimization given in Table 6.2. This reduction of current source flow will reduce the resistive losses in the circuit which generally results in an improvement to the power factor as well as transmission efficiency.

Based on the simulation results in Table 6.14, the final set of non-dominated solutions for Case I until Case IV is shown in Figure 6.7 until 6.10, respectively. In Figures 6.7a, 6.8a, 6.9a and 6.10a, the graph shows the closed-up Pareto front the best equally balanced trade-off between P_{LOSS} and THD_V. Although each of the figures shows different non-dominated solutions, for example the number of Pareto Front of Case II in Figures 6.8 has visibly less non-dominated solutions than Case III in Figures 6.9, the results still capture the most relevant trade-off part of the front between both objectives. Figures 6.7b, 6.8b, 6.9b and 6.10b show that from the last 20,000 evaluation, which is marks as small cross red on how MIDACO concentrates its search effort on that part of the Pareto front, which contains the MIDACO solution. The position of the individual MIDACO solution among the Pareto front is highlighted as semi-transparent green hexagon.

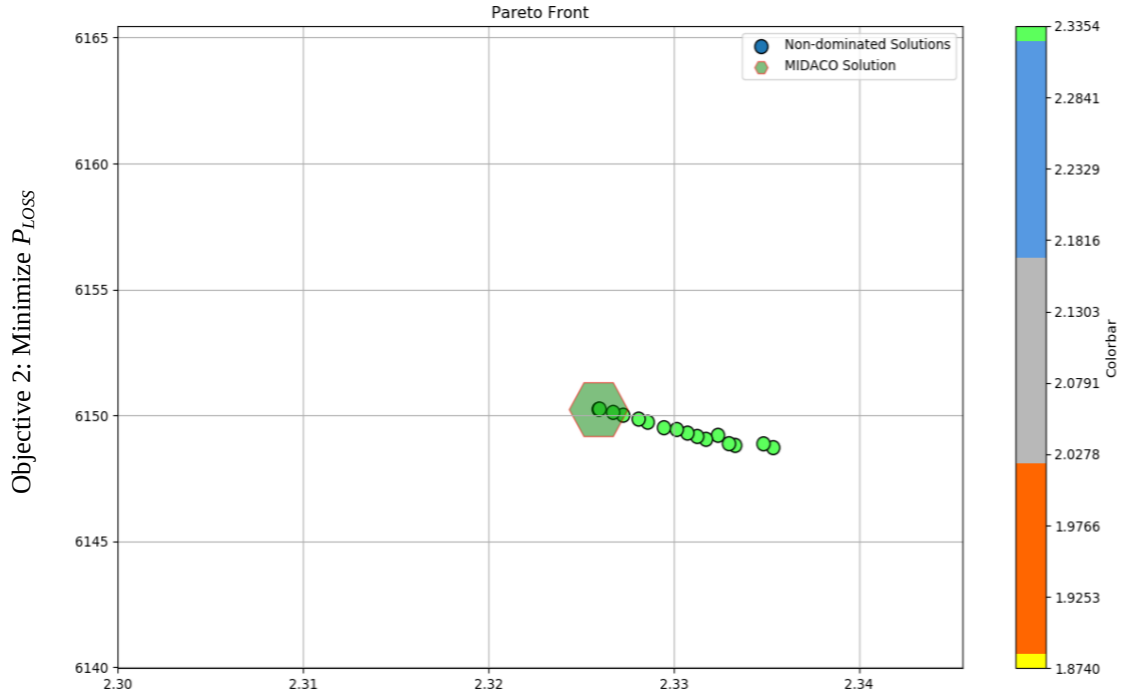

a) The set of non-dominated solutions

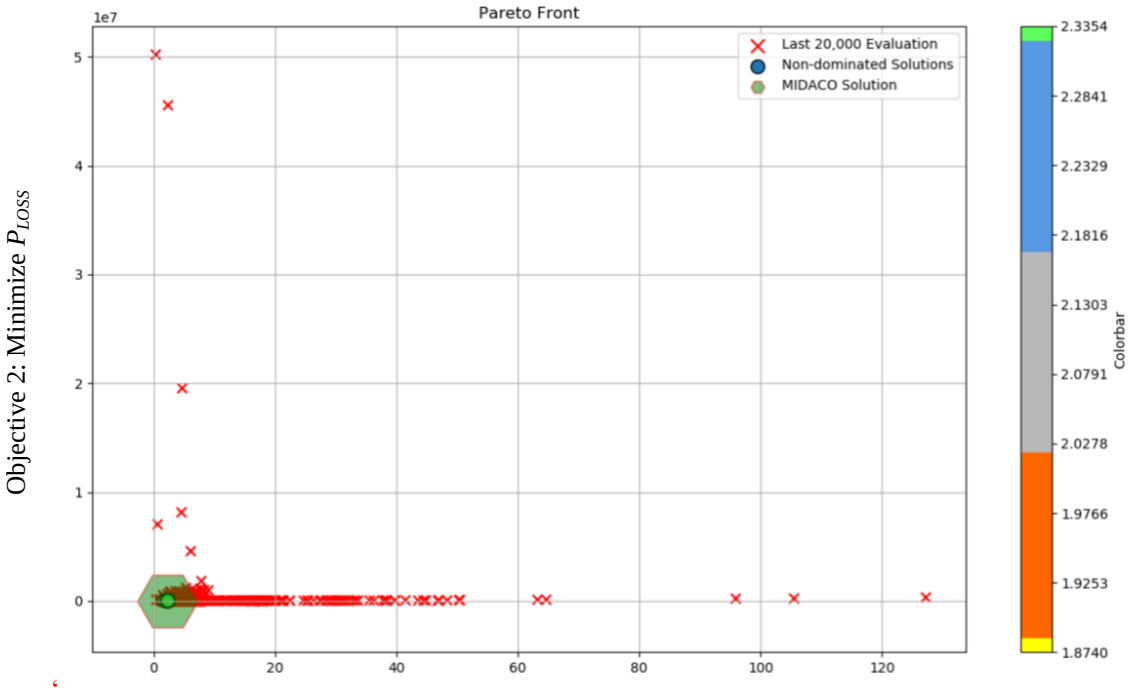

b) The set of non-dominated solutions with the last 20,000 evaluation

Figure 6.7: The best set of Pareto Fronts obtained for Case I

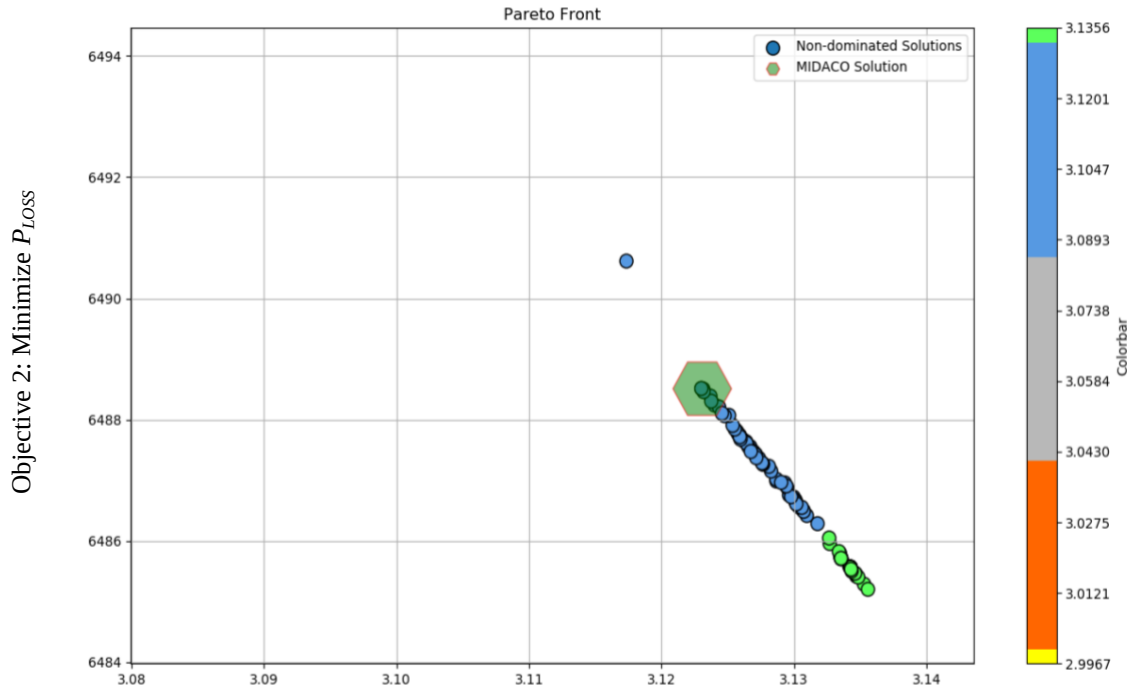

Objective 1: Minimize THD_V

a) The set of non-dominated solutions

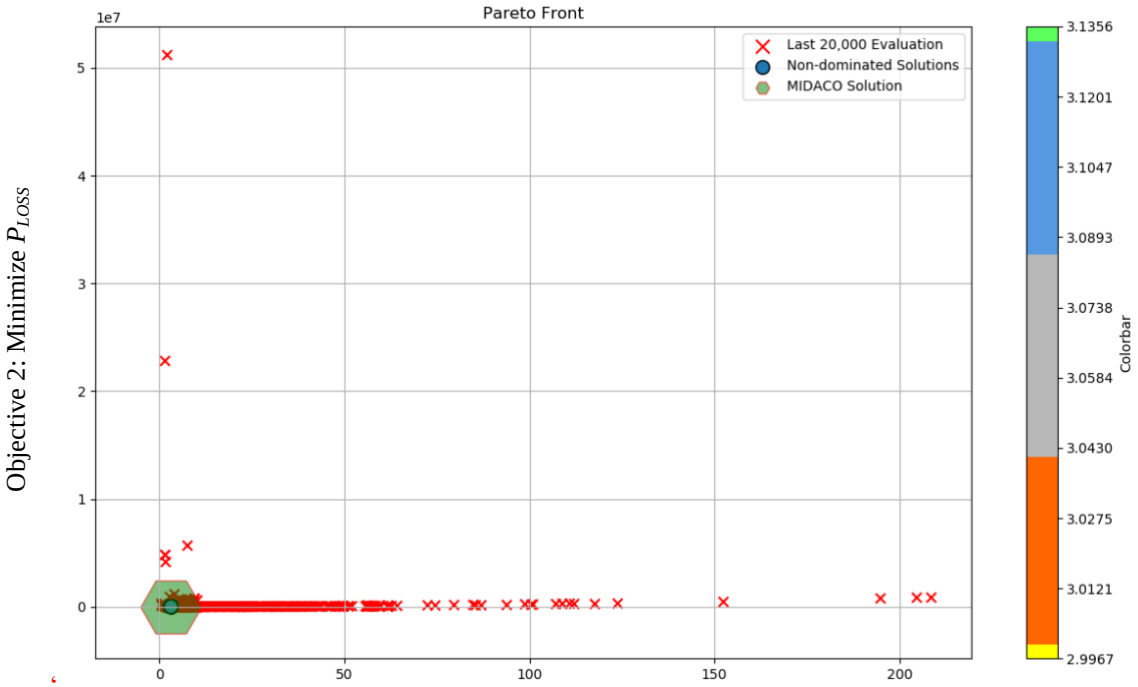

Objective 1: Minimize THD_V

b) The set of non-dominated solutions with the last 20,000 evaluation

Figure 6.8: The best set of Pareto Fronts obtained for Case II

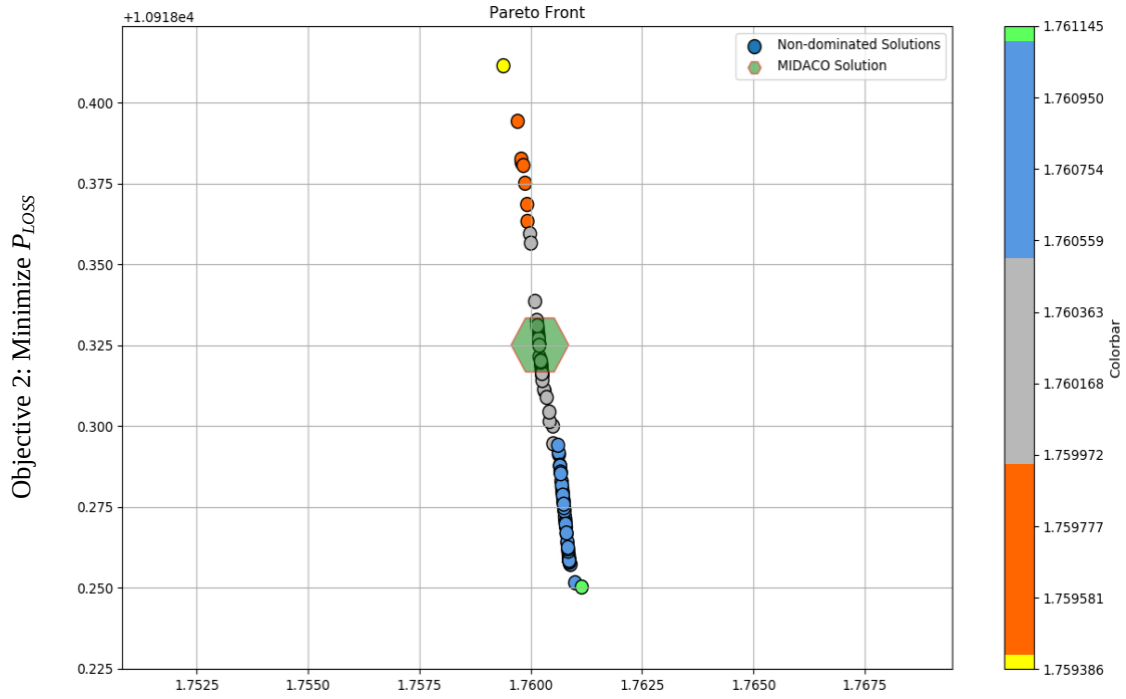

a) The set of non-dominated solutions

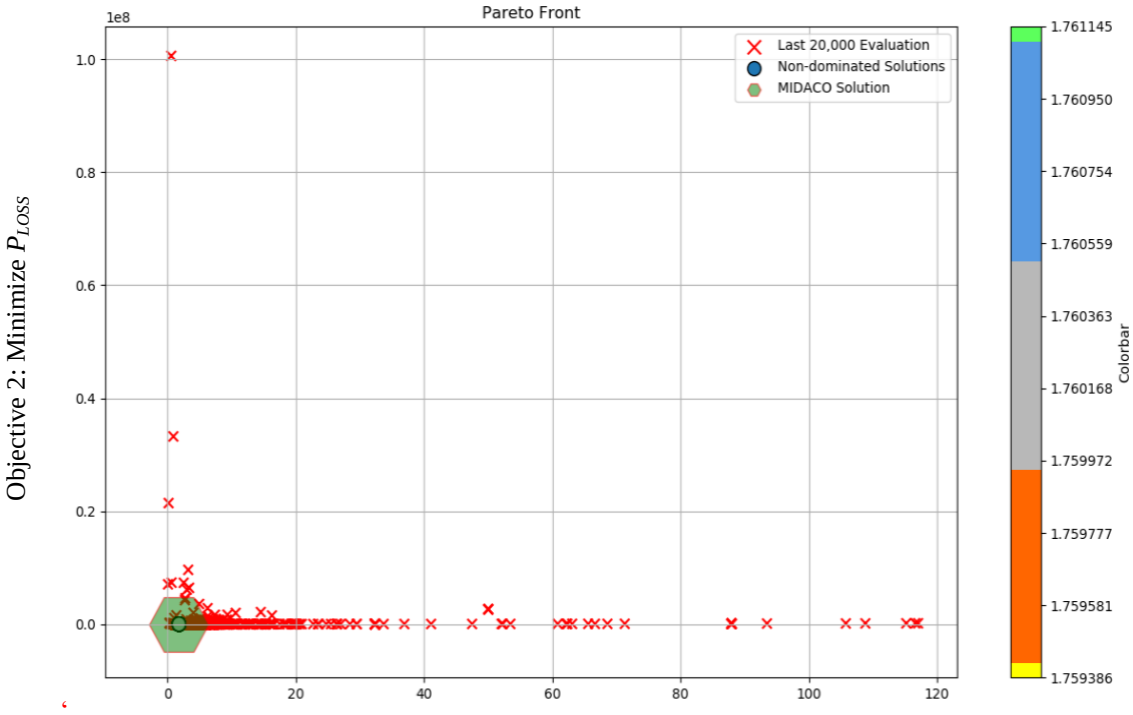

b) The set of non-dominated solutions with the last 20,000 evaluation

Figure 6.9: The best set of Pareto Fronts obtained for Case III

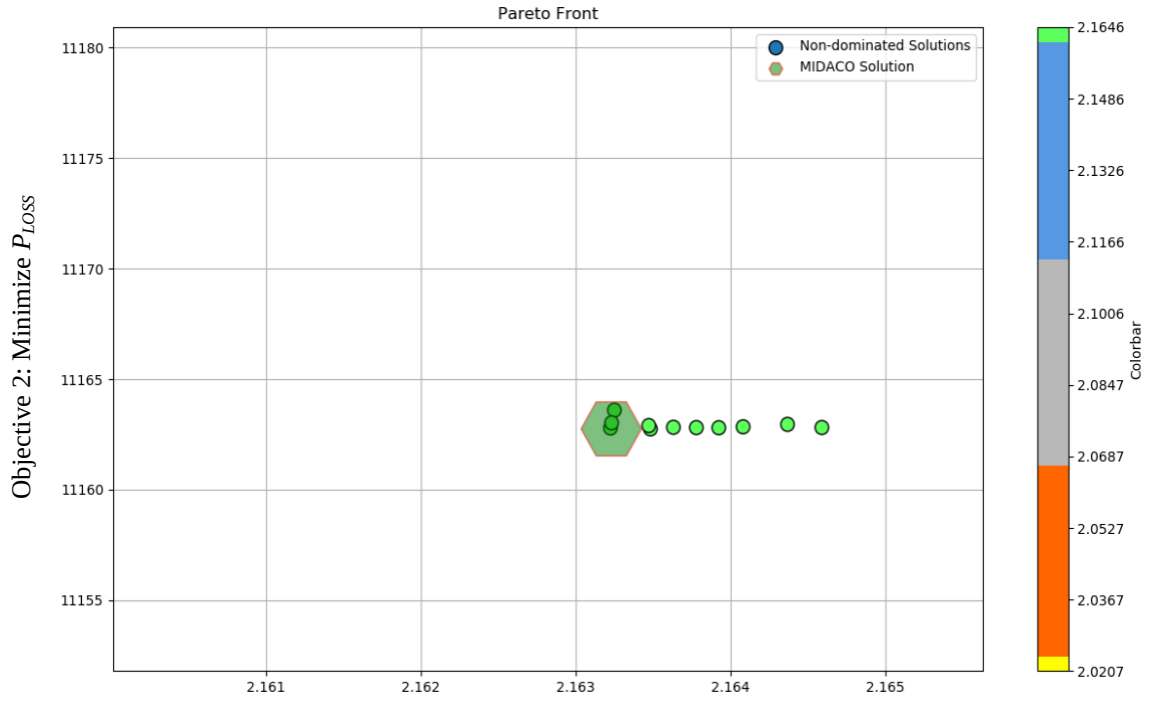

Objective 1: Minimize THD_V

a) The set of non-dominated solutions

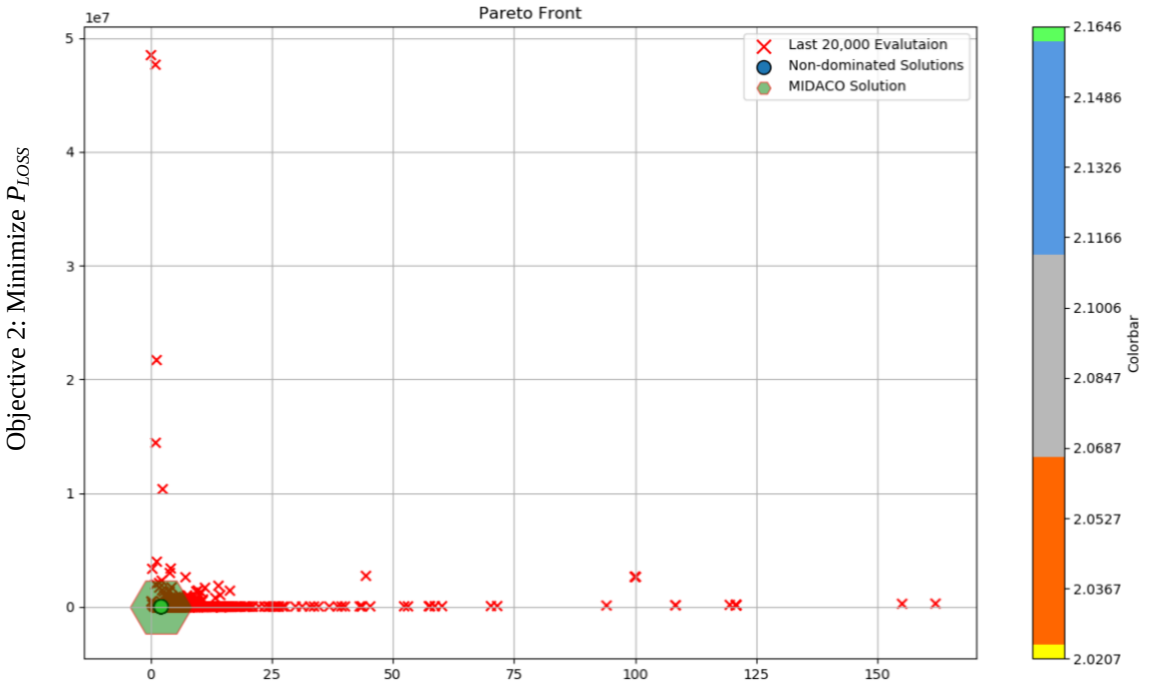

Objective 1: Minimize THD_V

b) The set of non-dominated solutions with the last 20,000 evaluation

Figure 6.10: The best set of Pareto Fronts obtained for Case IV

Table 6.15 shows the impact of varying BALANCE parameter on the optimal solutions where this parameter only assigned to non-priority between objectives. In contrast to the results in Figure 6.7, a more exceptional epsilon tolerance for the Pareto dominance filtering was used to create the plots in Figure 6.11 until Figure 6.15, which generally results generally in more display of non-dominated solutions. For this simulation, the EPSILON parameter is set to 0.0001.

Table 6.15: The simulated results with different BALANCE parameter

Set	BALANCE	X_{CF} (Ω)	R_{DF} (Ω)	X_{LF} (Ω)	PF (%)	η (%)	P_{LOSS} (kW)	THD_V (%)	I_S (A)
1	0	3.78	0.0083	0.1795	97.06	99.64	6.11	2.15	727.37
2	1.0	3.54	0.0069	0.1345	95.08	99.62	6.38	1.57	743.37
3	2.0	3.32	0.0070	0.1482	96.16	99.63	6.27	1.80	737.35
4	0.91	3.78	0.0080	0.1503	95.50	99.63	6.30	1.66	738.67
5	0.18	3.78	0.0083	0.1796	97.07	99.64	6.10	2.15	727.34

From Table 6.15, the results show five different set simulation with different BALANCE parameter where each of the simulations will results in different optimal solutions of the optimization. For the first setting, the BALANCE parameter is set to zero which means that the search effort on the part of the Pareto front which offers the best equally balanced trade-off between both objectives. When the BALANCE parameter is set to 1.0 and 2.0, MIDACO will be assigned to focus its search effort exclusively only to the first and second objective, respectively. For settings 4 and 5, the search effort represents some unequal priority between objectives. For setting 4, the simulation search effort focuses primarily on Objective 1 and minor on Objective 2. Setting 5 is vice versa to setting 4. Based on the table, the results show that the optimal filter can be obtained with different optimal solutions considering four objective functions simultaneously where the BALANCE parameter is significant and has a high impact to each of the solutions. Figure 6.11 until Figure 6.15 shows clearly the impact of different BALANCE parameter on the shape of the Pareto front for all five settings applied in Table 6.15.

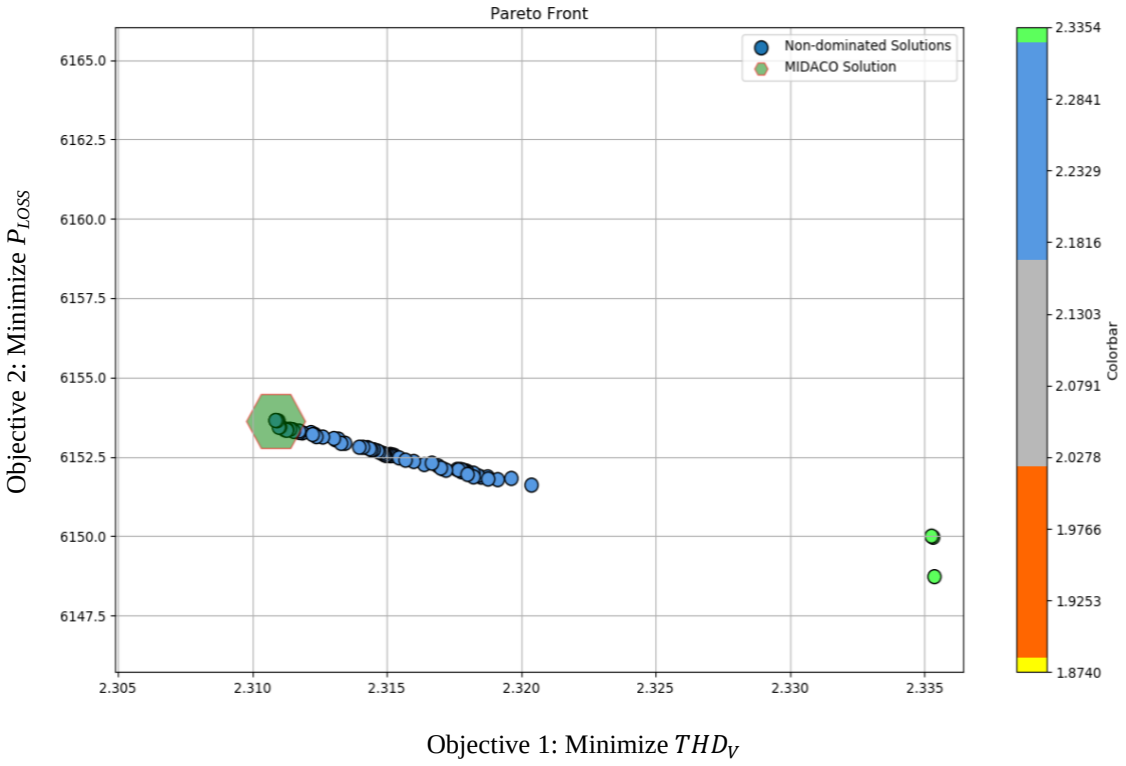

Figure 6.11: The set of non-dominated solutions when parameter BALANCE=0

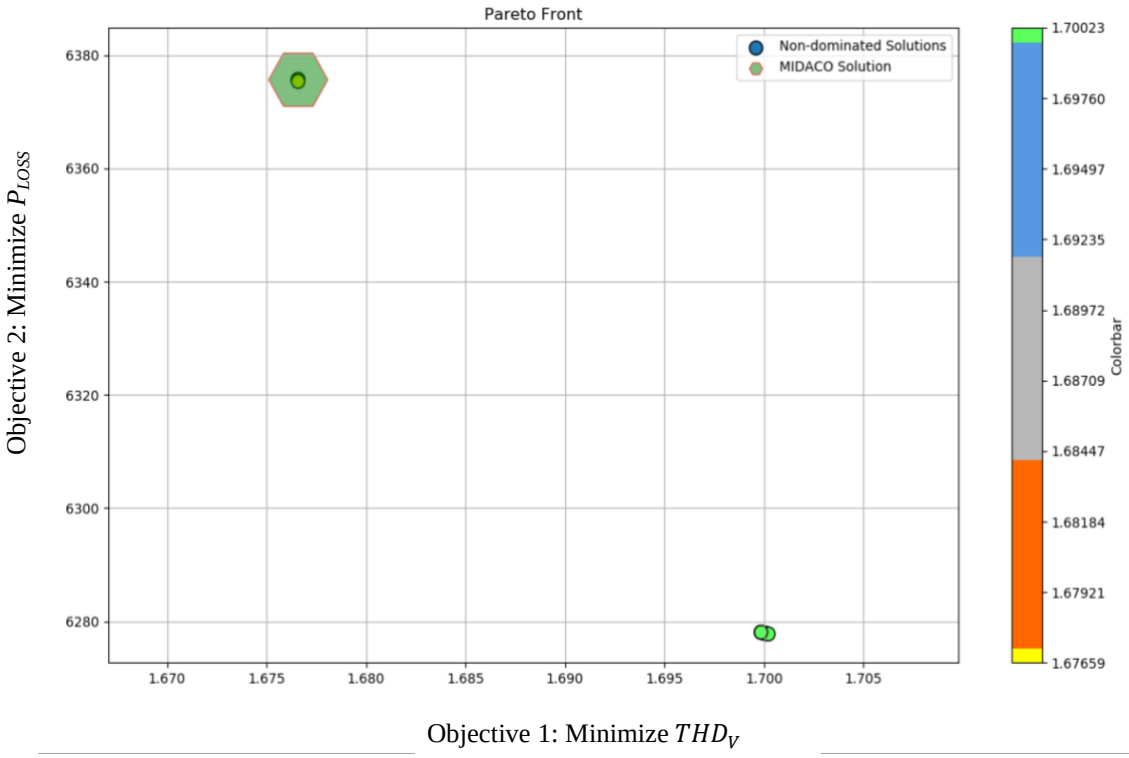

Figure 6.12: The set of non-dominated solutions when parameter BALANCE=1.0

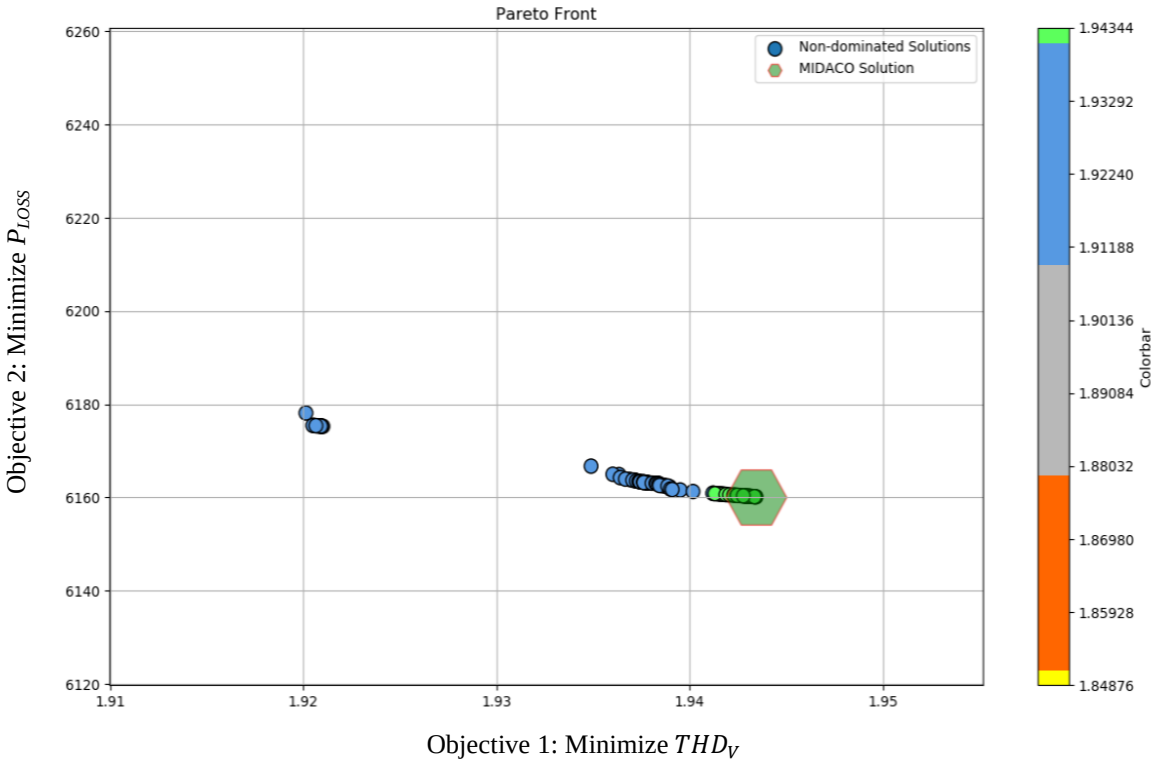

Figure 6.13: The set of non-dominated solutions when parameter BALANCE=2.0

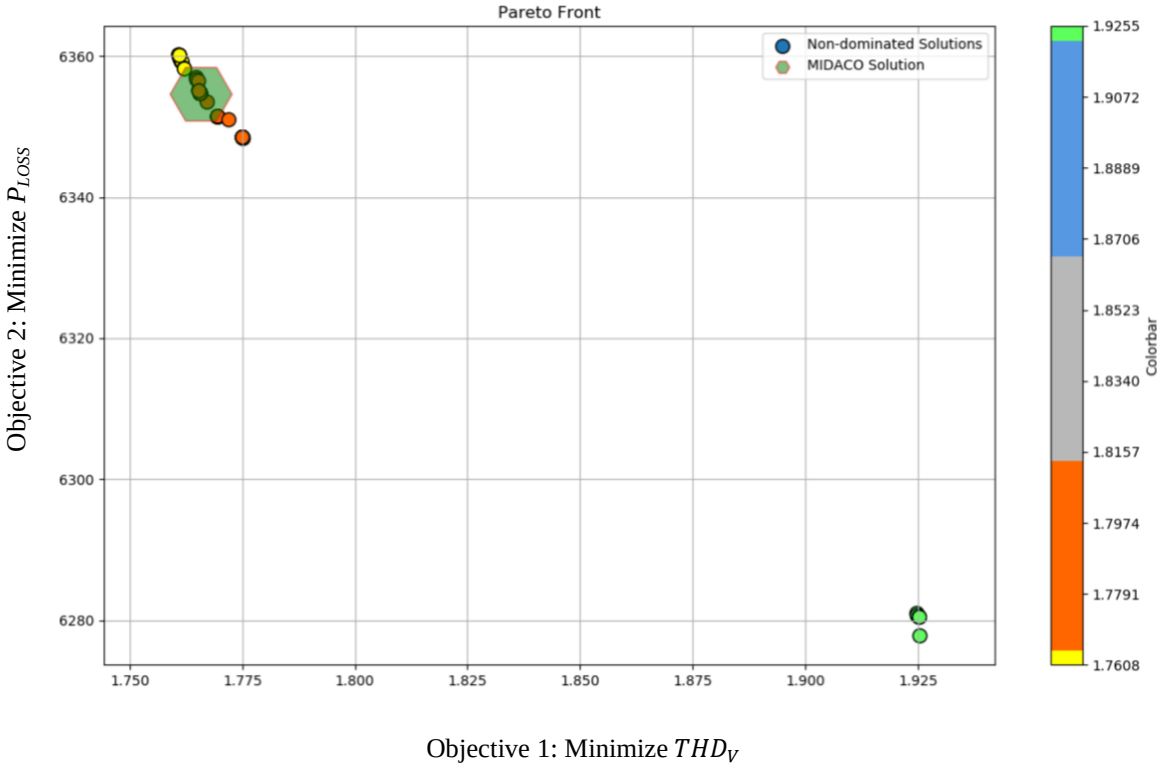

Figure 6.14: The set of non-dominated solutions when parameter BALANCE=0.91

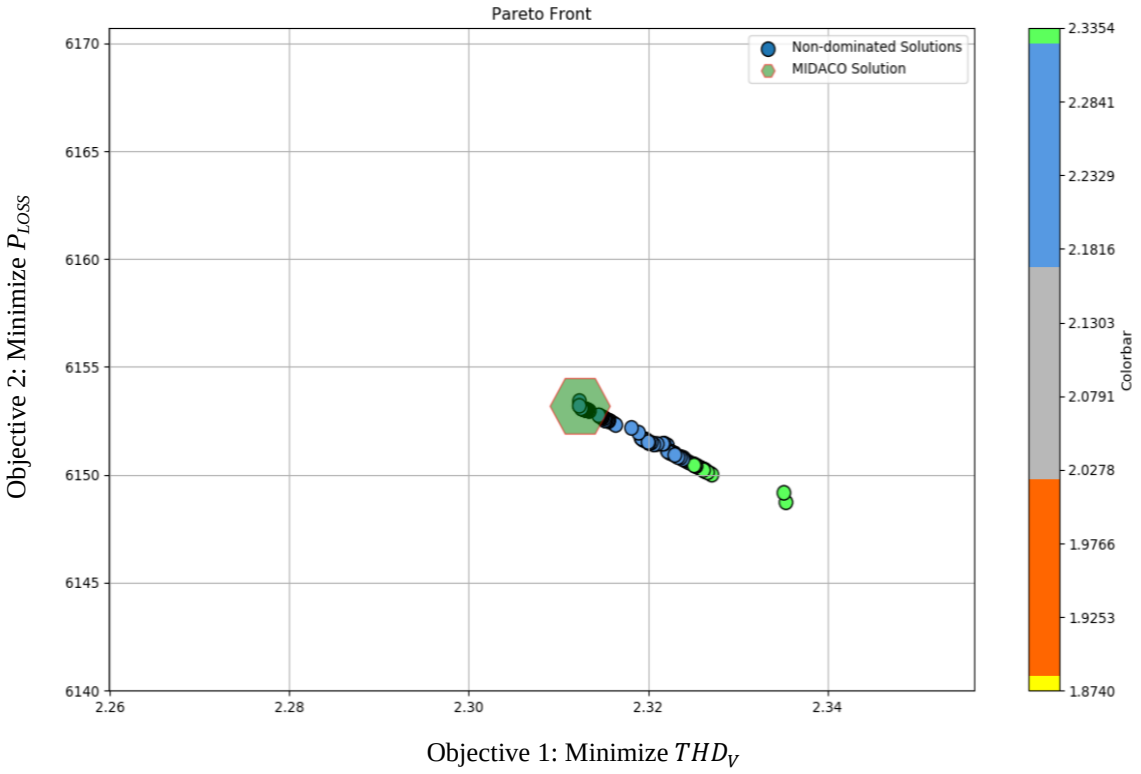

Figure 6.15: The set of non-dominated solutions when parameter BALANCE=0.18

6.7 Summary

In this chapter, the simulation of the previous chapter is continued with finding the optimal parameters in the same system with additional consideration of intrinsic resistance of the inductance as one of the variables that need to be optimised. Four cases that have been studied where the results obtained are based on three objectives. Then, the comparison results with GA and PSO highlighted the advantages of the proposed method. Lastly, the comparison of the damped and undamped single tuned filter is also discussed and proved that the value of the inductance resistor affects the performance of the power system. Overall, the numerical results revealed that the proposed method does highly benefit for multi-objective approaches over single-objective optimization on comprehensive passive filter design.

Chapter 7

Conclusions and Future Works

7.1 Conclusions

This research has raised the importance of harmonics in the power system, which is mainly because of the growth of the nonlinear load usage. The electrical pollution caused by power system harmonics such as voltage or current distortions and resonances has become a severe problem. This may result in the malfunctions, overvoltage, or overcurrent of the facility.

The research motivation and determination of this thesis have been presented in Chapter 1. The main aim of this research is to implement a metaheuristic optimization algorithm, MIDACO, for the design of passive harmonic filters. However, there are many types of shunt passive filter that has been proposed in previous wherein the single-tuned filter is the most common, and it is still extensively used in industry until today. Besides, there are many advantages of the single-tuned filter as it is simple, reliable, and cost-effective and because of the dual purpose of the filter, which does not only eliminate the harmonics but can improve the power factor, as well making it the first choice.

In designing a passive filter, it is a large task and challenge for engineers to meet the measurements, criteria, and practical standard that must be carefully followed. Therefore, Chapter 2 presented a comprehensive review on the effects of the filter, as well as the equipment connected to the source network, the choice of different types of

passive filter, and the previous methodologies with the selections of single-objective optimization and multiobjective optimization. Furthermore, the research gap that was not addressed and investigated by previous research was also identified. Hence, this research is introduced to overcome the previous studies with MIDACO as a first-time method to be used in the literature for power harmonics topic. This has led to the proposed main research objectives and contribution to investigate two types of single-tuned filter, namely, undamped and damped filter. The designs for both filters considered the parameters of the filters, which can avoid the harmonic resonance, at least to a minimum of 90% limit of power factor. In contrast, the voltage THD must not be greater than 5% to follow IEEE Std. 519-2014 and the capacitor value based on IEEE Std. 18-2012.

In Chapter 3, the general background of power system harmonics is presented, which includes the definition, source, and identification of harmonics. Various technologies of harmonics that aimed to eliminate harmonics have been explained in this chapter in order to solve the power quality problem where the main focus is on the technique when using a single-tuned passive filter. Although active filters are proven to be the most effective method in terms of improving power quality problem, nonetheless, most engineers still select PPF when planning the power system for harmonics elimination because it is economical, efficient, and reliable. Moreover, it requires only simple configurations of passive components.

In Chapter 4, the proposed method has been presented in detail. Apart from that, several explanations on the background of ant colony algorithm and the four new heuristic methods that were included in the MIDACO execution to develop the global competency of the ant colony algorithm were also included. Besides, this chapter also has included the concept of Utopia–nadir–balance, where this concept is specifically applied when solving the multiobjective problem. This chapter also presents specific descriptions of the parameter selection including the non-compulsory parameters when using MIDACO, where each of the parameters must be carefully chosen for the solution in order to achieve the best performance and results.

The first objective of this thesis has been executed where all of the performance results are presented in Chapter 5. There are four cases that have been tested, and the results were achieved, which satisfied four objective functions and the involved constraints.

The results of this investigation present the importance of adding single-tuned filter into an existing network, where overall the results highlight the importance of considering IEEE-18 for power shunt capacitors in order to solve the optimal solutions.

The results of this investigation also prove the robustness using MIDACO when compared with the simulated results using other two evolutionary computation optimizers in the literature, which is a GA and PSO. The main highlights of the results are on the better solution and the fastest computation time for the proposed method to reach an optimal solution compared to the other methods.

The accuracy of the proposed method is also proven when the proposed method is tested and compared to the prior publications. In contrast, the objective functions and constraints follow the comparative journal. The results of the investigation show that the voltage THD for the proposed method is below the standard limit, whereas the prior publications exceed the standard limit. Overall, the numerical performance for all methods has certified that the proposed method designates the robust software tool with better solution subject to constraint satisfaction with the fastest convergence capability to achieve the optimal solution subject to the condition applied.

In Chapter 6, this thesis continued with the concern of energy losses in the single-tuned filter that must be considered. Therefore, the simulation is continued with additional consideration of intrinsic resistance of the inductance as one of the variables that need to be optimized. Addition of resistance is a standard passive damping method, which aims to attenuate the peak of the LC filter resonance.

In this chapter, four cases were studied in which the results obtained are also based on four objectives functions. Besides, there is an additional constraint known as a quality factor that was added to the constraints involved in the previous chapter. Additionally, the aim of this research is also to compare this proposed technique with other metaheuristic techniques. The most apparent outcomes from the study displayed that the proposed technique recorded constraints satisfaction and better efficiency as the simulation findings exhibited that global maximum and minimum could be attained to satisfy all constrictions set and functions outlined. Besides, this research also exhibits the competency of fast convergence for the proposed technique toward obtaining the best solution to the issues highlighted. As such, a damping resistor of the single-tuned

filter was weighed in, whereby the benefits and glitches of damping filter over undamped filter were identified. Besides, the study in this chapter also has been to focus on solving the multiobjective problem. Overall, the numerical results revealed that the proposed method does highly benefit from multiobjective approaches over single-objective optimization on a comprehensive passive filter design. Also, the advantages and disadvantages of damping over the undamped filter were also presented in this thesis.

To summarize, the proposed method provides a helpful tool where the performance result is satisfactory, apart from exhibiting a reasonably good solution. Besides, the proposed method proved the precision and efficiency of this technique to reach the optimal solutions. In terms of single-tuned filter design, this proposed method guaranteed that this design is safe and that there are no risks of electrical resonance, and the capability of this design to operate following the standard limit is proven.

7.2 Future Work

The following describes the future research concerning the application of the proposed method designing passive filter for harmonics elimination:

- To include the cost such as cost for the maintenance, investment, and total filter as the objective function needs to be minimized to highlight the advantage of the single-tuned filter.

- The planning of the passive filter is very critical especially to the performance in order to satisfy the standard of harmonic filtering. Therefore, it is suggested to do multiset or different types of single-tuned filter at a high-voltage system with more complex harmonic situations using the proposed method.

- To test the proposed method with different industrial power system and more complicated case study.

- In this research, the proposed method only optimizes single-tuned filter, which only has up to three optimization variables. Therefore, it is suggested to extend the research using the proposed method for different types of passive filter such as double-tuned filter, C-type filter, and more, which consist of four or more optimization variables.

- To compare the proposed method with advanced DE, PSO, and ACO variants published in reputable journals including the recent winners of single-objective real-parameter optimization competitions on the IEEE Congress on Evolutionary Computation.

- The proposed method is also suitable for solving general many-objective single-tuned design problems with up to thousands of variables and hundreds of objectives. Therefore, in the future, it is suggested for future researchers to design different comprehensive passive filter designs through as many objective approaches as possible.

.

List of References

[1] I. Etxeberria-Otadui, D. Frey, S. Bacha, and B. Raison, “Medium Voltage Power Electronics Devices for Distribution Grids,” in *Advanced Solutions in Power Systems: HVDC, FACTS, and Artificial Intelligence*, First Edit., John Wiley & Sons, Inc., pp. 681–715, 2016.

[2] M. Rosu *et al.*, *Power Electronics and Drive Systems*, First Edit. John Wiley & Sons, Inc., 2018.

[3] W. M. Grady and S. Santoso, “Understanding power system harmonics,” *IEEE Power Eng. Rev.*, vol. 21, no. 11, pp. 8–11, 2001.

[4] E. Normanyo, “Mitigation of harmonics in a three-phase, four-wire distribution system using a system of shunt passive filters,” *Int. J. Eng. Technol.*, vol. 2, no. 5, pp. 761–774, 2012.

[5] M. M. Islam, *Power Quality : Harmonics*, First Edit. John Wiley & Sons, Inc., 2018.

[6] M. G. Simões and F. A. Farret., *Power quality analysis*, First Edit. John Wiley & Sons, Inc., 2017.

[7] S. Sakar, M. E. Balci, S. H. E. Abdel Aleem, and A. F. Zobaa, “Increasing PV hosting capacity in distorted distribution systems using passive harmonic filtering,” *Electr. Power Syst. Res.*, vol. 148, pp. 74–86, 2017.

[8] J. Zhang, “Power electronics in future electrical power grids,” *2013 4th IEEE Int. Symp. Power Electron. Distrib. Gener. Syst.*, pp. 1–3, 2013.

[9] V. Karthikeyan, S. Rajasekar, V. Das, P. Karuppanan, and A. K. Singh, “Grid-connected and off-grid solar photovoltaic system,” *Green Energy Technol.*, pp. 125–157, 2017.

[10] S. K. Rönnberg *et al.*, “On waveform distortion in the frequency range of 2 kHz–150 kHz—Review and research challenges,” *Electr. Power Syst. Res.*, vol. 150, pp. 1–10, 2017.

[11] R. K. Hartana and G. G. Richards, “Comparing capacitive and LC compensators

for power factor correction and voltage harmonic reduction," *Electr. Power Syst. Res.*, vol. 17, no. 1, pp. 57–64, 1989.

[12] G. G. Richards, P. Klinkhachorn, O. T. Tan, and R. K. Hartana, "Optimal LC compensators for nonlinear loads with uncertain nonsinusoidal source and load characteristics," *IEEE Trans. Power Syst.*, vol. 4, no. 1, pp. 30–36, 1989.

[13] S. H. E. Abdel Aleem, M. E. Balci, and S. Sakar, "Effective utilization of cables and transformers using passive filters for non-linear loads," *Int. J. Electr. Power Energy Syst.*, vol. 71, pp. 344–350, 2015.

[14] N. H. B. A. Kahar and A. F. Zobaa, "Application of mixed integer distributed ant colony optimization to the design of undamped single-tuned passive filters based harmonics mitigation," *Swarm Evol. Comput.*, vol. 44, pp. 187–199, 2018.

[15] M. Mamdouh, A. Aziz, E. E. A. El-zahab, A. M. Ibrahim, and A. F. Zobaa, "Practical considerations regarding power factor for nonlinear loads," *IEEE Trans. Power Deliv.*, vol. 19, no. 1, pp. 337–341, 2004.

[16] M. S. Almutairi and S. Hadjiloucas, "Harmonics mitigation based on the minimization of non-Linearity current in a power ystem," *Designs*, vol. 3, no. 2, p. 29, 2019.

[17] S. H. E. Abdel Aleem, A. F. Zobaa, and M. M. Abdel Aziz, "Optimal C-type passive filter based on minimization of the voltage harmonic distortion for nonlinear loads," *IEEE Trans. Ind. Electron.*, vol. 59, no. 1, pp. 281–289, 2012.

[18] S. H. E. A. Aleem and M. T. E. and A. F. Zobaa, "Different design approaches of shunt passive harmonic filters based on IEEE Std. 519-1992 and IEEE Std. 18-2002," *Recent Patents Electr. Electron. Eng.*, vol. 6, no. 1, pp. 68–75, 2013.

[19] G. W. Chang, S. Y. Chu, and H. L. Wang, "A new method of passive harmonic filter planning for controlling voltage distortion in a power system," *IEEE Trans. Power Deliv.*, vol. 21, no. 1, pp. 305–312, 2006.

[20] T. D. C. Busarello, J. A. Pomilio, and M. G. Simões, "Passive filter aided by shunt compensators based on the conservative power theory," *IEEE Trans. Ind. Appl.*, vol. 52, no. 4, pp. 3340–3347, 2016.

[21] C. Kawann and A. E. Emanucl, "Passive shunt harmonic filters for low and medium voltage: a cost comparison study," *IEEE Trans. Power Syst.*, vol. 11, no.

4, pp. 1825–1831, 1996.

[22] J. C. Das, *Power System Harmonics and Passive Filter Designs*. John Wiley & Sons, Inc., 2015.

[23] M. Singh and S. Mahapatra, "Implementation of passive filters for harmonics reduction," *Int. J. Adv. Sci. Technol.*, vol. 78, no. 1, pp. 1–12, 2015.

[24] M. Mohammadi, A. M. Rozbahani, and M. Montazeri, "Multi criteria simultaneous planning of passive filters and distributed generation simultaneously in distribution system considering nonlinear loads with adaptive bacterial foraging optimization approach," *Int. J. Electr. Power Energy Syst.*, vol. 79, pp. 253–262, 2016.

[25] P. E. Sutherland, "Harmonics in electrical power systems : Effects of new technologies," *IEEE Ind. Appl. Soc. Annu. Meet. IAS*, pp. 1–13, 2014.

[26] J. C. Leite, I. P. Abril, M. E. de L. Tostes, and R. C. L. de Oliveira, "Multi-objective optimization of passive filters in industrial power systems," *Electr. Eng.*, vol. 99, no. 1, pp. 387–395, 2017.

[27] P. P. Biswas, P. N. Suganthan, and G. A. J. Amaratunga, "Minimizing harmonic distortion in power system with optimal design of hybrid active power filter using differential evolution," *Appl. Soft Comput.*, vol. 61, pp. 486–496, 2017.

[28] M. E. Balci and S. Sakar, "Optimal design of single-tuned passive filters to minimize harmonic loss factor," *Middle East J. Sci. Res.*, vol. 21, no. 11, pp. 2149–2155, 2014.

[29] Y. Y. Hong and W. J. Liao, "Optimal passive filter planning considering probabilistic parameters using cumulant and adaptive dynamic clone selection algorithm," *Int. J. Electr. Power Energy Syst.*, vol. 45, no. 1, pp. 159–166, 2013.

[30] M. M. Elkholy, M. A. El-Hameed, and A. A. El-Fergany, "Harmonic analysis of hybrid renewable microgrids comprising optimal design of passive filters and uncertainties," *Electr. Power Syst. Res.*, vol. 163, pp. 491–501, 2018.

[31] G. W. Chang, H. L. Wang, and S. Y. Chu, "A probabilistic approach for optimal passive harmonic filter planning," *IEEE Trans. Power Deliv.*, vol. 22, no. 3, pp. 1790–1798, 2007.

[32] G. W. Chang, H. L. Wang, and S. Y. Chu, “Strategic placement and sizing of passive filters in a power system for controlling voltage distortion,” *IEEE Trans. Power Deliv.*, vol. 19, no. 3, pp. 1204–1211, 2004.

[33] H. H. Zeineldin and A. F. Zobaa, “Particle swarm optimization of passive filters for industrial plants in distribution networks,” *Electr. Power Components Syst.*, vol. 39, no. 16, pp. 1795–1808, 2011.

[34] A. A. A. El-Ela, S. Allam, and H. El-Arwash, “An optimal design of single tuned filter in distribution systems,” *Electr. Power Syst. Res.*, vol. 78, no. 6, pp. 967–974, Jun. 2008.

[35] J. C. Leite, I. P. Abril, and M. S. S.Azevedo, “Capacitor and passive filter placement in distribution systems by nondominated sorting genetic algorithm-II,” *Electr. Power Syst. Res.*, vol. 143, pp. 482–489, 2017.

[36] A. Menti, T. Zacharias, and J. Milias-Argitis, “Optimal sizing and limitations of passive filters in the presence of background harmonic distortion,” *Electr. Eng.*, vol. 91, no. 2, pp. 89–100, 2009.

[37] D. M. Soomro and M. M. Almelian, “Optimal design of a single tuned passive filter to mitigate harmonics in power frequency,” *ARPN J. Eng. Appl. Sci.*, vol. 10, no. 19, pp. 9009–9014, 2015.

[38] I. F. Mohamed, S. H. E. Abdel Aleem, A. M. Ibrahim, and A. F. Zobaa, “Optimal sizing of C-Type passive filters under non-sinusoidal conditions,” *Energy Technol. Policy*, vol. 1, no. 1, pp. 35–44, 2014.

[39] S. H. E. Abdel Aleem, A. F. Zobaa, and M. E. Balci, “Optimal resonance-free third-order high-pass filters based on minimization of the total cost of the filters using Crow Search Algorithm,” *Electr. Power Syst. Res.*, vol. 151, pp. 381–394, 2017.

[40] H. Hu, Z. He, and S. Gao, “Passive filter design for China high-speed railway with considering harmonic resonance and characteristic harmonics,” *IEEE Trans. Power Deliv.*, vol. 30, no. 1, pp. 505–514, 2015.

[41] A. Lamlom, A. Ibrahim, M. E. Balci, A. Karadeniz, and S. H. E. A. Aleem, “Optimal design and analysis of anti-resonance C-type high-pass filters,” in *Conference Proceedings - 2017 17th IEEE International Conference on*

Environment and Electrical Engineering and 2017 1st IEEE Industrial and Commercial Power Systems Europe, EEEIC / I and CPS Europe 2017, 2017.

[42] J. C. Das, "Passive filters - Potentialities and limitations," *IEEE Trans. Ind. Appl.*, vol. 40, no. 1, pp. 232–241, 2004.

[43] J. Arrillaga and N. R. Watson, *Power System Harmonics*. Chichester: Wiley, 2003.

[44] C. J. Chou, "Optimal planning of large passive-harmonic-filters set at high voltage level," *IEEE Trans. Power Syst.*, vol. 15, no. 1, pp. 433–441, 2000.

[45] W. Xu, T. Ding, X. Li, and H. Liang, "Resonance-free shunt capacitors - Configurations, design methods and comparative analysis," *IEEE Trans. Power Deliv.*, vol. 31, no. 5, pp. 2287–2295, 2016.

[46] A. B. Nassif, W. Xu, and W. Freitas, "An investigation on the selection of filter topologies for passive filter applications," *IEEE Trans. Power Deliv.*, vol. 24, no. 3, pp. 1710–1718, 2009.

[47] A. Karadeniz and M. E. Balci, "Comparative evaluation of common passive filter types regarding maximization of transformer's loading capability under non-sinusoidal conditions," *Electr. Power Syst. Res.*, vol. 158, pp. 324–334, 2018.

[48] M. Mohammadi, "Bacterial foraging optimization and adaptive version for economically optimum sitting, sizing and harmonic tuning orders setting of LC harmonic passive power filters in radial distribution systems with linear and nonlinear loads," *Appl. Soft Comput. J.*, vol. 29, pp. 345–356, 2015.

[49] A. F. Zobaa and S. H. E. Abdel Aleem, "A new approach for harmonic distortion minimization in power systems supplying nonlinear loads," *IEEE Trans. Ind. Informatics*, vol. 10, no. 2, pp. 1401–1412, 2014.

[50] X. R. Zhu, X. C. Shi, Y. L. Peng, and H. M. Li, "Simulated annealing based multi-object optimal planning of passive power filters," *Proc. IEEE Power Eng. Soc. Transm. Distrib. Conf.*, pp. 1–5, 2005.

[51] N. Yang and M. Le, "Multi-objective bat algorithm with time-varying inertia weights for optimal design of passive power filters set," *IET Gener. Transm. Distrib.*, vol. 9, no. 7, pp. 644–654, 2015.

[52] M. E. Balci and A. D. Karaoglan, “Optimal design of c-type passive filters based on response surface methodology for typical industrial power systems,” *Electr. Power Components Syst.*, vol. 41, no. 7, pp. 653–668, 2013.

[53] M. M. Ertay, S. Tosun, and A. Zengin, “Simulated annealing based passive power filter design for a medium voltage power system,” *Int. Rev. Electr. Eng.*, vol. 8, no. 1, pp. 354–361, 2013.

[54] V. Dzhankhotov and J. Pyrhönen, “Passive LC Filter design considerations for motor applications,” *IEEE Trans. Ind. Electron.*, vol. 60, no. 10, pp. 4–11, 2013.

[55] R. A. Vural, T. Yildirim, T. Kadioglu, and A. Basargan, “Performance evaluation of evolutionary algorithms for optimal filter design,” *IEEE Trans. Evol. Comput.*, vol. 16, no. 1, pp. 135–147, 2012.

[56] S. Russell and P. Norvig, *Artificial Intelligence: A Modern Approach*, no. 1–2. 1995.

[57] J. D. Farmer, N. H. Packard, and A. S. Perelson, “The immune system, adaptation, and machine learning,” *Phys. D Nonlinear Phenom.*, vol. 22, no. 1–3, pp. 187–204, 1986.

[58] S. Kirkpatrick, C. Gelati Jr, and M. Vecchi, “Optimization by simulated annealing,” *Biol. Comput. A Phys. Choice*, vol. 220, no. 4598, pp. 671–680, 1983.

[59] B. Mo, J. Yu, D. Tang, H. Liu, and J. Yu, “A remaining useful life prediction approach for lithium-ion batteries using Kalman filter and an improved particle filter,” *2016 IEEE Int. Conf. Progn. Heal. Manag.*, vol. 53, no. 6, pp. 805–810, 2016.

[60] R. Contreras, M. A. Pinninghoff, and J. Ortega, “Using ant colony optimization for edge detection in gray scale images,” *Lect. Notes Comput. Sci. (including Subser. Lect. Notes Artif. Intell. Lect. Notes Bioinformatics)*, vol. 7930 LNCS, no. PART 1, pp. 323–331, 2013.

[61] L. R. Costa, D. Aloise, and N. Mladenović, “Less is more: basic variable neighborhood search heuristic for balanced minimum sum-of-squares clustering,” *Inf. Sci. (Ny).*, vol. 415–416, pp. 247–253, 2017.

[62] A. Kalinli and N. Karaboga, “Artificial immune algorithm for IIR filter design,” *Engineering Applications of Artificial Intelligence*, vol. 18, no. 8. pp. 919–929,

2005, doi: 10.1016/j.engappai.2005.03.009.

[63] I. Fister, X. S. Yang, J. Brest, and D. Fister, “A brief review of nature-inspired algorithms for optimization,” *Elektroteh. Vestnik/Electrotechnical Rev.*, vol. 80, no. 3, pp. 116–122, 2013.

[64] Y. Song, *Modern Optimisation Techniques in Power Systems*. Kluwer Academic Publishers, 1999.

[65] D. E. Goldberg, “Sizing populations for serial and parallel genetic algorithms,” in *Proceedings of the Third International Conference on Genetic Algorithms*, pp. 70–79, 1989.

[66] A. Berizzi and C. Bovo, “The use of genetic algorithms for the localization and the sizing of passive filters,” in *Proceedings of International Conference on Harmonics and Quality of Power, ICHQP*, vol. 1, pp. 19–25, 2000.

[67] M. Ghiasi, V. Rashtchi, and S. H. Hoseini, “Optimum location and sizing of passive filters in distribution networks using genetic algorithm,” in *Proceedings - 4th IEEE International Conference on Emerging Technologies 2008, ICET 2008*, pp. 162–166, 2008.

[68] G. W. Chang, S. Chu, and H. Wang, “Sensitivity-based approach for passive harmonic filter planning in a power system,” *2002 IEEE Power Eng. Soc. Winter Meet. Conf. Proc. (Cat. No.02CH37309)*, vol. 2, pp. 937–940, 2002.

[69] N. Srinivas and K. Deb, “Muiltiobjective optimization using non-dominated sorting in genetic algorithms,” *Evol. Comput.*, vol. 2, no. 3, pp. 221–248, 1994.

[70] J. OuYang, F. Yang, S. W. Yang, and Z. P. Nie, “The improved NSGA-II approach,” *J. Electromagn. Waves Appl.*, vol. 22, no. 2–3, pp. 163–172, 2008.

[71] M. Dorigo, V. Maniezzo, A. Colorni, and M. Dorigo, “Positive feedback as a search strategy,” *Tech. Rep. 91-016*, pp. 1–20, 1991.

[72] M. Dorigo, V. Maniezzo, and A. Colorni, “Ant system: Optimization by a colony of cooperating agents,” *IEEE Trans. Syst. Man, Cybern. Part B Cybern.*, vol. 26, no. 1, pp. 29–41, 1996.

[73] T. Stützle and H. Hoos, “MAX–MIN ant system,” *Futur. Gener. Comput. Syst.*, vol. 16, pp. 889–914, 2000.

[74] M. Dorigo and L. M. Gambardella, “Ant colonies for the travelling salesman problem,” *BioSystems*, vol. 43, no. 2, pp. 73–81, 1997.

[75] Z. A. Hamid, I. Musirin, M. N. A. Rahim, and N. A. M. Kamari, “Application of electricity tracing theory and hybrid ant colony algorithm for ranking bus priority in power system,” *Int. J. Electr. Power Energy Syst.*, vol. 43, no. 1, pp. 1427–1434, 2012.

[76] P. Sarkar, A. Baral, K. Das, and P. Syam, “An ant colony system based control of shunt capacitor banks for bulk electricity consumers,” *Appl. Soft Comput. J.*, vol. 43, pp. 520–534, 2016.

[77] A. Ketabi and A. A. Babaee, “Application of the ant colony search algorithm to reactive power pricing in an open electricity market,” *Am. J. Appl. Sci.*, vol. 6, no. 5, pp. 956–963, 2009.

[78] W. Chen, Y. Shi, H. Teng, X. Lan, and L. Hu, “An efficient hybrid algorithm for resource-constrained project scheduling,” *Inf. Sci. (Ny).*, vol. 180, no. 6, pp. 1031–1039, 2010.

[79] M. López-Ibáñez and C. Blum, “Beam-ACO for the travelling salesman problem with time windows,” *Comput. Oper. Res.*, vol. 37, no. 9, pp. 1570–1583, 2010.

[80] A. Andziulis, D. Dzemydiene, R. Steponavičius, and S. Jakovlev, “Comparison of two heuristic approaches for solving the production scheduling problem,” *Inf. Technol. Control*, vol. 40, no. 2, pp. 118–122, 2011.

[81] J. Kennedy *et al.*, “Particle swarm optimization,” *Neural Networks, 1995. Proceedings., IEEE Int. Conf.*, vol. 4, no. 3, pp. 1942–1948, 1995.

[82] N. He, L. Huang, J. Wu, and D. Xu, “Study on optimal design method for passive power filters set at high voltage bus considering many practical aspects,” in *Conference Proceedings - IEEE Applied Power Electronics Conference and Exposition - APEC*, pp. 396–401, 2008.

[83] N. He, D. Xu, and L. Huang, “The application of particle swarm optimization to passive and hybrid active power filter design,” *IEEE Trans. Ind. Electron.*, vol. 56, no. 8, pp. 2841–2851, 2009.

[84] Y. P. Chang, “Optimal harmonic filters design of the Taiwan high speed rail traction system of distributer generation system with specially connected

transformers," *Int. J. Electr. Power Energy Syst.*, vol. 62, pp. 80–89, 2014.

[85] Y. P. Chang and C. N. Ko, "A PSO method with nonlinear time-varying evolution based on neural network for design of optimal harmonic filters," *Expert Syst. Appl.*, vol. 36, no. 3 PART 2, pp. 6809–6816, 2009.

[86] Y. P. Chang, "Integration of SQP and PSO for optimal planning of harmonic filters," *Expert Syst. Appl.*, vol. 37, no. 3, pp. 2522–2530, 2010.

[87] K. M. Passino, "Biomimicry of bacterial foraging for distributed optimization and control," *IEEE Control Syst.*, vol. 22, no. 3, pp. 52–67, 2002.

[88] X. S. Yang, "A new metaheuristic bat-inspired algorithm," *Stud. Comput. Intell.*, vol. 284, pp. 65–74, 2010.

[89] P. Kumar and S. Narayan, "Multi-objective bat algorithm tuned optimal FOPID controller for robust aircraft pitch control," *Int. J. Syst. Control Commun.*, vol. 8, no. 4, p. 348, 2017.

[90] M. R. A. Bakar, I. T. Abbas, M. A. Kalal, H. A. AlSattar, A. G. Khaddar Bakhayt, and B. A. Kalaf, "Solution for multi-objective optimisation master production scheduling problems based on swarm intelligence algorithms," *J. Comput. Theor. Nanosci.*, vol. 14, no. 11, pp. 5184–5194, 2017.

[91] A. Askarzadeh, "A novel metaheuristic method for solving constrained engineering optimization problems: Crow search algorithm," *Comput. Struct.*, vol. 169, pp. 1–12, 2016.

[92] A. Saha, A. Bhattacharya, P. Das, and A. K. Chakraborty, "Crow search algorithm for solving optimal power flow problem," in *Proceedings of the 2017 2nd IEEE International Conference on Electrical, Computer and Communication Technologies, ICECCT 2017*, 2017.

[93] L. Dos Santos Coelho, C. Richter, V. C. Mariani, and A. Askarzadeh, "Modified crow search approach applied to electromagnetic optimization," in *IEEE CEFC 2016 - 17th Biennial Conference on Electromagnetic Field Computation*, 2017.

[94] S. Kirkpatrick, C. D. Gelatt, and M. P. Vecchi, "Optimization by simulated annealing," *Ultrason. Sonochem.*, vol. 220, no. 4598, pp. 671–680, 1983.

[95] S. Z. Selim and K. Alsultan, "A simulated annealing algorithm for the clustering

problem," *Pattern Recognit.*, vol. 24, no. 10, pp. 1003–1008, 1991.

[96] A. F. Zobaa, "A new approach for voltage harmonic distortion minimization," *Electr. Power Syst. Res.*, vol. 70, no. 3, pp. 253–260, 2004.

[97] A. F. Zobaa, "Voltage harmonic reduction for randomly time-varying source characteristics and voltage harmonics," *IEEE Trans. Power Deliv.*, vol. 21, no. 2, pp. 816–822, 2006.

[98] A. E. Emanuel, "Harmonics in the early years of electrical engineering: A brief review of events, people and documents," in *Proceedings of International Conference on Harmonics and Quality of Power, ICHQP*, vol. 1, pp. 1–7, 2000.

[99] J. B. J. Fourier, *The analytical theory of heat*. Cambridge University Press, 2009.

[100] E. W. Schilling, "The distortion of current and voltage waves on transmission lines," 1933.

[101] C. Steinmetz, "Theory and Calculation of Alternating Current Phenomena," 1916.

[102] A. Kalair, N. Abas, A. R. Kalair, Z. Saleem, and N. Khan, "Review of harmonic analysis, modeling and mitigation techniques," *Renew. Sustain. Energy Rev.*, vol. 78, pp. 1152–1187, 2017.

[103] G. K. Singh, "Power system harmonics research: A survey," *Eur. Trans. Electr. Power*, vol. 19, no. 2, pp. 151–172, 2009.

[104] T. H. Ortmeyer, K. R. Chakravarthi, and A. A. Mahmoud, "The effects of power system harmonics on power system equipment and loads," *IEEE Trans. Power Appar. Syst.*, vol. PAS-104, no. 9, pp. 2555–2563, 1985.

[105] V. E. Wagner *et al.*, "Effects of harmonics on equipment," *IEEE Trans. Power Deliv.*, vol. 8, no. 2, pp. 672–680, 1993.

[106] S. K. Jain and S. N. Singh, "Harmonics estimation in emerging power system: Key issues and challenges," *Electr. Power Syst. Res.*, vol. 81, no. 9, pp. 1754–1766, 2011.

[107] M. H. J. Bollen, *Understanding Power Quality Problems:Voltage Sags and Interruptions*. 1999.

[108] B. C. Neagu, G. Georgescu, and O. Ivanov, "The impact of harmonic current flow on additional power losses in low voltage distribution networks," *2016 Int. Conf.*

Expo. Electr. Power Eng. (EPE 2016), pp. 20–22, 2016.

[109] T. J. M. S. Ragavi and R. S. Snekha, "Analysis of power quality disturbances using DWT and artificial neural network," *Int. J. Sci. Eng. Technol. Res.*, vol. 5, no. 4, pp. 1191–1196, 2016.

[110] Y. Chen, "Passive filter design using genetic algorithms," *IEEE Trans. Ind. Electron.*, vol. 50, no. 1, pp. 202–207, 2003.

[111] IEC 61000-2-1, "Electronic compatibility (EMC) - Part 2: Environment-Section 1: Description of the environment - Electromagnetic environment for low-frequency conducted disturbances and signalling in public power supply systems," 1990.

[112] V. J. Gosbell, S. Petera, and V. Smith, *Harmonic Distortion in the Electrical Supply System*. 2000.

[113] J. P. Nelson, "A better understanding of harmonic distortion in the petrochemical industry," *Ind. Appl. IEEE Trans.*, vol. 40, no. 1, pp. 220–231, 2004.

[114] A. Damnjanovic and G. M. J. Parsley, "Modeling of transformer nonlinearites taking hysteresis into account with consuming function and the harmonic balance method," *2004 IEEE Africon. 7th Africon Conf. Africa (IEEE Cat. No.04CH37590)*, vol. ol.1, pp. 741–744, 2004.

[115] D. Desai and S. Arya, "Reactive power compensation using FACTS device," in *International Conference on Research and Innovations in Science, Engineering and Technology, ICRISET2017*, vol. 1, pp. 175–168, 2018.

[116] S. Asawa and S. Al-Attiyah, "Impact of FACTS device in electrical power system," in *International Conference on Electrical, Electronics, and Optimization Techniques, ICEEOT 2016*, pp. 2488–2495, 2016.

[117] S. Dong, W. Zhonghong, J. Y. Chen, and Y. H. Song, "Harmonic resonance phenomena in STATCOM and relationship to parameters selection of passive components," *IEEE Trans. Power Deliv.*, vol. 16, no. 1, pp. 46–52, 2001.

[118] Q. Zhong, L. Lin, G. Wang, Y. Zhang, and Z. Wu, "Harmonic analysis model for voltage source converter under unbalanced conditions," *IET Gener. Transm. Distrib.*, vol. 9, no. 1, pp. 12–21, 2015.

[119] A. J. P. Ramos, P. C. C. Tavares, and L. R. Lins, "Application of static

compensators in radial power systems," in *IFAC Symposium on Planning and Operation of Electrical Energy System*, pp. 223–228, 1986.

[120] F. Z. G. H. Boudjella Houari, "Modeling and simulation of static Var modelling and simulation of static Var compensator with Matlab," in *4th International Conference on Computer Integrated Manufacturing CIP'2007 03-04*, 2007.

[121] A. Hewitt and T. Ahfock, "Harmonic injection due to negative phase sequence correction in static VAr compensators," in *Australasian Universities Power Engineering Conference: Challenges for Future Grids, AUPEC 2015*, 2015.

[122] "IEEE Std 519-2014. Recommended practice and requirements for harmonic control in electric power systems," *IEEE Std 519-2014*, vol. 2014, pp. 1–29, 2014.

[123] D. E. Steeper and R. P. Stratford, "Reactive compensation and harmonic suppression for industrial power systems using thyristor converters," *IEEE Trans. Ind. Appl.*, vol. IA-12, no. 3, pp. 232–254, 1976.

[124] G. Will and F. Haydock, "Industrial power quality considerations when installing adjustable speed drive systems," *IEEE Trans. Ind. Appl.*, 1995.

[125] M. M. G. Cardoso and B. J. C. Filho, "Thyristor switched series reactor for electric arc furnaces," in *Conference Record - IAS Annual Meeting (IEEE Industry Applications Society)*, vol. 1, pp. 124–130, 2006.

[126] H. Samet, T. Ghanbari, and J. Ghaisari, "Maximum performance of electric arc furnace by optimal setting of the series reactor and transformer taps using a nonlinear model," *IEEE Trans. Power Deliv.*, vol. 30, no. 2, pp. 764–772, 2015.

[127] Y. Li *et al.*, "A controllably inductive filtering method with transformer-integrated linear reactor for power quality improvement of shipboard power system," *IEEE Trans. Power Deliv.*, vol. 32, no. 4, pp. 1817–1827, 2017.

[128] A. Reznik, M. G. Simoes, A. Al-Durra, and S. M. Muyeen, "LCL Filter design and performance analysis for grid-interconnected systems," *IEEE Trans. Ind. Appl.*, vol. 50, no. 2, pp. 1225–1232, 2014.

[129] J. Rodríguez, J. S. Lai, and F. Z. Peng, "Multilevel inverters: A survey of topologies, controls, and applications," *IEEE Trans. Ind. Electron.*, vol. 49, no. 4, pp. 724–738, 2002.

[130] M. A. Chitsazan and A. M. Trzynadlowski, “Harmonic mitigation in interphase power controller using passive filter-based phase shifting transformer,” in *ECCE 2016 - IEEE Energy Conversion Congress and Exposition, Proceedings*, 2016.

[131] P. N. Parmar, “Harmonic mitigation for power quality improvement by designing phase-shifting transformers for non-linear,” *Int. J. Adv. Eng. Res. Dev.*, pp. 1418–1425, 2015.

[132] M. M. Swamy, “An electronically isolated 12-pulse autotransformer rectification scheme to improve input power factor and lower harmonic distortion in variable-frequency drives,” *IEEE Trans. Ind. Appl.*, vol. 51, no. 5, pp. 3986–3994, 2015.

[133] S. P. Ghayal and S. Gour, “Analysis of harmonics and neutral to ground (N to G) voltage diminutionusing isolation transformer,” in *ICONSTEM 2017 - Proceedings: 3rd IEEE International Conference on Science Technology, Engineering and Management*, pp. 571–574, 2018.

[134] P. Bagheri and W. Xu, “A technique to mitigate zero-sequence harmonics in power distribution systems,” *IEEE Trans. Power Deliv.*, vol. 29, no. 1, pp. 215–223, 2014.

[135] R. N. Jayasinghe and J. R. Lucas, “Power system harmonic effects on distribution transformers and new design considerations for K-factor transformers,” *IEE Sri Lanka Annu. Sess. – Sept.*, 2003.

[136] M. Tariq and M. T. Iqbal, “Power quality improvement by using multi-pulse AC-DC converters for DC drives: Modeling, simulation and its digital implementation,” *J. Electr. Syst. Inf. Technol.*, vol. 1, no. 3, pp. 255–265, 2014.

[137] K. Sozański, “Three phase active power filter with selective harmonics elimination,” *Arch. Electr. Eng.*, vol. 65, no. 1, pp. 33–44, 2016.

[138] T. L. Lee, Y. C. Wang, J. C. Li, and J. M. Guerrero, “Hybrid active filter with variable conductance for harmonic resonance suppression in industrial power systems,” *IEEE Trans. Ind. Electron.*, vol. 62, no. 2, pp. 746–756, 2015.

[139] W. H. Ko and J. C. Gu, “Impact of shunt active harmonic filter on harmonic current distortion of voltage source inverter-fed drives,” *IEEE Trans. Ind. Appl.*, vol. 52, no. 4, pp. 2816–2825, 2016.

[140] M. Mehrasa, E. Pouresmaeil, M. F. Akorede, B. N. Jørgensen, and J. P. S.

Catalão, “Multilevel converter control approach of active power filter for harmonics elimination in electric grids,” *Energy*, vol. 84, pp. 722–731, 2015.

[141] Danielle Collins, “Motion Control Tips,” *www.aurorabearing.com*, 2016. .

[142] K. Papp, G. Christiner, H. Popelka, and M. Schwan, “High voltage series reactors for load flow control,” *E&I Elektrotechnik und Informationstechnik*, vol. 121, no. 12, pp. 455–460, 2004.

[143] D. Shoup, J. Paserba, R. G. Colclaser, T. Rosenberger, L. Ganatra, and C. Isaac, “Transient recovery voltage requirements associated with the application of current-limiting series reactors,” *Electr. Power Syst. Res.*, vol. 77, no. 11, pp. 1466–1474, 2007.

[144] J. Vasilj, P. Sarajcev, and R. Goic, “Modeling of current-limiting air-core series reactor for transient recovery voltage studies,” *Electr. Power Syst. Res.*, vol. 117, pp. 185–191, 2014.

[145] H. John, “Line Reactors and VFDs,” *EC&M*, 2002. .

[146] B. Singh, A. Chandra, and K. Al-Haddad, *Power Quality : Problems and Mitigation Techniques*. Wiley, 2014.

[147] M. N. Alam, B. Das, and V. Pant, “A comparative study of metaheuristic optimization approaches for directional overcurrent relays coordination,” *Electr. Power Syst. Res.*, vol. 128, pp. 39–52, 2015.

[148] Z. A. Memon, M. A. Uquaili, and M. A. L. I. Unar, “Harmonics mitigation of industrial power system using passive filters,” vol. 31, no. 2, pp. 355–360, 2012.

[149] K. K. Srivastava, S. Shakil, and A. V. Pandey, “Harmonics and its mitigation technique by passive shunt filter,” *Int. J. Soft Comput. Eng.*, vol. 3, no. 2, pp. 325–331, 2013.

[150] J. Bladow and A. Montoya, “Experiences with parallel EHV phase shifting transformers,” *IEEE Trans. Power Deliv.*, vol. 6, no. 3, pp. 1096–1100, 1991.

[151] P. Bresesti, M. Sforna, V. Allegranza, D. Canever, and R. Vailati, “Application of phase shifting transformers for a secure and efficient operation of the interconnection corridors,” *IEEE Power Eng. Soc. Gen. Meet. 2004.*, pp. 1–6, 2004.

[152] R. M. G. Castro, F. M. R. Batista, and J. M. Medeiros Pinto, “Application of FACTS in the Portuguese transmission system: Investigation on the use of Phase-Shift Transformers,” in *2001 IEEE Porto Power Tech Proceedings*, vol. 4, pp. 40–43, 2001.

[153] G. M. Carvajal, G. O. Plata, W. G. Picon, and J. C. C. Velasco, “Investigation of phase shifting transformers in distribution systems for harmonics mitigation,” in *2014 Clemson University Power Systems Conference, PSC 2014*, 2014.

[154] E. A. Sobhy and S. Hoyos, “A multiphase multipath technique with digital phase shifters for harmonic distortion cancellation,” *IEEE Trans. Circuits Syst. II Express Briefs*, vol. 57, no. 12, pp. 921–925, 2010.

[155] S. Z. Djokic and A. J. Collin, “Cancellation and attenuation of harmonics in low voltage networks,” in *Proceedings of International Conference on Harmonics and Quality of Power, ICHQP*, pp. 137–141, 2014.

[156] P. Rodríguez, J. I. Candela, A. Luna, L. Asiminoaei, R. Teodorescu, and F. Blaabjerg, “Current harmonics cancellation in three-phase four-wire systems by using a four-branch star filtering topology,” *IEEE Trans. Power Electron.*, vol. 24, no. 8, pp. 1939–1950, 2009.

[157] A. J. Collin, S. Z. Djokic, C. E. Cresswell, A. M. Blanco, and J. Meyer, “Cancellation of harmonics between groups of modern compact fluorescent lamps,” *2014 Int. Symp. Power Electron. Electr. Drives, Autom. Motion, SPEEDAM 2014*, pp. 1190–1194, 2014.

[158] J. Kaiwar, “A study on harmonic mitigation by using isolation transformer,” *Res. J. Eng. Sci.*, vol. 6, no. 9, pp. 29–31, 2017.

[159] M. A. Shafie, H. Singh, and M. Q. A. Rahman, “Harmonic and neutral to ground voltage reduction using isolation transformer,” *PECon2010 - 2010 IEEE Int. Conf. Power Energy*, no. November 2010, pp. 561–566, 2010.

[160] G. Sandoval, J. Houdek, G. W. Chang, W. Xu, and P. F. Ribeiro, “A review of harmonic mitigation techniques,” *Power*, pp. 1–17, 2005.

[161] E. F. Fuchs, D. Yildirim, and W. M. Grady, “Measurement of eddy-current loss coefficient P EC-R, derating of single-phase transformers, and comparison with K-factor approach,” *IEEE Trans. Power Deliv.*, vol. 15, no. 1, pp. 148–154, 2000.

[162] O. Gouda, G. Amer, and W. Salem, “A study of K-factor power transformer characteristics by modeling simulation,” *Eng. Technol. Appl.*, vol. 1, no. 3, pp. 114–120, 2011.

[163] G. W. Massey, “Estimation methods for power system harmonic effects on power distribution transformers,” *IEEE Trans. Ind. Appl.*, vol. 30, no. 2, pp. 485–489, 1994.

[164] T. Committee, I. Power, and E. Society, *IEEE Recommended Practice for Establishing Liquid-Filled and Dry-Type Power and Distribution Transformer Capability When Supplying Nonsinusoidal Load Currents*, vol. 2008, no. August. IEEE, 2008.

[165] “Isolation Transformer,” *Protek Power.com. All Rights Reserved 2012*, 2012. .

[166] F. Z. Peng, “Application issues of active power filters,” *IEEE Ind. Appl. Mag.*, vol. 4, no. 5, pp. 21–30, 1998.

[167] B. Singh, K. Al-Haddad, and A. Chandra, “A review of active filters for power quality improvement,” *IEEE Trans. Ind. Electron.*, vol. 46, no. 5, pp. 960–971, 1999.

[168] S. Moran, “A line voltage regulator/conditioner for harmonic-sensitive load isolation,” in *Conference Record of the IEEE Industry Applications Society Annual Meeting*, pp. 947–951, 1989.

[169] J. Nastran, R. Cajhen, P. Jereb, and M. Seliger, “Active power filter for nonlinear AC loads,” *IEEE Trans. Power Electron.*, vol. 9, no. 1, pp. 92–96, 1994.

[170] H. L. Jou and J. C. Wu, “A new UPS scheme provides harmonic suppression and input power factor correction,” *IEEE Trans. Ind. Electron.*, vol. 42, no. 6, pp. 629–635, 1995.

[171] C. Y. Hsu and H. Y. Wu, “A new single-phase active power filter with reduced energy-storage capacity,” *IEEE Proc. - Electr. Power Appl.*, vol. 143, no. 1, pp. 25–30, 1996.

[172] E. Epstein, A. Yair, and A. Alexandrovitz, “Analysis of a reactive current source used to improve current drawn by static inverters,” *IEEE Trans. Ind. Electron. Control Instrum.*, vol. IECI-26, no. 3, pp. 172–177, 1979.

[173] F. Harashima, H. Inaba, and K. Tsuboi, “A closed-loop control system for the reduction of reactive power required by electronic converters,” *IEEE Trans. Ind. Electron. Control Instrum.*, vol. IECI-23, no. 2, pp. 162–166, 1976.

[174] H. Sasaki and T. Machida, “A new method to eliminate AC harmonic currents by magnetic flux compensation — Considerations on basic design,” *IEEE Trans. Power Appar. Syst.*, vol. PAS-90, no. 5, pp. 2009–2019, 1971.

[175] L. Malesani, P. Mattavelli, and P. Tomasin, “High-performance hysteresis modulation technique for active filters,” *IEEE Trans. Power Electron.*, vol. 12, no. 5, pp. 876–884, 1997.

[176] S. Bhattacharya, P. T. Cheng, and D. M. Divan, “Hybrid solutions for improving passive filter performance in high power applications,” *IEEE Trans. Ind. Appl.*, vol. 33, no. 3, pp. 732–747, 1997.

[177] G. Rim, I. Kang, W. Kim, and J. Kim, “A shunt hybrid active filter with two passive filters in tandem,” in *Proceedings of Applied Power Electronics Conference. APEC ’96*, vol. 1, pp. 361–366, 1996.

[178] J. W. Dixon, J. J. García, and L. Morán, “Control system for three-phase active power filter which simultaneously compensates power factor and unbalanced loads,” *IEEE Trans. Ind. Electron.*, vol. 42, no. 6, pp. 636–641, 1995.

[179] H. L. Jou, “Performance comparison of the three-phase active-power-filter algorithms,” *IEE Proc. - Gener. Transm. Distrib.*, vol. 142, no. 6, p. 646, 1995.

[180] J. W. Dixon, “A series active power filter based on a sinusoidal current-controlled voltage-source inverter,” *IEEE Trans. Ind. Electron.*, vol. 44, no. 5, pp. 612–620, 1997.

[181] S. Bhattacharya and D. Divan, “Synchronous frame based controller implementation for a hybrid series active filter system,” in *IAS ’95. Conference Record of the 1995 IEEE Industry Applications Conference Thirtieth IAS Annual Meeting*, vol. 3, pp. 2531–2540 vol.3, 1995.

[182] M. Ucar, E. Ozdemir, and M. Kale, “An analysis of three-phase four-wire active power filter for harmonic elimination reactive power compensation and load balancing under non-ideal mains voltage,” *PESC Rec. - IEEE Annu. Power Electron. Spec. Conf.*, vol. 4, pp. 3089–3094, 2004.

[183] M. Aredes, J. Hafner, and K. Heumann, “Three-phase four-wire shunt active filter control strategies,” *IEEE Trans. Power Electron.*, vol. 12, no. 2, pp. 311–318, 1997.

[184] B. Li and M. Tong, “Control method of the three-phase four-leg shunt active power filter,” in *Energy Procedia*, vol. 14, 2012.

[185] C. Madtharad and S. Premrudeepreechacharn, “Active power filter for three-phase four-wire electric systems using neural networks,” *Electr. Power Syst. Res.*, vol. 60, no. 3, pp. 179–192, 2002.

[186] G. J. Wakileh, *Power System Harmonics: Fundamental, Analysis and Filter Design*. Austria: Springer, 2001.

[187] M. Z. El-Sadek, *Power System Harmonics*. Egypt, 2006.

[188] M. Schlueter, M. Munetomo, “MIDACO SOLVER-User Manual,” vol. 6, 2018.

[189] M. Dorigo, G. Di Caro, and L. M. Gambardella, “Ant algorithms for discrete optimization,” *Artif. Life*, vol. 5, no. 2, pp. 137–172, 1999.

[190] M. Schlüter and M. Gerdts, “The oracle penalty method,” *J. Glob. Optim.*, vol. 47, no. 2, pp. 293–325, 2010.

[191] J. Dréo, “Shortest path find by an ant colony,” *Wikipedia Commons*. https://commons.wikimedia.org/wiki/File:Aco_branches.svg.

[192] M. Dorigo and C. Blum, “Ant colony optimization theory: A survey,” *Theor. Comput. Sci.*, vol. 344, no. 2–3, pp. 243–278, 2005.

[193] M. Huang, “Improved ant colony algorithm in the distribution of reactive power compensation device and optimization,” in *Procedia Engineering*, vol. 7, pp. 256–264, 2010.

[194] D. Prayogo, M. Y. Cheng, and D. K. Wibowo, “Minimizing construction cost and CO 2 emission problem by imitating the behavior of ant colony,” in *1st International Conference on Sustainable Civil Engineering Structures and Construction Materials*, 2012.

[195] K. Socha and M. Dorigo, “Ant colony optimization for continuous domains,” *Eur. J. Oper. Res.*, vol. 185, no. 3, pp. 1155–1173, 2008.

[196] M. Schlüter, J. A. Egea, and J. R. Banga, “Extended ant colony optimization for

non-convex mixed integer nonlinear programming," *Comput. Oper. Res.*, vol. 36, no. 7, pp. 2217–2229, 2009.

[197] G. E. P. Box and M. E. Muller, "A Note on the Generation of Random Normal Deviates," *Ann. Math. Stat.*, vol. 29, no. 2, pp. 610–611, 1958.

[198] M. Schlueter, C. H. Yam, T. Watanabe, and A. Oyama, "Parallelization Impact on Many-Objective Optimization for Space Trajectory Design," vol. 6, no. 1, pp. 1–6, 2016.

[199] IEEE, "IEEE Standard for Shunt Power Capacitors IEEE Power and Energy Society," 2013.

[200] B. Singh, A. Chandra, and K. Al-Haddad, *Power Quality Problems and Mitigation Techniques*. Chichester: Wiley Blackwell, 2015.

[201] IEEE, "IEEE Recommended Practices and Requirements for Harmonic Control in Electrical Power Systems," pp. 1–112, 1992.

[202] "Parallel Resonant Circuit," *Electronics Tutorial*. https://www.electronics-tutorials.ws/accircuits/parallel-resonance.html.

[203] "Series Resonant Circuit," *Electronics Tutorial*. https://www.electronics-tutorials.ws/accircuits/series-resonance.html.

[204] D. E. Goldberg, *Genetic Algorithms in Search, Optimization, and Machine Learning*. 1989.

[205] J. Kennedy, R. C. Eberhart, and Y. Shi, *Swarm Intelligence*, vol. 78, no. 2. 2001.

[206] A. A. Abou El-Ela, S. M. Allam, and M. M. Shatla, "Maximal optimal benefits of distributed generation using genetic algorithms," *Electr. Power Syst. Res.*, vol. 80, no. 7, pp. 869–877, 2010.